Year : 2022

Touch and wound responses in Arabidopsis thaliana

Yang Tsu-Hao

Yang Tsu-Hao, 2022, Touch and wound responses in Arabidopsis thaliana

Originally published at : Thesis, University of Lausanne

Posted at the University of Lausanne Open Archive http://serval.unil.ch
Document URN : urn:nbn:ch:serval-BIB_CEF3FEB5F28D3

UNIL | Université de Lausanne
Faculté de biologie et de médecine

Département de Biologie Moléculaire Végétale (DBMV)

Touch and wound responses in *Arabidopsis thaliana*

Thèse de doctorat ès sciences de la vie (PhD)

présentée à la

Faculté de biologie et de médecine
de l'Université de Lausanne

par

Tsu-Hao YANG

Master of Science
National Tsing Hua University, Taiwan

Jury

Prof. Richard Benton, President
Prof. Edward Elliston Farmer, Thesis Director
Prof. Matthew Gilliham, Expert
Dr. Stephan Kellenberger, Expert
Prof. Niko Geldner, Expert

Lausanne
2022

UNIL | Université de Lausanne

Faculté de biologie et de médecine

Ecole Doctorale

Doctorat ès sciences de la vie

Imprimatur

Vu le rapport présenté par le jury d'examen, composé de

Président·e	Monsieur	Prof.	Richard	**Benton**
Directeur·trice de thèse	Monsieur	Prof.	Edward Elliston	**Farmer**
Expert·e·s	Monsieur	Prof.	Matthew	**Gilliham**
	Monsieur	Dr	Stephan	**Kellenberger**
	Monsieur	Prof.	Niko	**Geldner**

le Conseil de Faculté autorise l'impression de la thèse de

Tsu-Hao Yang

Master of Science, National Tsing Hua University, Taiwan

intitulée

Touch and wound responses in *Arabidopsis thaliana*

Lausanne, le 29 novembre 2022

pour le Doyen
de la Faculté de biologie et de médecine

Prof. Richard Benton

Abstract:

Land plants rely on inducible defenses to survive in nature. Inducible defenses are triggered reactively by environmental stimuli such as touch or wounding. We focused on the role of plant vascular tissues in sensing and responding to mechanical stimulations. A novel mechanostimulation method is developed in this thesis to study mechanical force sensation in plants. With the use of this method, forces ranging from 3 mN to 76 mN are applied to *Arabidopsis thaliana* leaves. We thus characterized the touch-induced electrical signal to optimize our stimulation protocol. Three breakthroughs were achieved in this study. Firstly, the mechanostimulated electrical signals are identified in the phloem sieve element. The amplitudes of the touch-induced sieve element signal were consistent with the touch-induced surface potential. Second, rosette mechano-responsiveness depends on the time of day. *A. thaliana* and *Mimosa pudica* both showed consistent time-of-day-associated mechano-responses. Thirdly, plasma membrane proton pump activity plays a key role in mechano-response electrical signal production. Gain-of-function and null-mutations of the plasma membrane proton pump both attenuate the mechanostimulated electrical signal. Furthermore, mechanostimulation induces jasmonate-responsive gene transcripts. The 13-lipoxygenases (13-LOX) genes *LOX2* and *LOX6* are the major jasmonate precursor-producing genes involved in mechanostimulation-induced jasmonate synthesis. Meanwhile, *LOX3* and *LOX4* were found to be essential for wound-response growth inhibition in *Arabidopsis*. In summary, we find that plant vascular tissues play an important role in mechanical force sensation. Plasma membrane proton pumps are required for maintaining the proper plasma membrane potential in touch responses. In summary, we performed a comprehensive study of mechanostimulation-induced electrical signals in *Arabidopsis.* This study improves our understanding of mechanical force sensation in plants.

Résumé

Les plantes terrestres dépendent de défenses inductibles pour survivre dans la nature. Les défenses inductibles sont déclenchées de manière réactive par des stimuli environnementaux tels que le toucher ou la blessure. Nous nous sommes concentrés sur le rôle des tissus vasculaires des plantes dans la détection et la réponse aux stimulations mécaniques. Une nouvelle méthode de mécanostimulation est développée dans cette thèse pour étudier la sensation de force mécanique chez les plantes. Grâce à cette méthode, des forces allant de 3 mN à 76 mN sont appliquées aux feuilles d'*Arabidopsis thaliana*. Nous avons ainsi caractérisé le signal électrique induit par le toucher afin d'optimiser notre protocole de stimulation. Trois percées ont été réalisées dans cette étude. Premièrement, les signaux électriques mécanostimulés sont identifiés dans le tube criblé du phloème. Les amplitudes du signal de la phloème induit par le toucher étaient cohérentes avec le potentiel de surface induit par le toucher. Deuxièmement, la mécanosensibilité des rosettes dépend de l'heure de la journée. *A. thaliana* et *Mimosa pudica* ont tous deux montré des réponses mécaniques associées à l'heure du jour. Troisièmement, l'activité de la pompe à protons de la membrane plasmique joue un rôle clé dans la production du signal électrique de la mécano-réponse. Les mutations par gain de fonction et les mutations nulles de la pompe à protons de la membrane plasmique atténuent toutes deux le signal électrique mécanostimulé. De plus, la mécanostimulation induit la transcription de gènes répondant au jasmonate. Les gènes des 13-lipoxygénases (13-LOX) *LOX2* et *LOX6* sont les principaux gènes producteurs de précurseurs de jasmonate impliqués dans la synthèse de jasmonate induite par la mécanostimulation. Par ailleurs, LOX3 et LOX4 se sont avérés essentiels pour l'inhibition de la croissance en réponse aux blessures chez Arabidopsis. En résumé, nous constatons que les tissus vasculaires des plantes jouent un rôle important dans la sensation de force mécanique. Les pompes à protons de la membrane

plasmique sont nécessaires pour maintenir le potentiel adéquat de la membrane plasmique dans les réponses tactiles. En résumé, nous avons réalisé une étude des signaux électriques induits par la mécanostimulation chez Arabidopsis. Cette étude améliore notre compréhension de la sensation de force mécanique chez les plantes.

Summary for general audience:

La sensibilité au toucher peut aider les plantes à se protéger en produisant le jasmonate une hormone de défense. Nous avons développé une nouvelle méthode pour en savoir plus sur la façon dont les plantes ressentent le toucher. Nous avons constaté que les signaux électriques induits par le toucher étaient transmis à travers le système vasculaire. Une force minimale de 3 mN, similaire à la force du vent appliquée par un vent d'échelle Beaufort 3 (12-19 Km/h) soufflant contre une surface de feuille de 2 cm2, était nécessaire pour induire des signaux électriques. Après une première stimulation tactile, les plantes ont besoin de plus de 30 minutes pour ressentir un second toucher. En général, les plantes sont plus sensibles au toucher l'après-midi que le matin. Les signaux électriques induits par le toucher ont besoin de l'activité des pompes à protons qui maintiennent le potentiel de la membrane plasmique. Toucher des mutants qui ont une l'expression reduité des pompes à protons dans les veines déclenche la production de signaux électriques faibles. De plus, les pompes à protons hyperactives diminuent le signal électrique induit par le toucher. Le toucher active les gènes producteurs de précurseurs de jasmonate pour induire la signalisation et la défense du jasmonate. Ceci est différent de l'inhibition de la croissance induite par la blessure qui nécessite d'autres gènes produisant des précurseurs de jasmonate. En résumé, nous trouvons que le toucher induit des signaux électriques dans le système vasculaire de la plante. Cette réponse dépend de l'heure de la journée et nécessite l'activité des pompes à protons de la membrane plasmique dans le phloème. Deux paires de gènes qui produisent des précurseurs du jasmonate jouent des rôles différents mais essentiels dans les réponses au toucher et à la blessure.

Chapter 1: INTRODUCTION

The great canopy of land plants provides essential nutrition and shelter for the animals on earth. Unlike their animal counterparts, land plants rely on the root system to support their growth. Plants cannot escape from aggressors in response to the attack. Therefore, plants have developed elegant strategies to defend themselves. An important strategy which I studied in this thesis is inducible defense. Inducible gene expression reactively boosts plant defense in response to direct or indirect stimuli. The activation of inducible defense mechanisms depends on various plant hormones, such as jasmonic acid, salicylic acid, and ethylene.

Jasmonate is the major hormone that activates defense mechanisms in response to mechanical wounding and helps plants fight against aggressors like herbivores. This hormone is known to be involved in the transcriptional reprogramming of many herbivore-induced genes (Reymond et al. 2004). The first discovered wound-inducible defense response was the accumulation of a protease inhibitor in tomatoes (Green and Ryan 1972). In the 1990s, a small organic compound called jasmonic acid was identified to be the signal which controlled the protease inhibitors in tomatoes (Farmer and Ryan 1990, Farmer and Ryan 1992). More and more publications underscored the importance of jasmonate in plant defense and the mechanism of action of jasmonate and its unclear receptor are now known (Howe et al., 2018). Also, it is now known that electrical signals are essential for long-distance wound signaling and activating the jasmonate pathway in leaves distal to wounds (Mousavi et al., 2013). The propagation velocity of wound-induced electrical signals through the plant vasculature is similar to the velocity of cytosolic calcium increases (Nguyen et al., 2018). Both wound-induced electrical signals and calcium signals depended on the clade 3 *GLUTAMATE RECEPTOR-LIKE* genes (*GLR*s) to propagate from leaf to leaf. But how signals originate from a wound and how signals activate the jasmonate pathway remain little understood.

The wound response in plants depends on various hormone signaling pathways. Herbivores are the major source of wounds in nature and insect damage is one of the main causes of yield loss in agriculture. When plant tissues are broken, fragments from the cell wall and other cell-derived molecules (known as damage-associated molecular patterns) are released from wounds (Ferrari et al., 2013; Choi and Klessig, 2016; Mielke and Gasperini, 2019). These molecules are sensed by self-recognition mechanisms and this triggers jasmonate synthesis and signaling (Heil et al., 2012). Both leaf extract application and mechanical wounding can induce increases in the endogenous jasmonate concentration (Reymond et al. 2004). Transcriptional reprogramming shares similar patterns in response to either wounding, leaf extract application, or jasmonate application (Reymond et al. 2004). In addition to damage-associated molecular patterns, other signals such as reactive oxygen species (ROS), electrical signals, and hydraulic signals are also involved in the systemic response induced by wounding (Steinhorst and Kudla, 2013; Mousavi et al., 2013; Huber and Bauerle, 2016).

Jasmonate biosynthesis and signaling

The complex jasmonate biosynthetic pathway operates in at least three cellular compartments and involve approximately 10 intermediates (Acosta and Farmer 2010). The synthesis of jasmonate begins in the chloroplasts where triunsaturated fatty acids are oxygenated by 13-LIPOXYGENASES (LOXs) (Wasternack and Hause, 2013)(Figure 1.1). The dioxygenation of 16:3 and 18:3 triunsaturated fatty acids is the first and essential step for jasmonate production. The four 13-LOXs in *Arabidopsis* are organized in two pairs which react differently in response to wounding (Chauvin et al., 2016). Following dioxygenation, the fatty acids are dehydrated by the enzyme ALLENE OXIDE SYNTHASE (AOS). AOS (also called CYP74A) belongs to the cytochrome P450 superfamily and uniquely catalyzes this dehydration step. Loss-of-function *aos* single mutants stop jasmonate production in early steps allowing

researchers access phenomenon in the jasmonate-null condition (Park et al., 2002). AOS produces short-lived, allene oxide intermediates. These are cyclized by ALLENE OXIDE CYCLASE (AOC) enzymes which rearrange the allene oxide intermediates into 12-oxo-phytodienoic acid (OPDA) and dinor-oxo-phytodienoic acid (dnOPDA). OPDA has the property of triggering jasmonate-independent signaling (Ribot et al., 2008). Transportation of OPDA out of chloroplasts requires the JASSY protein which is localized on the outer membrane of the chloroplast (Guan et al., 2019). Impaired JASSY gene function causes failed OPDA transport and impaired jasmonate accumulation after wounding. Therefore, OPDA is another crucial intermediate in jasmonate biosynthesis. The steps following OPDA production take place in another cellular compartment outside of chloroplast. OPDA and dnOPDA are transported into the peroxisome, the second cellular compartment crucial for jasmonate biosynthesis. In peroxisomes, OPDA REDUCTASE 3 enzyme reduces the cyclopentenones OPDA and dnOPDA into cyclopentanones. Then the cyclopentanones undergo 3 rounds of successive β-oxidation to produce OPC8, OPC6, and the prohormone jasmonic acid (Schaller and Stintzi, 2009). Then jasmonic acid is exported from the peroxisome to the cytosol for final modifications. Jasmonic acid can be methylated or can be conjugated to amino acids in the cytosol. Methyl-jasmonate is a volatile derivate which can spread through the air. The enzyme JASMONATE RESISTANT 1 (JAR1) produces jasmonyl-isoleucine (JA-Ile) which is the major biological active jasmonate (Staswick et al., 2002; Staswick et al., 2005).

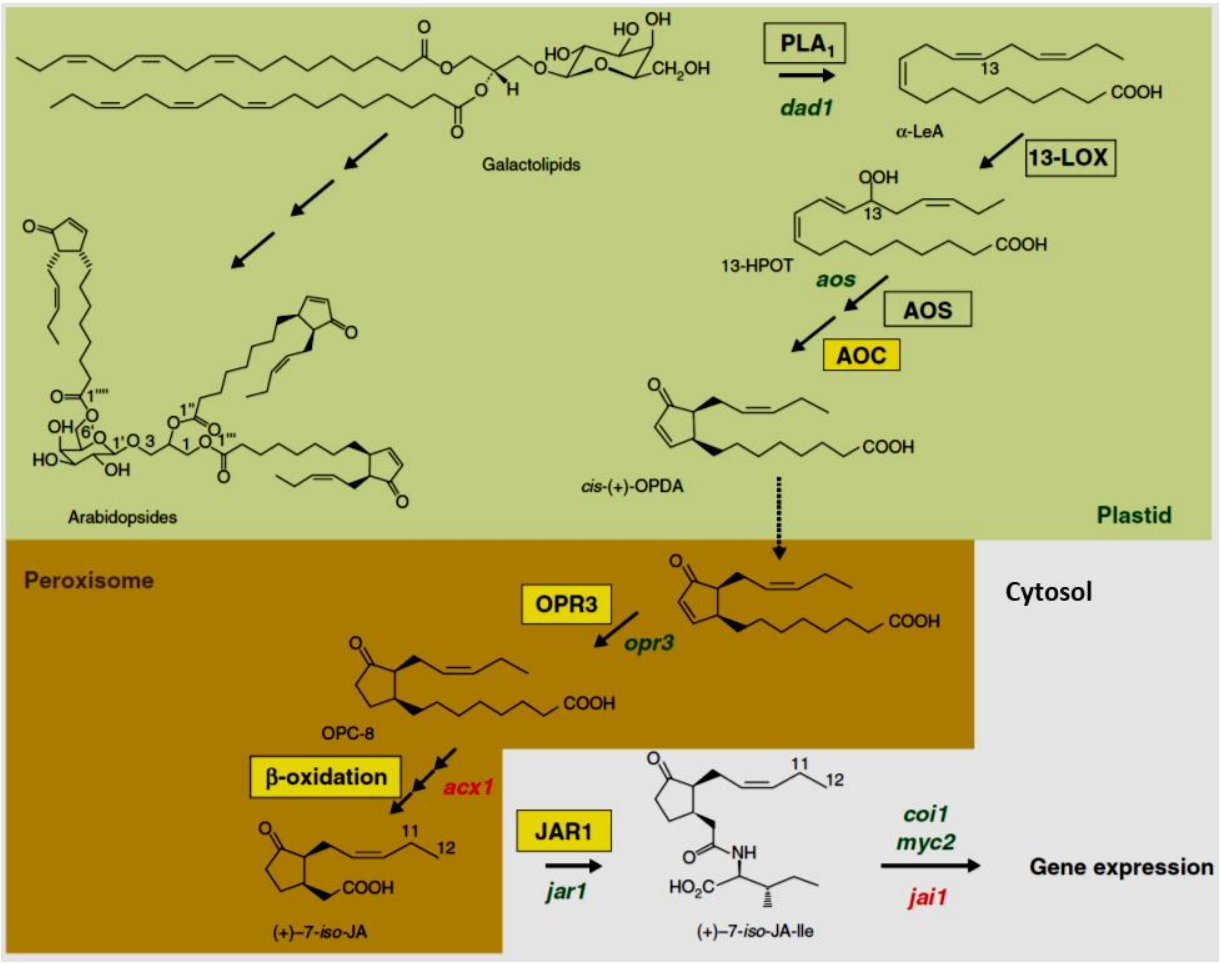

Figure 1.1 Jasmonate biosynthesis. 13-LOXs oxygenate fatty acids in the plastids as the first step of jasmonate synthesis. The products are processed by AOS and AOC to generate OPDA. OPDA is then transported to peroxisomes and is reduced by OPR3. This is followed by 3 rounds of β-oxidation. The prohormone jasmonic acid is then conjugated with isoleucine by JAR1 in the cytosol. Jasmonyl-isoleucine is the main biological active hormone (Figure from Wasternack and Hause, 2013).

Arabidopsis thaliana has four 13-lipoxygenases (*LOX2*, *LOX3*, *LOX4*, and *LOX6*) that initiate jasmonate biosynthesis in the chloroplasts. This is an early and potentially regulatory step in jasmonate synthesis. All four 13-LOXs contribute to jasmonate synthesis in response to wounding (Chauvin et al., 2013). Moreover, the 13-LOXs are likely active in pairs: the LOX2, LOX6 pair and the LOX3, LOX4 pair (Chauvin et al., 2016). Activation of *LOX2* and *LOX6*

upregulated the transcripts of *LOX3* and *LOX4* suggesting the relationship between pairs might be hierarchical. Of the four 13-LOXs, LOX6 is the main contributor which produces jasmonate in the distal leaf shortly after wounding (Gasperini et al. 2015). The induction levels of transcripts from the *JAZ10* gene, a jasmonate signalling marker gene, in the *lox2 lox3 lox4* triple mutants which retains *LOX6* are similar to those in the WT. *LOX6* is specifically expressed in xylem contact cells in leaves. The oxylipins produced from *LOX6* are exported from the contact cells into the rest of the leaf (Gasperini et al. 2015). Both *LOX2* and *LOX6* are required for a full WT-level jasmonate response. *LOX2* is important for the production of high levels of jasmonate in the proximity of a wound (Glauser et al. 2009). This *LOX* is expressed broadly in soft tissues in the leaf blade, but its expression is excluded from mature veins (Chauvin et al., 2016). *LOX2* expression is wound-inducible and it is also the most abundant 13-LOX under resting conditions. Thus, a *lox2* single mutant was significantly more susceptible than the WT to the larvae of *Spodoptera littoralis* (Glauser et al. 2009; Chauvin et al., 2016). While *LOX3* and *LOX4* have a minor role in rapid jasmonate induction by wounding, they are crucial for male fertility and wound-response growth inhibition in Arabidopsis (Chauvin et al., 2013; Caldelari et al. 2011; Yang et al., 2020). *LOX3* is expressed in the xylem and phloem, and in the blades of developing leaves (Chauvin et al., 2016). *LOX4* is strictly expressed in or near the phloem. Both *LOX3* and *LOX4* are wound-inducible at the mRNA level. Finally, lack of *LOX4* increases the susceptibility in the root to the root-knot nematode *Meloidogyne javanica* (Ozalvo et al., 2014). However, the effect of lacking both *LOX3* and *LOX4* is not significant to the growth of caterpillar *Spodoptera littoralis* (Chauvin et al., 2016).

The jasmonate signaling pathway is highly regulated. The expression of jasmonate-responsive genes is repressed by members of the JASMONATE ZIM-DOMAIN (JAZ) family. In the *Arabidopsis* genome, there are 13 JAZs that repress the activity of transcription factors

while JA-Ile concentrations are low (Howe et al., 2018). Environmental cues can stimulate the rapid production of biologically-active JA-Ile within 90 seconds (Chauvin et al., 2013). JA-Ile binds to the receptor CORONATINE INSENSITIVE 1 (COI1) in the nucleus. The COI1 is an SKP1-CUL1-F-Box-Protein (SCF) E3 Ubiquitin Ligase (Katsir et al., 2008). Hormone recognition favors the formation of the COI1-JAZ complex through the binding of COI1 to the Jas motif present in JAZ proteins (Thines et al., 2007). COI1-JAZ complex formation promotes the ubiquitination and degradation of JAZ through 26S proteasomes (Chini et al., 2007). This degradation requires the Jas motif and a JAZ10 splicing variant which lacks its Jas motif had a jasmonate-insensitive phenotype (Chung and Howe, 2009). JAZ degradation relieves transcription factors from the repression. Thus, transcription factors such as MYC2 recruit RNA polymerase II to promote the transcription of jasmonate-responsive genes (Chini et al., 2007; Acosta and Farmer 2010) (Figure 1.2).

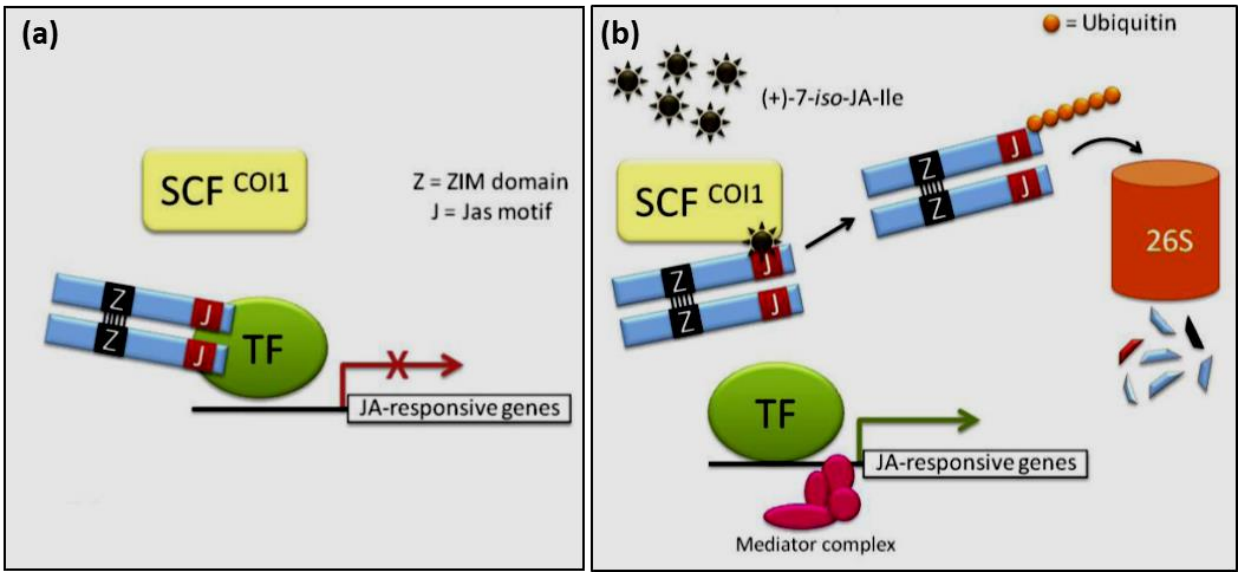

Figure 1.2 Jasmonate signaling. (a) In the absence of jasmonate, JAZ proteins bind to and repress transcription factors like MYC2. The transcription of JA-responsive genes is inhibited. (b) In the presence of jasmonyl-isoleucine, hormone binding facilitates the formation of COI1-JAZ complexes. COI1 binding to the Jas motif of a JAZ protein promotes its ubiquitination and

following degradation by 26S proteasomes. Transcription factors relieved from JAZ-repression can thus induce JA-responsive gene expression (Figure from Acosta and Farmer 2010).

Long-distance wound signaling

The rapid production of jasmonate accumulation at long distances from stimuli such as wounding is an amazing feature. Both jasmonate biosynthesis and jasmonate signaling are not restricted in the wounding site (Koo and Howe 2009). By the time of the first discovery of a wound-inducible protease inhibitor in tomatoes, it had been noticed that the wound response occured in leaves distal to wounds (Green and Ryan 1972). Experiments with airborne methyl jasmonate application provided further insights (Farmer and Ryan 1990). Both methyl jasmonate-sprayed tomato plants and unsprayed control tomato plants have protease inhibitor induction if these plants are sealed in the same Plexiglas box. Also, in an air-tight glass chamber, the airborne methyl jasmonate can travel through a 4-6 cm distance from cotton-tipped wooden dowels to the tomato plants and induce protease inhibitors in a dose-dependent manner. The volatile hormone derivatives traveling through air to receive plants was the first described long-distance signaling mechanism in the jasmonate pathway.

Grafting experiments revealed that the oxylipin jasmonate and its precursors can be transported axially from the shoot to the root in *Arabidopsis* (Gasperini et al., 2015). The WT shoot grafted onto *aos* roots had normal induction of jasmonate-responsive genes in the root following wounding of the shoot. The *aos* mutant shoot grafted onto the WT cannot induce such a response. Further, the radial transport of oxylipins can also occur. The oxylipins produced by LOX6 are transported from xylem contact cells to the entire vasculature and the leaf blade. The lipoxygenase triple mutant, *lox2 lox3 lox4*, in which only LOX6 produces jasmonate precursors, shows a near WT level of jasmonate-responsive gene induction in either

wounded leaf 8 or distal leaf 13 (Gasperini et al., 2015). However, LOX2 activity is required for a full WT level of response in grafted seedlings. Wounded *lox2* mutants show much weaker induction of jasmonate responsive genes than the WT in both the cotyledon and the root (Gasperini et al., 2015). To sum up, although oxylipins are transported both axially and radially, a full response of jasmonate signaling requires de novo jasmonate synthesis. The axial and radial transportation of oxylipins provides one mode of long-distance signaling in the jasmonate pathway.

In adult *Arabidopsis*, wounding induces jasmonate-responsive genes such as *JAZ10* and *LOX2* via signalling mechanisms that require interleaf vascular connections (Glauser et al., 2009, Chauvin et al., 2013). This suggests that the induction of wound-response genes is determined by vascular architecture. Wounding results in various types of signals (Figure 1.3) (Farmer et al., 2020). From the breakage site, damage-associated molecular patterns are released into extracellular spaces (Creelman and Mullet, 1997; Ferrari et al., 2013). The membrane potential of the living cells collapses rapidly in response to wounding. Membrane depolarization of groups of cells due to wounding can be measured as electrical signals with surface or intracellular electrodes (Mousavi et al., 2013; Salvador-Recatala et al., 2014). The electrical signal in the undamaged leaf petiole distal to wounded leaves coincides with tissue deformations due to changes in turgor pressure (Kurenda et al., 2019). Also, damage to the phloem and xylem from wounding is thought to lead to changes in their intracellular pressures. Such a change of pressure in the vascular tissues may produce a hydraulic pressure wave that serves as a wound-induced hydraulic signal (Boari and Malone 1993).

The speed of wound signals propagating leaf-to-leaf must preceed jasmonate induction in the distal leaf and occurs in this leaf within 90 seconds of wounding (Chauvin et al., 2013). Signals originating from the wound travel throughout the wounded *Arabidopsis* leaf in less than

40 seconds. Calculations performed according to the size of adult *Arabidopsis* rosettes and induction of jasmonate synthesis in leaves distal to wounds led to estimated leaf-to-leaf signal velocities of approximately 7.5 cm per minute (Chauvin et al., 2013). This estimated velocity was similar to another velocity estimation experiment measuring the jasmonate-independent velocity of wound-induced reactive oxygen species accumulation from the leaf to the inflorescence stem (Miller et al., 2009). These estimated velocities created a starting point to study the long-distance wound signals which activate hormone biosynthesis and wound responses.

Further research showed that wound-associated electrical signals propagated from leaf to leaf with an average velocity of 8.5 cm per minute (Mousavi et al., 2013). This speed closely matches previous estimations of the wound-induced responses (Miller et al., 2009; Chauvin et al., 2013). Electrical signal propagation can cover almost 1/3 of the entire rosette in 5-week-old *Arabidopsis* and this is identical to the wound-induced expression domain of wound-induced *JAZ10* expression. Electrical signal propagation in wounded Arabidopsis rosettes depends on GLUTAMATE RECEPTER-LIKE (GLR) genes. The mutant *glr3.3 glr3.6* eliminates the long-distance electrical signal and also eliminates the wound-induced *JAZ10* expression in the distal leaf (Mousavi et al., 2013). Also, the consistent phenotype of plants lacking long-distance electrical signal and wound-induced *JAZ10* expression is found in *glr3.1 glr3.3* mutants as well (Nguyen et al., 2018). Finally, caterpillar larvae gain weight faster on both *glr3.1 glr3.3* and *glr3.3 glr3.6* mutants suggesting the defenses are attenuated. These findings suggest that the long-distance propagated electrical signal is a key to activating wound-response jasmonate synthesis.

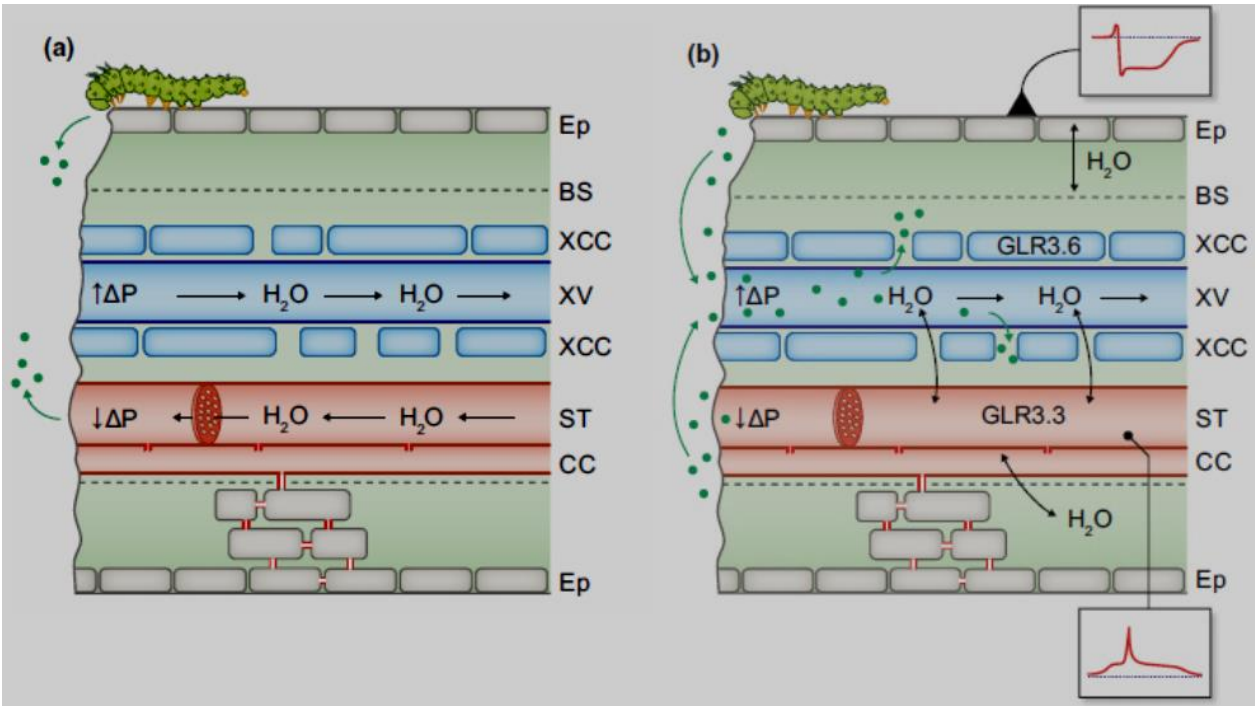

Figure 1.3 Wound-induced signals in *Arabidopsis*: a model. (a) Wounding by a caterpillar causes pressure changes in the phloem and the xylem. (b) The pressure changes and transpiration drive the elicitors along xylem vessels. These elicitors trigger membrane depolarization in xylem contact cells. Such electrical signals can be measured with intracellular electrodes or with surface electrodes (Figure from Farmer et al., 2020).

Electrical, hydraulic, and chemical wound signals in plants

Electrical signals: Certain environmental stimuli induce electrical responses in plants. Such electrical signals include slow wave potentials, action potentials, system potentials, sieve element wound signals, and single-cell damage signals (Figure 1.4) (Farmer et al., 2020). The wound-response slow wave potential propagates leaf-to-leaf through vascular connections. This signal route is similar to that of wound-induced jasmonate synthesis (Chauvin et al., 2013). The slow wave potential consists of a rapid depolarization phase and a long repolarization phase. It takes minutes from depolarization to repolarization for the complete slow wave potential. It was found that GLUTAMATE-RECEPTOR-LIKE ion channels were necessary for

propagation of slow wave potentials (Mousavi et al., 2013). Plants lacking certain functional clade 3 GLR genes cannot induce jasmonate signalling in leaves distal to wounds. Also, the plasma membrane proton pump *AHA1* is necessary for the repolarization phase of the leaf-to-leaf slow wave potential (Kumari et al, 2019). The *aha1* mutant has extended durations of the depolarization phase and also shows stronger wound-induced responses. A small hyperpolarization which is often found at the beginning of slow wave potential in the distal leaf of *Arabidopsis* does not show any link to stress responses yet. A slow wave potential includes the components of the phloem action potential, the system potential, and single cell damage signals (van Bel et al., 2014; Farmer et al., 2020).

The action potential is an all-or-nothing electrical signal which, in plants, is best known in carnivores such as the Venus flytrap (*Dionaea*) (Sibaoka, 1966). An extremely fast velocity is one of its characteristics. For example, the velocity of action potential propagation in the Venus flytrap can reach at least 10 meters per minute (Sibaoka, 1966). Also, action potentials in the Venus flytrap have relatively short durations. Each action potential lasts no more than a few seconds (Simons, 1981; Hodick and Sievers, 1988). If the stimuli do not produce a wound, the stimulated action potential does not move from organ to organ (Fromm and Lautner, 2007). For example, a touch-induced action potential is found propagating within the same leaf in *Arabidopsis* (Degli Agosti, 2014). But its velocity, 6 cm per minute, is much slower than the action potentials recorded in Venus flytrap. Furthermore, the action potential in the sieve element of *Mimosa pudica* has been recorded with aphid electrodes (Fromm, 1991). There are papers suggesting that the action potential, as a component of the slow wave potential, plays a major role in depolarizing cells prior to the long depolarization phase (Davies and Stankovic, 2006).

The system potential is a hyperpolarization induced by adding cations or glutamate into a wound (Zimmermann et al., 2009). It can travel from leaf-to-leaf and is proposed as a long-distance signal in plants. Either monocots, barley (*Hordeum vulgare*) and corn (*Zea mays*) or dicots, tobacco (*Nicotiana tabacum*) and fava bean (*Vicia faba*) all have system potentials (Zimmermann et al., 2009). System potentials are recorded through extracellular electrodes placed in substomatal cavities and reference electrodes on the tip of the same leaf. This electrical signal also relies on the activity of plasma membrane proton pumps. Inhibition of plasma membrane proton pumps suppresses the propagation of system potentials. The velocity of system potential propagation is between 5 cm per minute and 10 cm per minute.

In order to probe specific electrical signals in phloem sieve elements, aphids can be glued onto gold wires and used as a living electrodes (Tjallingii, 1990). These are intracellular electrodes since the aphid feeds in the sieve element. This method, originally used to study aphid electrophysiology, was adopted for plant-derived electrical signals (Salvador-Recatala et al., 2014). Stimuli such as caterpillar feeding or mechanical wounding trigger sieve element wound signals. The estimated velocity of this signal is around 6 cm per minute (Salvador-Recatala et al., 2014). Sieve element wound signals have a sharp, spike-like peak which is embedded in a long and slow wave. To date, it is still not fully clear whether the slow wave of the sieve element wound signal corresponds to the slow wave potential or not. Also, the spike-like peak, duration of a few seconds, shares similar characteristics with the action potential.

Single-cell damage signals can be measured through surface electrodes placed on the root of *Arabidopsis* seedlings (Marhavy et al., 2019). Individual cortex cells are damaged with the laser of a 2-photon microscope. Damage-induced membrane depolarization spreads through the neighboring cells. At a 100 µm distance from the wounded cell, the single cell damage signal is measured with an amplitude of 80 mV. It decays with the increase of distance from

the wounded cell. For example, the amplitude at a distance of 200 µm is decreased down to 25 mV. It is almost undetectable if measured at a distance of 400 µm from the wound (Marhavy et al., 2019). This short-distance electrical signal is partially attenuated by chemical or genetic inhibition of calcium channels, chloride channels, potassium channels, and proton pumps. Furthermore, the single-cell damage signal induces a regional ethylene response in the root.

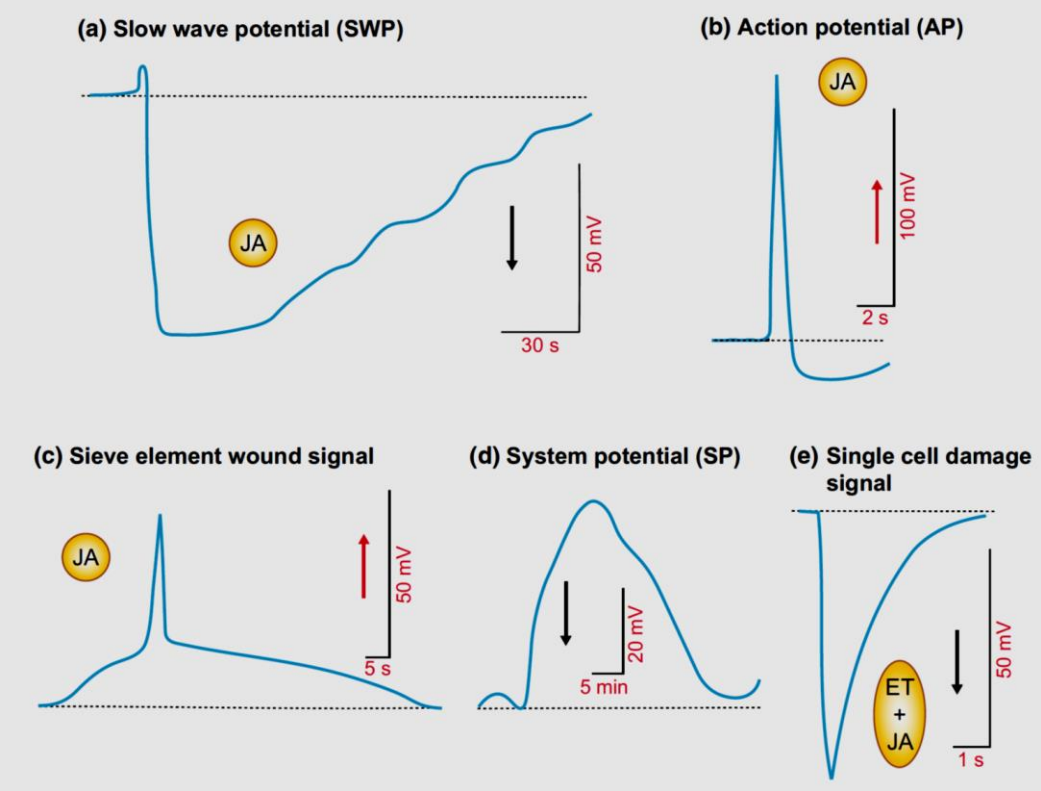

Figure 1.4 Environmental stimuli-induced electrical responses in plants. (a) Wound-induced slow wave potentials that trigger jasmonate synthesis. (b) Touch-triggered action potential from Venus flytrap (*Dionaea muscipula*). (c) Wound-induced depolarization in the sieve element. This signal is measured with living aphid electrode. (d) System potential measured with an extracellular electrode in a substomatal cavity. This is a hyperpolarization signal. (e) Single cell damage signal, single root cell was damaged in *Arabidopsis* triggering the short-distance depolarization. (Figure from Farmer et al., 2020).

Hydraulic signals: Most plant cells contain a large vacuole that helps to maintain turgor pressure in the cell. Turgor pressure pushes the cytoplasm and plasma membrane (protoplasm)

toward the cell wall. Loss of turgor pressure shrinks the cell volume and pulls the protoplasm backwards, detaching it from the cell wall (plasmolysis). At the tissue level, the xylem and phloem are two major vascular tissues transporting ions, nutrients, and water. The xylem is under tension caused by transpiration. The phloem has high turgor pressure to drive phloem sap movement in the source-to-sink direction. Wounding a leaf causes water loss from the wound and generates hydraulic pressure changes. In an experiment on the hypocotyl of cucumber (*Cucumis sativa*), cutting its root eliminated the xylem tension immediately and caused a regional membrane depolarization near the cut (Stahlberg and Cosgrove, 1997). Caterpillars (e.g. *Spodoptera littoralis*) cut leaf tissues repeatedly while feeding and this also causes systemic hydraulic signals in tomato plants (Malone et al., 1994). The wound-induced hydraulic signal is able to deliver solutes throughout the shoot as though by mass flow. Wound-induced mass flows through the xylem carry elicitors that cause long-distance wound signaling in tomatoes (Malone et al., 1994). In theory, hydraulic signal propagation does not depend on living cells and waves of pressure changes can pass through the xylem or even dead tissues. Thus, the velocity of the wound-induced hydraulic signal might be faster than the velocity of the wound-induced electrical signal (Vodeneev et al., 2012). Pressure changes in the xylem are often linked with the initiation of slow wave potential (Stahlberg and Cosgrove, 1996).

Wound-induced electrical signals are caused by the ion fluxes traveling across membranes which depolarize the electrical charges on the plasma membrane. A recent study finds pressure changes in *Arabidopsis* leaf petiole are triggered by insect damage (Kurenda et al., 2019). This deformation of the petiole is transient and coincident with the slow wave potential. The double mutant *glr3.3 glr3.6* has no leaf-to-leaf wound-response electrical signal and an attenuated force was measured from the petiole deformation. This showed that GLRs and wound-induced electrical signals were required for insect damage-induced turgor changes

leading to tissue deformation. Furthermore, *irregular xylem* (*irx*) mutants have abnormal xylem vessel development which affects the depolarization slope of the slow wave potential (Kurenda et al., 2019). That again highlights the importance of the xylem in wound-induced turgor-driven deformation. Also, wound-induced electrical signals might be closely linked to wound-induced hydraulic pressure changes.

In the 'squeeze cell' hypothesis (Farmer et al., 2014), wound-produced pressure changes travel beyond the xylem vessels to reach the contact cells and even other nearby cells. Because the cell wall is rigid, pressure changes in the xylem may influence the turgor pressure significantly in the neighboring cells. Wound-induced pressure changes and hydraulic signals travel through xylem vessels in the axial direction. Until these hydraulic signal reach the distal leaf, pressure changes are proposed to spread into the radial direction which then squeezes the xylem contact cells. This might be how wound-induced hydraulic signals and long-distance electrical signals activate jasmonate production in the distal leaf. Evidence consistent with this has come from more recent studies of the root. The cellulose biosynthesis mutant *korrigan1* (*kor1*) has enlarged cortex cells that mechanically squeeze inner root tissues and constitutively activate jasmonate production in the root (Mielke et al., 2021). Complementing *korrigan1* in the cortex perfectly restored auto-activated jasmonate signalling. Furthermore, hyperosmotic treatment decreases the turgor pressure in *kor1* cells and also abolishes the auto-activated jasmonate signaling. In contrast, hypoosmotic treatment induces jasmonate signalling predominantly in the endodermis and pericycle cells which are localized inner the cortex cells.

Chemical signals: Cell wall fragments derived from pectin and cellulose are known to be effective stimuli in activating the jasmonate response (Mielke and Gasperini, 2019). The mixture of chemicals released from a wound (e.g., damage-associated molecular patterns) is much more complex than just fragments of the cell wall (Choi and Klessig, 2016). A famous

theory about chemical elicitors is the "Ricca's Factor" theory (Ricca, 1926). In this theory, damage causes elicitor release through the xylem in *Mimosa pudica.* These unknown elicitors trigger the movement of distal leaves. Using a mathematical modeling procedure, chemical signal transport in the xylem was found to better explain elicitor movement than simple diffusion (Evans and Morris, 2017). Theoretically, simple diffusion has a velocity that is orders of magnitude smaller than the velocity of the electrical signal. Unlike simple diffusion, chemical elicitor transport by the mass flow in the xylem can likely recapitulate the velocity of electrical signal propagation. However, the diverse chemicals that might be released in a wound add huge complexity to searching for possible elicitors. For instance, glutamate is thought to be one possible chemical in wound-response signalling (Toyota et al., 2018). Depending on different aggressors, there are microbe-associated molecular patterns, nematode-associated molecular patterns, and endogenous damage-associated molecular patterns that can be potential elicitors (Choi and Klessig, 2016). Thus, the wound signal in the local, wounded leaf would be more complicated to study than in the distal leaf.

Organ mechanosensitivity

The plant has inducible defenses and the defense hormone jasmonate facilitates plant survival in a competitive environment. Hydraulic signals or osmotic changes which are not associated with wounding can activate jasmonate signaling in unwounded plants. For example, *Arabidopsis* treated with hypotonic solutions shows jasmonate-responsive gene induction in the root (Mielke et al., 2021). Non-wounding touch stimulation also triggers electrical signals in plants as in the example of touch-induced action potentials in the Venus flytrap (Sibaoka, 1966). It has been known for over a hundred years that two consecutive action potentials are required to induce the trap closure (Stuhlman and Darden, 1950; Forterre et al., 2005). The sensory hair is the most important mechanosensing tissue in the traps of Venus flytraps (Stuhlman and

Darden, 1950; Hedrich and Neher, 2018). The carnivorous Venus flytrap uses this mechanosensing mechanism to control the traps that capture insects for food. Furthermore, the mechanical force sensing machinery is different in another well-known mechanosensitive plant: *Mimosa pudica.* Leaf movement in *M. pudica* relies on specialized tissues named pulvini (Bose, 1927). Pulvinar motor cells have high levels of plasma membrane proton pumps that are thought to regulate leaf movements (Fleurat-Lessard et al., 1997). Leaflet closure and downward leaf movement would reduce the visibility to herbivores (Bose, 1926). Instead of capturing prey, *M. pudica* uses the mechanosensing mechanism to avoid aggressors.

Unlike action potentials in the Venus flytrap, many other touch-induced responses are relatively slow. Touch-induced growth inhibition (thigmomorphogenesis) occurs over a longer timescale than do electrical signals. For example, trees grow under in windy conditions develop thicker trunks and show less trunk elongation (Coutand et al., 2008). Also, repeated touch delays flowering time in *Arabidopsis* (Chehab et al., 2012). *Arabidopsis* that received repeated touch treatments over four weeks developed shorter inflorescence stems in comparison to the untouched control. This touch-induced morphological/developmental regulation is jasmonate-dependent. No detectable effect is found in the *aos* mutant which cannot produce jasmonate. Furthermore, OPDA Reductase 3 over-expressing plants accumulate more jasmonate than WT plants and have an even stronger phenotype in response to repeated touches (Chehab et al., 2012). These experiments, among others, showed that mechanical touch can induce jasmonate-dependent responses. Other experiments have been performed to test whether or not touch triggers jasmonate production. For example, the reporter *JAZ10 promoter::GUS* was used to address this question. Forceps-touched inflorescence stems showed clear GUS staining suggesting a local jasmonate response is induced with touch (Sehr et al., 2010). Furthermore, Chehab et al. (2012) analyzed jasmonate levels in the rosette leaves and inflorescence stem.

They found that endogenous jasmonate levels were elevated in the touched leaf and in the inflorescence stem. Although the inflorescence stem was not directly touched, jasmonate may move from the touched leaf or other signals may travel through vascular connections to activate jasmonate production in the inflorescence stem. Moreover, touch-induced jasmonate production boosts the jasmonate-dependent defense response: touched plants are better defended against fungus infection and caterpillar feeding (Chehab et al., 2012). Fungal lesion size and the caterpillar weight gain are both reduced in a jasmonate-dependent manner. Moreover, *aos* mutants do not show such jasmonate-dependent phenotypes in response to touch (Figure1.5 form Chehab et al., 2012).

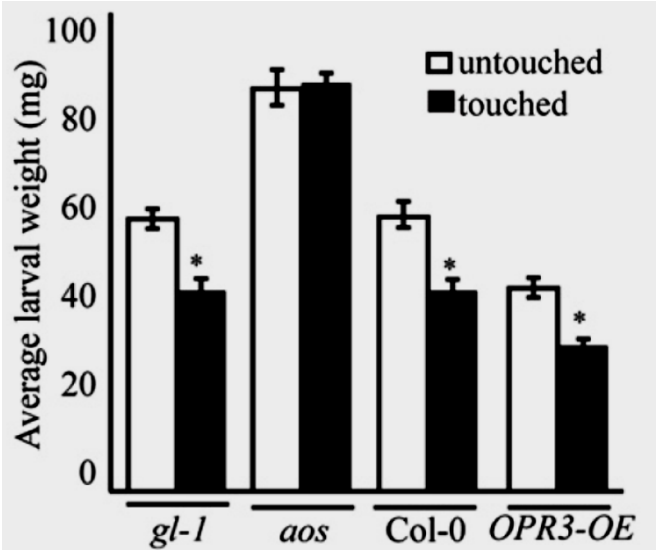

Figure 1.5 Repeatedly touched plants showed increased jasmonate-dependent resistance to *Trichoplusia ni*. Weights of T. ni. Larvae after 12 days of feeding on the indicated genotypes and treatments. Each genotype treatment was fed on by a newly hatched larvae. Mean ± SE of more than 15 larvae per genotype treatment are shown. Asterisk indicates significant difference (student *t* test, $P<0.0001$) (Figure from Chehab et al., 2012).

Thigmomorphogenesis, touch-induced growth regulation, depends on jasmonate signalling (Chehab et al., 2012). Activation of jasmonate biosynthesis requires mechanisms

underlying the touch response. Degli-Agosti (2014) recorded touch-induced action potential in *Arabidopsis* leaves (Figure 1.6). However, this work used invasive electrodes and this is a major concern since wounding *Arabidopsis* leaves also induces electrical signals. It has been proposed that the mechanosensitive channel MscS-LIKE 10 (MSL10) can be a component of wind force perception in *Arabidopsis* (Tran et al., 2021). Also, the *msl10* mutant shows a reduction in the wound-induced slow wave potential suggesting its role in the perception of mechanical wounding (Moe-Lange et al., 2021). Furthermore, vascular tissues appear to be essential to wound-induced mechanical signalling in *Arabidopsis* (Nguyen et al., 2018; Kurenda et al., 2019), but whether leaf vascular tissues within the bundle sheath are mechanosensitive to non-wounding stimulations remain largely unknown. The well-known PIEZO channels are the key to mechanical force sensing in animals (Coste et al., 2010; Coste et al., 2012; Kefauver et al., 2020). *Arabidopsis* PIEZO1 (*PZO1*) is highly expressed in the root vasculature, root hair, and root caps (Mousavi et al., 2021). *pzo1* mutant fail to penetrate hard media, suggesting that PIEZO1 is important in the mechanical force transduction in the root. However, a study focused on touch-response gene expression found that *PZO1* has no major role in touch-induced gene expression and thigmomorphogenesis in shoots (Darwish et al., 2022). Thigmomorphogenesis is almost abolished in the calmodulin-binding transcriptional activator *campta3* mutant. CAMPTA3 can bind directly to the promoter region of touch-responsive genes *in vitro*. The *campta1/2/3* triple mutant reduces both jasmonate-dependent and jasmonate-independent touch-response gene expression (Darwish et al., 2022). These findings indicate that CAMTA transcription factors play a key role in touch-induced transcriptional regulation and development.

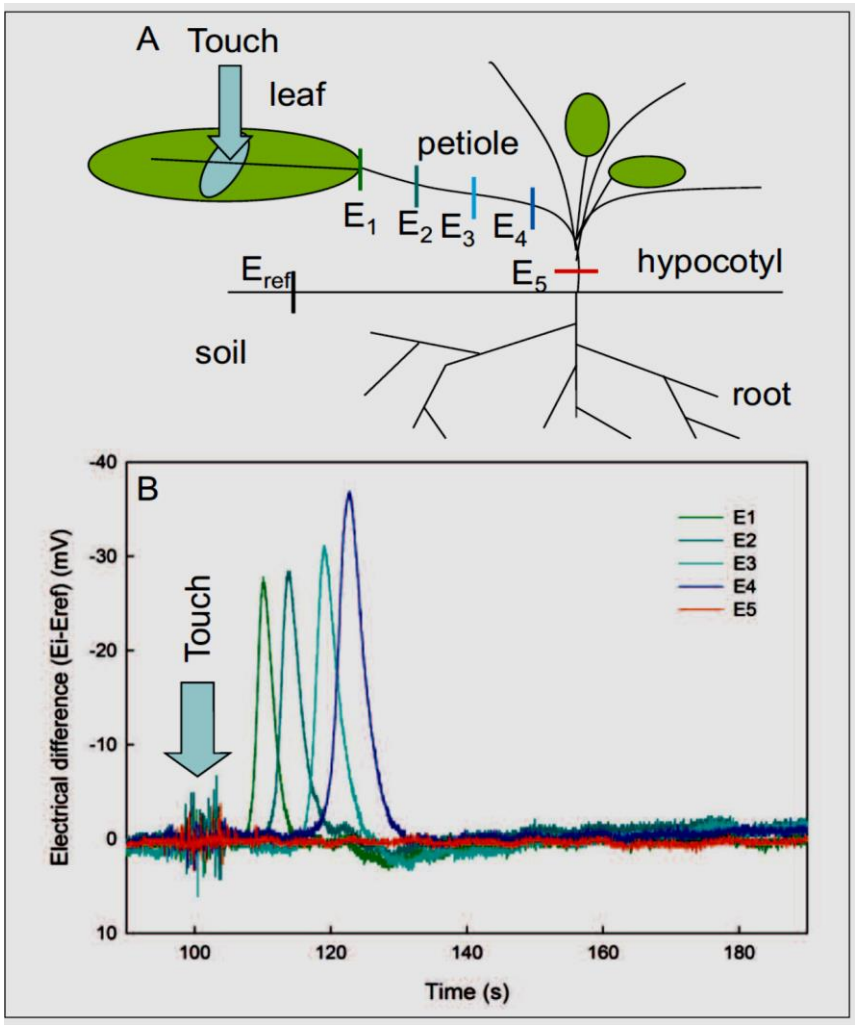

Figure 1.6 Touch-induced action potentials in *Arabidopsis*. Measured with dry (non-chloridized) silver electrodes. (A) 5 electrodes placed in an *Arabidopsis thaliana* plant. A paint brush (weight ~1-2 g, for ~ 2 s) stimulated the light blue zone as indicated. (B) Electrical potential differences of each electrode with respect to a silver reference electrode (Eref) inserted in the soil. Touch-stimulated depolarization is transmitted from E1 to E4 but not E5 (Figure from Degli-Agosti, 2014).

Tissue-specific touch responses: trichomes

Trichomes are three-dimensional hair-like structures on leaf surfaces. Unlike many hair cells in animals, trichomes are often rigid. As such, they provide a mechanical barrier that

protects against herbivores. Although stiffness limits movement, the trichome can, by acting like a lever, concentrate mechanical compressions and transduce them to the adjacent skirt cells (Zhou et al., 2017). A computational model suggests axial and lateral compressive forces would increase the forces in different parts of the trichome structure. Bending and pulling a single trichome triggers cytosolic calcium oscillations and apoplastic pH changes in the adjacent skirt cells. Mechanical stimulation-induced cytosolic calcium increases in and around trichomes was further investigated in a recent study (Figure 1.7 form Matsumura et al., 2022). In that study, the GFP-based, cytosolic calcium reporter GCaMP3 is used, providing good visual resolution. Brushing triggered cytosolic calcium increases in the area surrounding the trichome.

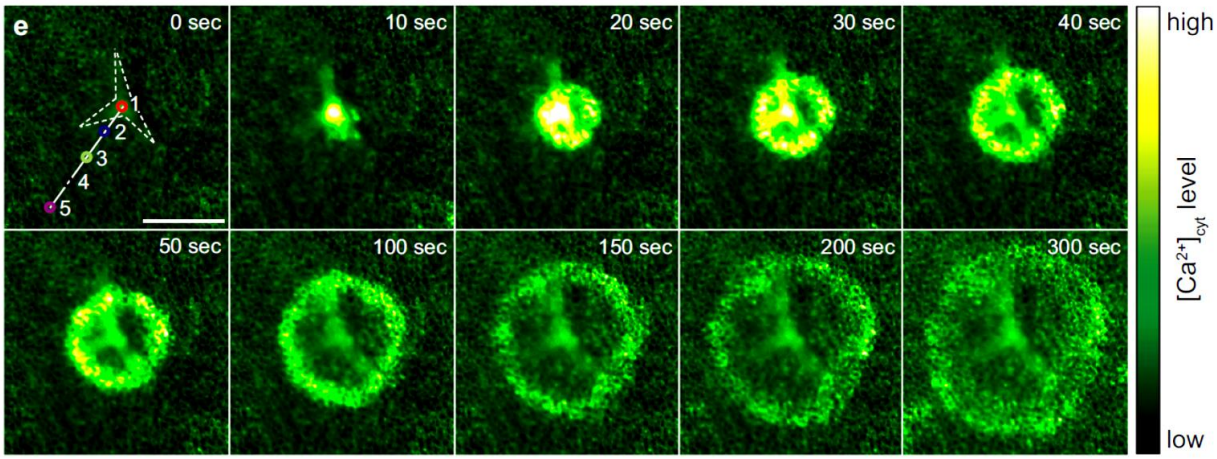

Figure 1.7 Touch-triggered cytosolic calcium signal surrounding the trichome. Calcium imaging monitored with *35Spro::GCaMP3* in a 2-week-old *Arabidopsis* (Col-0). A trichome was pushed with a silver chloride wire (Scale bar = 0.2 mm). Mechanostimulation-induced calcium waves propagated from the stimulated trichome (dashed line) (Figure from Matsumura et al., 2022).

A ring-shaped calcium wave propagates at a velocity of 1 µm per second away from the brushed trichome and skirt cells (Matsumura et al., 2022). This brushing-triggered cytosolic calcium wave was attenuated in the *glabrous1* mutant (*gl1*). *gl1* lacks an essential transcription

factor, and has almost no trichomes on the leaf surface (Oppenheimer et al., 1991; Xia et al., 2010). Moreover, 70% of brushing-induced gene expression and touch-induced immunity were both compromised in the *gl1* mutant, which indicates trichome is important to mechanosensation (Matsumura et al., 2022). However, an earlier study found that repeated leaf bending increased jasmonate-dependent defense and that this was not attenuated in *gl1* (Chehab et al., 2012). These two studies therefore found distinct touch-induced immunity outputs in the same *gl1* mutant (Chehab et al., 2012; Matsumura et al., 2022). This suggests that this may be due to the differences in mechanical stimulation methods. In fact, each study employs different methods which may stimulate different cell types and this may cause different effects on immunity. That raises a common problem in this field: a simple, robust, and reproducible method is needed. Thus, we developed a new mechanostimulation method to improve reproducibility and quantitation.

In the thesis I used two very different approaches to activate the jasmonate pathway: crush wounding of large leaf areas and gentle non-wounding mechanostimulation of small leaf areas. Electrical signals produced following large wounds are well characterized. However, mechanostimulation-induced electrical signals are poorly understood in terms of their architectures and abilities to stimulate jasmonate synthesis.The first part of the thesis employed crush wounding. The second part of the thesis studied touch-induced electrical signals. This thesis research was based on the use of *Arabidopsis thaliana*. Several experiments on *Mimosa pudica* were also performed.

Goals of the thesis:

- Deepen our understanding of wound-induced growth inhibition by identifying jasmonate biosynthesis enzymes (lipozygenases) necessary for this response.
- Use gain-of-function cation channel mutants to activate growth inhibition in the absence of wounding.
- Develop and optimize a new mechanostimulation method to improve the quantitation and reproducibility of experiments on touch responses.
- Characterize electrical signals produced in response to single mechanostimulations.
- Investigate the role of vascular tissues in touch-response electrical signalling.
- Identify how mechanostimulation activates jasmonate precursor biosynthesis to induce jasmonate signalling.
- Examine the necessity of proton pumps and ion channels in the mechanostimulation-induced electrical signal.

Chapter 2: JASMONATE PRECURSOR BIOSYNTHETIC ENZYMES LOX3 AND LOX4 CONTROL WOUND-RESPONSE GROWTH RESTRICTION

Published in Yang et al. (2020) Plant physiology 184, 1172-1180.

Introduction:

Jasmonate is the major hormone that activates defense mechanisms in response to wounding and helps plants fight against aggressors such as herbivores. An early step in jasmonate synthesis involves linolenic acid oxygenation by 13-lipoxygenases (13-LOXs). *Arabidopsis thaliana* has four 13-LOXs that initiate jasmonate biosynthesis. This is a critical and potentially regulatory step in jasmonate synthesis. All four 13-LOXs contribute to rapid jasmonate synthesis after leaf wounding (Chauvin et al., 2013). Of them, *LOX6* is the main contributor which produces jasmonate in the distal leaf after wounding (Gasperini et al. 2015). *LOX2* is important for the production of high levels of jasmonate in the proximity of a wound (Glauser et al. 2009). While *LOX3* and *LOX4* have a minor role in rapid jasmonate induction following leaf wounding, both are crucial for male fertility in Arabidopsis (Chauvin et al., 2013; Caldelari et al. 2011).

The activation of defenses often comes at a cost of reduction in plant growth. Repeatedly activating the jasmonate pathway by wounding or touching causes rosette growth restriction (Yan et al. 2007; Chehab et al., 2012). But how jasmonate-activated defense and growth reduction are regulated by 13-LOXs is not yet clear. The *A. thaliana fatty acid oxygenation up-regulated 2* (*fou2*) mutant was identified due to its enhanced 13-LOX activity, higher basal jasmonate levels, and a wound mimic phenotype i.e. stunted growth with short petioles (Bonaventure et al., 2007). This mutant increases the activity of the non-selective voltage-gated vacuolar cation channel TPC1 (Bonaventure et al., 2007; Beyhl et al., 2009; Lenglet et al.,

2017). Employing a series of 13-LOX mutants, I successfully identified the LOXs that play a major role in wound-induced growth regulation. In order to identify cell types that contribute to wound-response growth inhibition we expressed derivatives of the *fou2* cDNA in distinct cell niches. We found that the phloem region is essential for the growth reducing effects of *fou2*. These findings were published in Yang et al. (2020).

My contribution to Yang et al. (2020) Plant physiology 184, 1172-1180. I produced main figures 2, 3, 4, 5 and supplemental figures 1, 2B, and 3.

Jasmonate Precursor Biosynthetic Enzymes LOX3 and LOX4 Control Wound-Response Growth Restriction[1][OPEN]

Tsu-Hao Yang,[a,2] Aurore Lenglet-Hilfiker,[a,2] Stéphanie Stolz,[a] Gaëtan Glauser,[b] and Edward E. Farmer[a,3,4]

[a]Department of Plant Molecular Biology, University of Lausanne, Lausanne, Switzerland 1015
[b]Neuchâtel Platform of Analytical Chemistry, University of Neuchâtel, Neuchâtel, Switzerland 2000

ORCID IDs: 0000-0002-9414-4632 (T.-H.Y.); 0000-0002-0983-8614 (G.G.); 0000-0002-6572-5024 (E.E.F.).

Wound-response plant growth restriction requires the synthesis of potent mediators called jasmonates (JAs). Four 13-lipoxygenases (13-LOXs) produce JA precursors in Arabidopsis (*Arabidopsis thaliana*) leaves, but the 13-LOXs responsible for growth restriction have not yet been identified. Through loss-of-function genetic analyses, we identified LOX3 and LOX4 as the principal 13-LOXs responsible for vegetative growth restriction after repetitive wounding. Additional genetic studies were carried out in the gain-of-function *fatty acid oxygenation 2* (*fou2*) mutant that, even when undamaged, shows JA-dependent leaf growth restriction. The *fou2 lox3 lox4* triple mutant suppressed the *fou2* JA-dependent growth phenotype, confirming that LOX3 and LOX4 function in leaf growth restriction. The *fou2* mutation affects the TWO PORE CHANNEL1 (TPC1) ion channel. Additional genetic approaches based on this gene were used to further investigate LOX3 function in relation to leaf growth. To activate LOX3-dependent JA production in unwounded plants, we employed hyperactive TPC1 variants. Expression of the *TPC1ΔCa$_i$* variant in phloem companion cells caused strongly reduced rosette growth in the absence of wounding. Summarizing, in parallel to their established roles in male reproductive development in Arabidopsis, LOX3 and LOX4 control leaf growth rates after wounding. The process of wound-response growth restriction can be recapitulated in unwounded plants when the LOX3 pathway is activated genetically using a hyperactive vacuolar cation channel.

Herbivore damage can lead to spectacular changes in the growth of long-lived plants. Similarly, long-term plant growth can be modified strikingly as a result of repetitive leaf wounding inflicted by skilled bonsai gardeners. These effects are characterized by altered vegetative growth often leading to stunted plants. In the laboratory, and over briefer timescales, comparable effects on plant growth can be observed in short-lived species including Arabidopsis (*Arabidopsis thaliana*). For example, when the rosettes of this species are subject to repetitive wounds over a period of ~3 weeks, the newly formed leaves they produce are smaller with shortened petioles compared to those on unwounded plants (Yan et al., 2007). These effects on growth were found to depend on the production of the lipidic regulator jasmonate (JA). Specifically, leaf and petiole growth restriction was strongly attenuated in the JA-synthesis mutant *allene oxide synthase* (*aos*; Yan et al., 2007) and in a JA-signaling mutant (Zhang and Turner, 2008). Therefore, a key function of JA pathway-activating signals produced in damaged organs is to travel to apical tissues to reprogram future growth, allowing plants to optimize their defense strategies (Huot et al., 2014; Guo et al., 2018; Ballaré and Austin, 2019; Fernández-Milmanda et al., 2020). Importantly, the activation of JA signaling after wounding requires the de novo synthesis of JA (Browse, 2009; Chini et al., 2016; Howe et al., 2018). Specifically, JA biosynthesis in the aerial tissues of Arabidopsis depends on four distinct 13-lipoxygenases (13-LOXs), namely LOX2, LOX3, LOX4, and LOX6. Each of these 13-LOXs can produce JA precursors in leaves and each LOX appears to contribute in a different way to defense gene expression (Chauvin et al., 2013, 2016; Grebner et al., 2013). However, unlike for reproductive development, the contributions of individual 13-LOXs to vegetative growth modulation in Arabidopsis remains poorly understood.

Like wound-response leaf growth restriction (Zhang and Turner, 2008), Arabidopsis reproductive development requires the *CORONATINE-INSENSITIVE1* gene (Xie et al., 1998). *CORONATINE-INSENSITIVE1* encodes the receptor for jasmonoyl-Ile (JA-Ile; Sheard et al., 2010; Howe et al., 2018) and 12-hydroxy-JA-Ile (Jimenez-Aleman et al., 2019; Poudel et al., 2019), a compound implicated, together with JA-Ile, in the control of wound-induced growth restriction (Poudel et al., 2019). In terms of JA biosynthetic enzymes, a LOX was found to be essential

[1]This work was supported by the Swiss National Science Foundation (grants nos. 31003A–155960 and 31003A–175566/1 to E.E.F.).
[2]These authors contributed equally to this article.
[3]Author for contact: edward.farmer@unil.ch.
[4]Senior author.
The author responsible for distribution of materials integral to the findings presented in this article in accordance with the policy described in the Instructions for Authors (www.plantphysiol.org) is: Edward E. Farmer (edward.farmer@unil.ch).
T-H.Y., A.L-H., and S.S. performed genetics experiments; G.G. performed jasmonate analyses; T-H.Y., A.L-H., and E.E.F. analyzed data; E.E.F. wrote the article.
[OPEN]Articles can be viewed without a subscription.
www.plantphysiol.org/cgi/doi/10.1104/pp.20.00471

for male flower formation in maize (Acosta et al., 2009), Subsequently, LOX3 and LOX4 were identified as the 13-LOXs that produce the JA precursors necessary for normal reproductive development in Arabidopsis (Caldelari et al., 2011). That is, although all four Arabidopsis 13-LOXs produce precursors for JA synthesis, LOX2 and LOX6 cannot replace LOX3 and LOX4 to maintain male fertility. The study of the roles of JA in reproductive development has been extended to the cellular level, and the cells in floral organs that are necessary for JA signaling leading to fertility have been identified (Jewell and Browse, 2016). By contrast, the roles of 13-LOXs in vegetative development in Arabidopsis remain poorly understood. To our knowledge, no specific 13-LOXs have an attributed role in any aspect of leaf growth. We therefore set out to address this gap in our knowledge. We used a collection of reduced-function *lox* single and multiple mutants. In each case, two alleles for each LOX were previously characterized biochemically for their ability to make JAs in wounded leaves (Caldelari et al., 2011; Chauvin et al., 2013). One of each allele was used in this study, allowing the individual inputs of each LOX on rosette growth to be assessed genetically.

To complement loss-of-function studies and to further investigate the activity of 13-LOXs in rosette growth restriction, we also took an opposite, gain-of-function approach. Here, we attempted to activate growth-regulating 13-LOXs in Arabidopsis in the absence of wounding. Our strategy was based on the *fatty acid oxygenation upregulated2* (*fou2*) mutant (Bonaventure et al., 2007a). At the molecular level, the *fou2* mutation affects TWO-PORE CHANNEL1 (Peiter et al., 2005; Hedrich et al., 2018; Pottosin and Dobrovinskaya, 2018), increasing the open-probability of this vacuolar cation channel (Bonaventure et al., 2007a; Beyhl et al., 2009; Lenglet et al., 2017). In the undamaged state, adult-phase *fou2* leaves have elevated levels of JA compared to the wild type, and the *fou2* transcriptome indicates high JA pathway activity (Bonaventure et al., 2007b). Relevant to that study is the fact that *fou2* has small, epinastic leaves with short petioles. Generation of *fou2 aos* double mutants that cannot produce JA is known to suppress much of the effect of *fou2* on leaf growth, although this double mutant does not completely rescue the leaf epinasty that is typical of *fou2* (Bonaventure et al., 2007b). We investigated whether *fou2* complementary DNA (cDNA; $TPC1^{D454N}$) could be used to activate JA signaling leading to rosette growth restriction. The results reveal roles for specific 13-LOXs in leaf growth and also identify a cell population likely to play critical roles in wound-response vegetative growth plasticity.

RESULTS

Damaged Plants Are Smaller, with Greater Defense Capabilities than Their Undamaged Counterparts

Wild-type plants that had been fed on by *Spodoptera littoralis* larvae for 11 d under controlled conditions showed obvious signs of damage and their rosettes appeared to be smaller than the undamaged wild type (Fig. 1A). However, each leaf showed variable signs of damage, and a more controlled wounding protocol was therefore employed. We used serial mechanical wounding to better control for the effects of leaf damage and to test whether plants that had been damaged were more resistant to herbivores. Starting with 2-week-old plants, developing leaves were wounded at 3-d intervals in such a way that leaf 1 was damaged first by crushing 50% of the lamina, then leaf 2, and so forth. In total, seven leaves were wounded. As a control, plants were handled identically but not wounded. At the end of the treatment, and 3 d after the last of seven wounds (or handling, as was the case of the control unwounded plants), wounded wild-type rosettes were smaller than

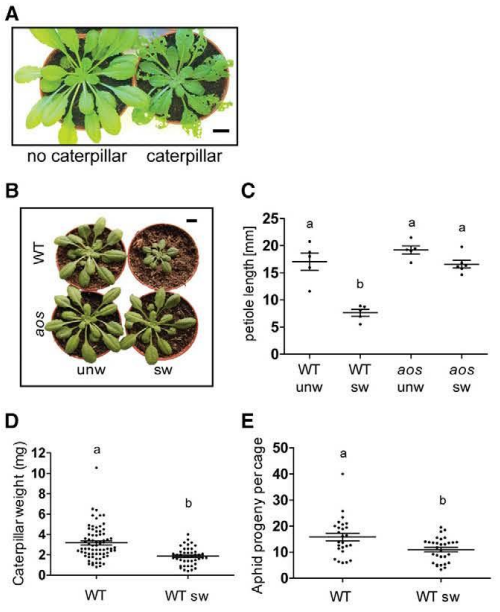

Figure 1. Enhanced defense in serially wounded plants. A, Rosette morphology of undamaged wild-type (WT) plant and plant after 11 d of *S. littoralis* feeding. Scale bar = 1 cm. B, Rosette morphology of wild type and *aos* after serial wounding. The background was digitally rendered in white in the image. unw, Unwounded; sw, serially wounded. Scale bar = 1 cm. C, Petiole length after serial wounding in wild type and *aos* mutant. The mean petiole length of leaves number 6, 7, and 8 in each plant is counted as one biological replicate. Bars represent the means (±SEM), n = 5 to 6 D, Biomass of *S. littoralis* after 11 d feeding on unwounded wild type or serially wounded wild type (WT sw). Bars are means (±SEM) of three combined experiments. Wild type, n = 73; wild type sw, n = 44. E, Reproductive success of cabbage aphids (*B. brassicae*) on unwounded or serially wounded plants. Aphid success was monitored 14 d after placing nymphs on plants. Bars are means (±SEM) of three combined experiments; wild type, n = 26; wild type sw, n = 30. Lowercase letters indicate significant difference as determined by Tukey's HSD test ($P < 0.001$).

those of unwounded plants (Fig. 1B) and showed reduced petiole extension (Fig. 1C). The effects of wounding on petiole growth were reduced in the *aos* mutant relative to the wild type (Fig. 1, B and C). Reduced growth due to JA pathway activity has been linked to increased levels of defense (Huot et al., 2014; Guo et al., 2018). We compared herbivore performance on unwounded plants and plants that had been mechanically wounded in bioassays using the lepidopteran herbivore *S. littoralis* and the cabbage aphid *Brevicoryne brassicae*. Weight gain by *S. littoralis* was reduced on the prewounded plants compared to undamaged plants (Fig. 1D). Similarly, aphid fecundity, as judged by the production of adult aphids, was reduced on the prewounded plants relative to the undamaged plants (Fig. 1E).

Identification of 13-LOXs that Operate in Wound-Activated Rosette Growth Responses

Because wound-response growth restriction is JA-dependent and is associated with decreased defense against herbivores, we sought to identify the branch of the JA synthesis pathway necessary for this process. Four 13-LOXs contribute to JA production in wounded leaves (Chauvin et al., 2013; 2016). The effects of serial wounding on growth restriction in single *lox* mutants for each of these genes was tested. Figure 2, A and B, shows that the wild type and all single *lox* mutants displayed wound-response growth restriction. Next, *lox* triple mutants (Chauvin et al., 2013) were wounded repetitively. Each of these lines retains a single functional JA precursor-producing LOX. When subjected to serial wounding, the *lox2 lox4 lox6* mutant displayed growth restriction similar to the wild type (Fig. 2, C and D), whereas the other triple mutants showed less wound-response growth restriction relative to the wild type. In the triple mutants, mass reduction in response to wounding was lowest in *lox2 lox3 lox4*, followed by *lox3 lox4 lox6*, then *lox2 lox3 lox6*. The *lox* quadruple mutant that cannot produce JA (Chauvin et al., 2013) showed relatively little wound-response growth restriction. A final series of experiments compared the

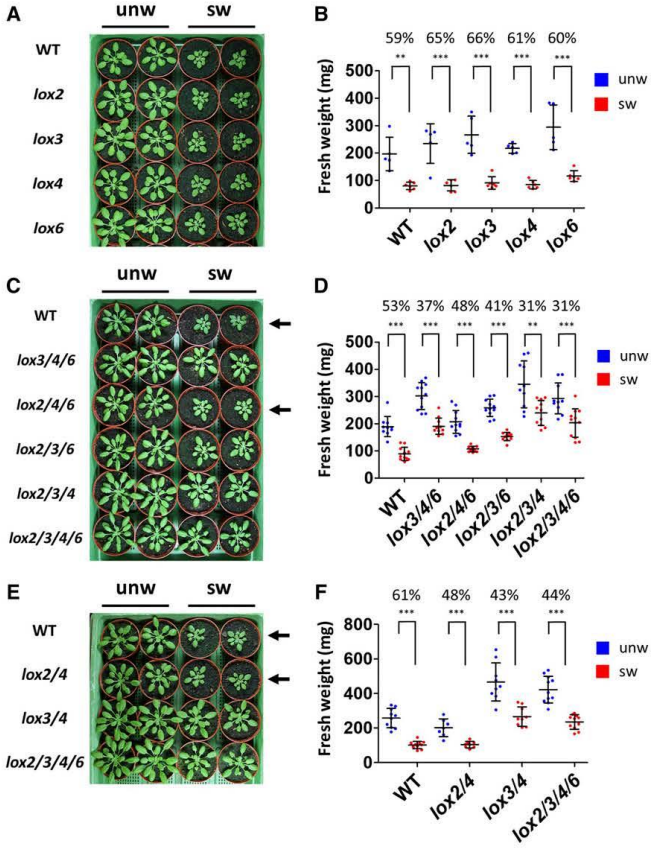

Figure 2. Effect of serial leaf wounding on rosette growth of *lox* mutants. Rosette morphology of unwounded and serially wounded wild type (WT) and *lox* mutants. unw, Unwounded; sw, serially wounded. In each case, two representative plants are shown. The ratios (percent) represent fresh weight reduction resulted by wounding. A, Rosettes of wild type and *lox* single mutants. B, Fresh weights of unwounded and serially wounded wild type and *lox* single mutants. $n = 5$ to 6. C, Rosette morphology of wild type, *lox* triple mutants, and the *lox* quadruple mutant. D, Fresh weights of unwounded and serially wounded plants. $n \geq 10$. E, Rosette morphology of wild type, *lox* double mutants, and the *lox* quadruple mutant. F, Fresh weights of unwounded and serially wounded plants. $n \geq 7$. Arrows in C and E indicate genotypes showing strong growth restriction after wounding. Bars represent the mean of fresh weight (±SD). Asterisks indicate significant difference as determined by Student *t* test (**$P < 0.01$ and ***$P < 0.001$).

growth of the *lox2 lox4* and *lox3 lox4* double mutants in response to serial wounding. In these assays, the *lox3 lox4* double mutant behaved like the quadruple *lox* mutant. The *lox2 lox4* double mutant showed slightly stronger growth restriction than *lox3 lox4* (Fig. 2, E and F). Comparison of fresh weights of unwounded plants from the same dataset (Supplemental Fig. S1) showed that the fresh masses of the quadruple and triple *lox* mutants and the *lox3 lox4* double mutant were greater than the wild type. In summary, these results based on biochemically and genetically verified loss-of-function *lox* alleles show that LOX3, and, to a lesser extent, LOX4, produce the majority of JA precursors necessary for wound-response rosette growth restriction.

The *fou2* Phenotype Is Suppressed When *LOX3* and *LOX4* Are Mutated

A mutant that affects petiole length is *fou2*, a plant gene that overproduces JA in the adult phase (Bonaventure et al., 2007a). JA production in *fou2* is necessary for the shorter-than-wild-type petioles typical of this mutant, and petiole length was restored in *fou2 aos* double mutants that cannot produce JA (Bonaventure et al., 2007b). Based on the results of the serial wounding assays shown in Figure 2, we therefore generated *fou2 lox3 lox4* triple mutants. We found that the strong JA-dependent phenotype of *fou2* was suppressed in the *fou2 lox3 lox4* triple mutant (Fig. 3). The level of suppression of the *fou2* phenotype was similar to that reported for the *fou2 aos* double mutant (Bonaventure et al., 2007a), which was used as a control in these experiments. These results further confirm the roles for LOX3 and LOX4 in JA-dependent growth control and raise the intriguing possibility that stunted, bonsai-like wound phenotypes could be recapitulated through the genetic activation of 13-LOXs in the absence of wounding. To do this, we chose LOX3 because it had the strongest effect among the four 13-LOXs on wound-response growth restriction. The xylem and phloem were chosen as target tissues because (1) the *LOX3* promoter activity domain spans both these regions (Chauvin et al., 2016), and (2) both the phloem and xylem are known to play critical roles in leaf-to-leaf wound signaling (Nguyen et al., 2018). Methods to activate JA production via LOX3, and therefore mimic wound-response growth restriction, were developed taking advantage of the gain-of-function nature of the *fou2* mutation.

Hyperactive TPC1 Stimulates LOX3-Dependent Growth Restriction

In *fou2*, the Asp 454 to Asn (D454N) mutation in TWO-PORE CHANNEL1 (TPC1^{D454N}) increases the open probability of this channel (Bonaventure et al., 2007a; Beyhl et al., 2009). This is because Asp 454, along with other acidic residues in TPC1, binds inhibitory Ca^{2+} in

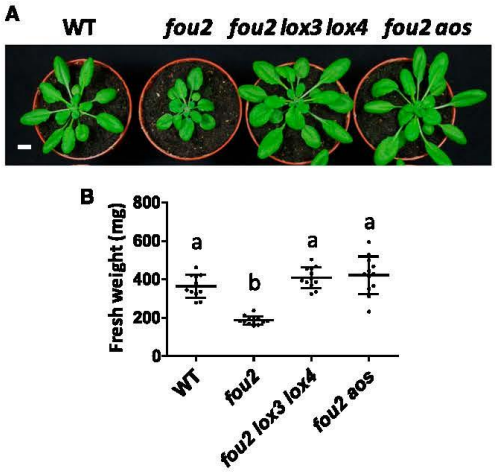

Figure 3. Mutations in *LOX3* and *LOX4* genes largely suppress the *fou2* phenotype. Plants were grown for 5 weeks in short-day conditions. A, Rosette morphology of wild type (WT), *fou2*, *fou2 lox3 lox4*, and *fou2 aos*. Scale bar = 1 cm. The phenotype of the *fou2 aos* mutant was as reported in Bonaventure et al. (2007b). B, Fresh weights of wild type, *fou2*, *fou2 lox3 lox4*, and *fou2 aos*. Data are means (±SD), $n = 11$ to 12. Lowercase letters indicate statistically significant differences as determined by Tukey's HSD test ($P < 0.05$).

the vacuolar lumen, changing the voltage sensitivity of this voltage-gated cation channel (Guo et al., 2017). However, the *fou2* mutation is semidominant, and wild-type *TPC1* alleles inhibit the effects of TPC1^{D454N} (Bonaventure et al., 2007a). In preliminary experiments to activate JA-dependent growth phenotypes with TPC1^{D454N}, and to overcome its semidominance, *TPC1^{D454N}* was expressed in the *tpc1-2* null background (Peiter et al., 2005), with expression in the phloem driven by the *SUC TRANSPORTER2* (*SUC2*) promoter (Truernit and Sauer, 1995), with expression in xylem contact cells driven by the *LIPOXYGENASE6* (*LOX6*) promoter (Chauvin et al., 2013), or with expression in the bundle sheath driven by the *SCARECROW* (*SCR*) promoter (Wysocka-Diller et al., 2000). The 5-week-old *SCRpro::TPC1^{D454N}* plants (Supplemental Fig. S2A) did not display a *fou2*-like phenotype, and the *LOX6pro::TPC1^{D454N}* plants (Supplemental Fig. S2B) displayed only a slight *fou2*-like phenotype at this stage. By contrast, *SUC2pro::TPC1^{D454N}* expressed in *tpc1-2* phenocopied *fou2* (Supplemental Fig. S2C), including causing elevated expression of the JA-signaling marker *JAZ10* (Supplemental Fig. S2D). As expected, when the wild-type *TPC1* sequence was expressed under the *SUC2* promoter in the *fou2* background, the *TPC1* cDNA partially reverted the *fou2* phenotype toward that of the wild type (Supplemental Fig. S2E) and suppressed the elevated levels of *JAZ10* transcript detected in *fou2* (Supplemental Fig. S2F).

These initial findings raised the possibility that JA precursor production by LOX3 could be activated through the expression of hyperactive TPC1 variants, provided that these variants had sufficient genetic penetrance to overcome the presence of wild-type *TPC1* alleles. The single D454N mutation in TPC1^{D454N} reduces Ca^{2+} binding to a vacuole lumen-located inhibitory sensor (Beyhl et al., 2009). More recently, and together with Asp 454, the residues Asp 240 and Glu 528 were also found to participate in channel-inhibiting Ca^{2+} coordination. The TPC1 ^{D240A,D454A,E528A} variant, termed "TPC1ΔCa$_i$," largely removes luminal calcium inhibition without affecting the cation permeation specificity observed in the wild-type channel (Guo et al., 2017). We reasoned that hyperactive TPC1ΔCa$_i$ might display sufficient genetic penetrance to be employed in backgrounds harboring wild-type *TPC1* alleles to activate growth restriction through LOX3. Experiments were thus designed to test this.

Based on preliminary results (Supplemental Fig. S2), *TPC1ΔCa$_i$* was expressed in the phloem. For this, *SUC2*pro::*TPC1ΔCa$_i$* was transformed into the wild

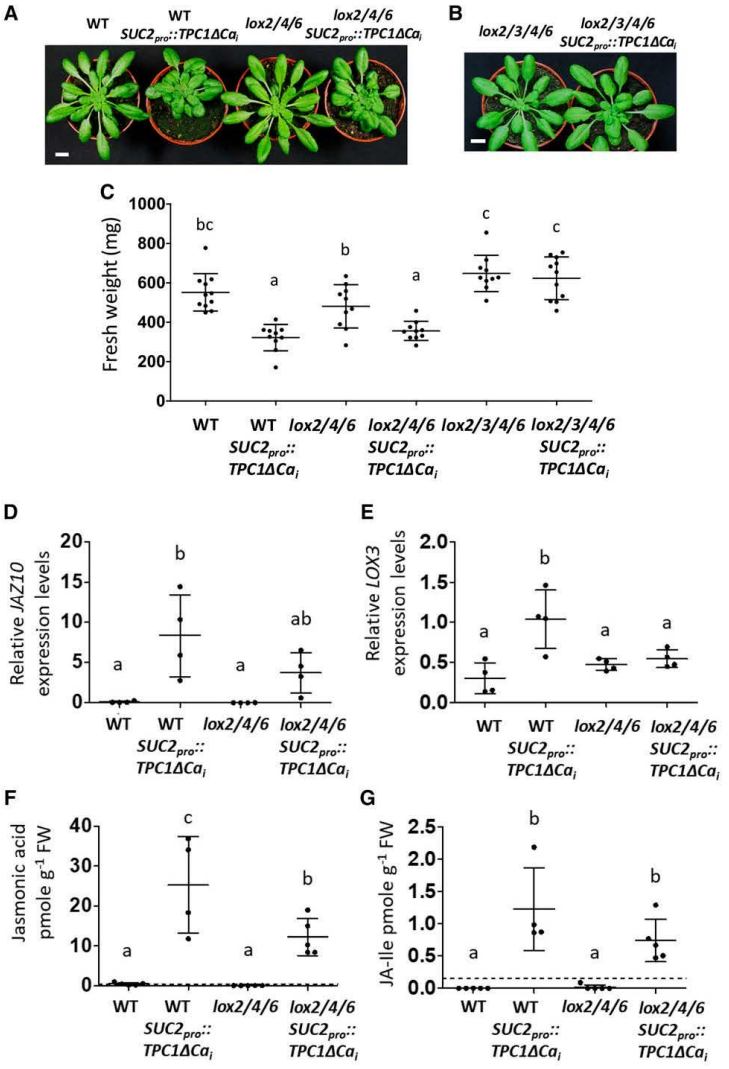

Figure 4. Expressing *TPC1ΔCa$_i$* in phloem companion cells stimulates LOX3-dependent growth restriction. All plants were 5 weeks old. A, Rosette morphology of wild type (WT), the wild type expressing *SUC2$_{pro}$::TPC1ΔCa$_i$*, *lox2/4/6*, and *lox2/4/6*-expressing *SUC2$_{pro}$::TPC1ΔCa$_i$*. B, Rosette morphologies of the *lox* quadruple mutant and the same plant transformed with *SUC2$_{pro}$::TPC1ΔCa$_i$*. Scale bars = 1 cm. C, Fresh weights of wild type, the wild type expressing *SUC2$_{pro}$::TPC1ΔCa$_i$*, *lox2/4/6*, *lox2/4/6* expressing *SUC2$_{pro}$::TPC1ΔCa$_i$*, *lox* quadruple mutant, and *lox* quadruple mutant expressing *SUC2$_{pro}$::TPC1ΔCa$_i$*. D, *JAZ10* transcript levels relative to reference gene *UBC21*. E, *LOX3* transcript levels relative to *UBC21*. F, JA levels in the leaves of the wild type, the wild type expressing *SUC2$_{pro}$::TPC1ΔCa$_i$*, *lox2/4/6*, and *lox2/4/6* expressing *SUC2$_{pro}$::TPC1ΔCa$_i$*. The dashed horizontal line shows the limit of quantification. G, JA-Ile levels in the leaves of the wild type, the wild type expressing *SUC2$_{pro}$::TPC1ΔCa$_i$*, *lox2/4/6*, and *lox2/4/6* expressing *SUC2$_{pro}$::TPC1ΔCa$_i$*. The dashed horizontal line shows the limit of quantification. Data are means (±SD); $n = 10$ to 11 (C), $n = 4$ (D and E), and $n = 4$ to 5 (F and G). Lowercase letters indicate statistically significant differences as determined by Tukey's HSD test ($P < 0.05$).

type and into the *lox2 lox4 lox6* triple mutant that retains *LOX3* as the only functional 13-LOX gene. Both the wild type and the *lox2 lox4 lox6* lines expressing *SUC2*-pro::*TPC1ΔCa*$_i$ displayed *fou2*-like phenotypes (Fig. 4A; Supplemental Fig. S3). As a control, *SUC2*pro::*TPC1ΔCa*$_i$ was transformed into the *lox2 lox3 lox4 lox6* quadruple mutant that lacks the ability to make JA. The transformed quadruple mutant displayed a weak phenotype at the rosette center (Fig. 4B; Supplemental Fig. S3), consistent with the fact that part of the effect of *fou2* on leaf growth is JA-independent (Bonaventure et al., 2007a, 2007b). Further analyses of the transformants revealed that *TPC1ΔCa*$_i$ expression in the wild type and in *lox2 lox 4 lox6* reduced rosette fresh weight, but this was not significantly affected in the *lox* quadruple mutant that does not produce JA (Fig. 4C). *JAZ10* levels were found to be elevated in wild type and in *lox2 lox4 lox6* triple mutant plants expressing *SUC2*pro::*TPC1ΔCa*$_i$ (Fig. 4D). The relative levels of the LOX3 mRNA were also measured in the wild type, the wild type expressing *TPC1ΔCa*$_i$, and in the *lox2 lox4 lox6* triple mutant without and with the *TPC1ΔCa*$_i$ transgene. Whereas expression of *TPC1ΔCa*$_i$ in the wild type increased *LOX3* mRNA levels ~3-fold, there was no corresponding increase in *LOX3* mRNA level in the triple-mutant background (Fig. 4E).

Finally, to investigate whether expression of *SUC2*-pro::*TPC1ΔCa*$_i$ in the wild type and in the *lox2 lox4 lox6* triple mutant altered the levels of jasmonic acid and JA-Ile in leaves, the levels of these molecules were measured. Increases in both jasmonic acid (Fig. 4F) and JA-Ile (Fig. 4G) were detected in both genetic backgrounds expressing *TPC1ΔCa*$_i$ relative to the control genetic backgrounds.

DISCUSSION

JA-controlled leaf growth restriction is likely to be widespread in nature and can be activated by repetitive wounding (Yan et al., 2007) or by repeated mechanostimulation (Chehab et al., 2012). This process is, at least in part, a consequence of repression of cell division (Noir et al., 2013) and is controlled by MYC transcription factors (Major et al., 2017). Although growth and defense can be at least partially uncoupled (Campos et al., 2016), the ability of plants to channel resources from growth to defense is likely to have adaptive value (Huot et al., 2014; Guo et al., 2018). Consistent with this, we found that repetitively wounded plants slowed weight gain in a lepidopteran, and also limited reproduction in a hemipteran, herbivore. The fact that repetitive wounding affected plant growth and that this correlated with resistance to insects prompted us to investigate which branch of the JA biosynthesis pathway operates to control post-wounding leaf growth.

A Role for LOX3 and LOX4 in Wound-Response Growth

Here, we were able to identify LOX3 and LOX4 as the key 13-LOXs that act, through the production of JA precursors, in wound-response leaf growth restriction. We also noted that multiple *lox* mutations generally caused an increase in the fresh mass of unwounded plants. This was expected because *aos* mutants in JA biosynthesis have higher dry masses than the wild type (Yan et al., 2007). LOX3 and LOX4 are known to contribute to JA production in response to osmotic stress (Grebner et al., 2013) and after leaf wounding (Chauvin et al., 2013). This same 13-LOX pair in Arabidopsis is essential for male reproductive development (Caldelari et al., 2011) and the two 13-LOXs also play roles in root defense against nematodes (Ozalvo et al., 2014).

With this work, all four JA precursor-producing 13-LOXs in Arabidopsis now have attributed roles in wounded rosettes (Fig. 5). In addition to the functions of LOX3 and LOX4 described herein, LOX2 produces JA precursors as well as defense-related metabolites called "arabidopsides," which accumulate rapidly in and near wounds (Glauser et al., 2009). Concerning *LOX6*, corresponding loss-of-function mutants are compromised in rapid JA synthesis in leaves distal to damage sites (Chauvin et al., 2013; Grebner et al., 2013; Gasperini et al., 2015). LOX2 and LOX6 also function together to upregulate LOX3 and LOX4 (Chauvin et al., 2016). In this work, expression of *TPC1ΔCa*$_i$ in the wild-type background caused increases in *LOX3* mRNA levels. However, and consistent with the model for *LOX3*/*LOX4* regulation by LOX2 and LOX6 proposed in Chauvin et al. (2016), no increases in *LOX3* mRNA were detectable in the *lox2 lox4 lox6* triple mutant. The result suggests that hyperactive TPC1 variants exert their activating effect on LOX3-dependent JA precursor synthesis at the post-transcriptional level.

A question emerging from this study is raised by the fact that all four 13-LOXs produce JAs after leaf wounding (Chauvin et al., 2013). LOX3, LOX4, and

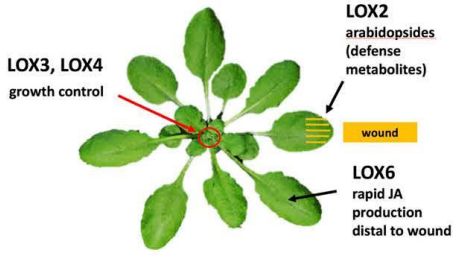

Figure 5. Specific 13-LOX functions in wounded Arabidopsis rosettes. All four 13-LOXs produce JA precursors in wounded leaves and all four play roles in defense against lepidopteran herbivores. LOX2 is expressed throughout soft tissues (including the mesophyll) but not (or at very low levels) in the mature leaf vasculature. LOX3, LOX4, and LOX6 are primarily expressed in phloem- and xylem-associated cells in both developing and mature leaf veins. Only the functions that are largely specific to distinct LOXs in Arabidopsis leaves are emphasized. From Chauvin et al. (2013, 2016), Glauser et al. (2009), Grebner et al. (2013), and this work.

LOX6 are expressed principally in phloem- and xylem-associated cells in adult-phase primary leaf veins (Chauvin et al., 2013). Moreover, JA precursors made by LOX6 in xylem contact cells can move out of these cell populations (Gasperini et al., 2015). Why, then, do LOX3 and LOX4 and not LOX2 and/or LOX6 operate in the control of wound-response leaf growth restriction? It is possible that JA precursors or JAs produced by LOX6 and LOX2 in response to wounding do not reach the stem cell populations that determine the rate of leaf primordia development. In a potentially interesting parallel, we note that transcripts for all four Arabidopsis 13-LOXs are found in developing flowers (Klepikova et al., 2016), and yet only LOX3 and LOX4 produce JAs essential for reproductive development in this plant (Caldelari et al., 2011).

Phloem-Derived Signals Can Activate the JA Pathway

Which cell types produce the signals that lead to wound-response rosette growth restriction? To investigate this, we sought to control this process genetically in the absence of wounding. The *LOX3* promoter activity domain in primary leaf veins spans both the regions of xylem and phloem (Chauvin et al., 2016). Cells in one or both of these tissues were candidates that might produce the signals that stimulate environmentally linked growth restriction. In this respect, the phloem was of particular interest because this tissue plays central roles in growth plasticity (López-Salmerón et al., 2019). Additionally, key roles of the phloem in the induction of antiherbivore defense mechanisms in leaves have been discovered (Nguyen et al., 2018). Remarkably, expressing $TPC1^{D454N}$ in the null background *tpc1-2* under the phloem-companion-cell–specific *SUC2* promoter phenocopied *fou2*. To increase the dominance of *fou2*, we exploited *TPC1ΔCa*$_i$ ($TPC1^{D240A,D454A,E528A}$), which strongly increases the open probability of the channel (Guo et al., 2017). The first key test with the *TPC1ΔCa*$_i$ cDNA was to express it in a restricted cellular domain under the *SUC2* promoter in the *lox2 lox3 lox4 lox6* quadruple mutant background that does not produce biologically active JAs in response to wounding (Chauvin et al., 2013). This test (Fig. 4B; Supplemental Fig. S3) revealed that the rosette diameters and leaf shapes of the *lox* quadruple mutants with or without *TPC1ΔCa*$_i$ were similar. In 5-week-old plants, only a few of the younger leaves in the rosette of the quadruple mutant transformed with *TPC1ΔCa*$_i$, displayed some epinasty. This experiment served as the basis for transforming the *lox2 lox4 lox6* triple mutant with *TPC1ΔCa*$_i$ to try to activate LOX3, and thereby control rosette growth. A further control was expression of *TPC1ΔCa*$_i$ in the wild-type background. The wild-type plants expressing *SUC2::TPC1ΔCa*$_i$ displayed a *fou2*-like phenotype.

By extending this approach to a *lox2 lox4 lox6* background that carries the functional *LOX3* gene, we found that *TPC1ΔCa*$_i$-dependent ion fluxes generated in the phloem could activate the LOX3 branch of the JA synthesis pathway. The mechanism underlying this phenomenon is unknown, but membrane depolarization after wounding appears to play a role in JA pathway activation in Arabidopsis leaves (e.g. Lenglet et al., 2017; Nguyen et al., 2018). Phloem cells are highly excitable (Sibaoka, 1962; Hafke and van Bel, 2013; Hedrich et al., 2016), and wounding may therefore activate JA synthesis by altering membrane potentials and Ca^{2+} fluxes in these cells. Such a scenario may be widespread in plants subjected to repetitive wounding. The art of bonsai may rest on related mechanisms.

CONCLUSION

Loss-of-function genetic studies show that LOX3 and LOX4 together control wound-response leaf growth in Arabidopsis. These two 13-LOXs operate in both vegetative growth and reproductive development, highlighting that their functions are distinct from those of LOX2 and LOX6. Further demonstrating a role of LOX3 in controlling leaf growth, we were also able to activate LOX3-dependent JA production in unwounded leaves. This was accomplished using a novel approach based on gain-of-function mutations in a vacuolar ion channel. In terms of future work, hyperactive ion channel variants could find broader use in investigating mechanisms of cell-to-cell signaling within the vasculature, a phenomenon that underlies much of plant physiology.

MATERIALS AND METHODS

Plant Material and Growth Conditions

Transfer-DNA insertion lines were obtained from the Nottingham Arabidopsis Stock Center (http://arabidopsis.info/). Arabidopsis (*Arabidopsis thaliana*) Columbia (Col-0) was the wild type and the background for *lox* mutants. The *lox* alleles used were *lox2-1* (Glauser et al., 2009), *lox3b* (SALK_147830), *lox4a* (SALK_071732), and *lox6a* (SALK_138907). Other mutants used were *tpc1-2* (*SALK_145413*), *fou2* (At4g03560, $TPC1^{D454N}$; Bonaventure et al., 2007a), and *aos* (At5g42650; Park et al., 2002), which were all in the wild-type background. Plants were grown individually in 7-cm–diameter pots on soil at 70% humidity and 100 $\mu E\ m^{-2}\ s^{-1}$ photosynthetically available radiation under short-day conditions (10-h light at 22°C).

Serial Wounding

For serial wounding, a series of wounds was inflicted from d 14 of growth when the first two leaves were slightly bigger than the cotyledons. Fifty percent of the tip of leaf 1 was wounded with forceps. Control plants were handled identically but not wounded. Plants were then incubated for 3 d before 50% wounding of leaf 2. The same schema was repeated with 3 d of resting between each wound event and the series of wounds was stopped 3 d after leaf 7 was wounded. Five to six plants of each genotype (wild type or *aos*) were used for petiole measurements. For each plant, petiole lengths of the leaves 6, 7, and 8 were measured from photographs using the software ImageJ (https://imagej.nih.gov/ij/index.html) and their combined lengths were averaged.

Insect Bioassays

No-choice bioassays were performed with neonate *Spodoptera littoralis* placed on 5-week-old plants grown under short-day conditions identical to those described above. Six larvae were placed on each individual plant (11 plants per genotype) and allowed to feed for 11 d. Larvae were then weighted

on a precision balance XP205 DeltaRang (Mettler-Toledo). Aphid bioassays performed with *Brevicoryne brassicae*. Unwounded or serially wounded plants were placed in cages (11 plants per cage) and five adult aphids were deposed on each plant. After 48 h (day0), the adults were removed. After 72 h, nymphs were removed, leaving only five nymphs on each plant. Nymphs were counted at day 11 and the nymphs and adult aphids were counted at day 14. The aphid performance was calculated as follows: ([number of nymphs on day 11 + number of nymphs on day 14]/ number of adults on day 14).

Gene Expression Analysis

At the time of tissue collection, the leaves (unwounded or wounded) were collected and immediately frozen in liquid N_2. RNA isolation and reverse transcription quantitative PCR was as described by Gfeller et al. (2011) using the following primer pairs: *UBC21* (At5g25760) transcripts were quantified using the primers 5′-CAGTCTGTGTGTAGAGCTATCATAGCAT-3′ (ubc21F) and 5′-AGAAGATTCCCTGAGTCGCAGTT-3′ (ubc21R). *JAZ10* (At5g13220) transcripts were quantified using primers 5′-ATCCCGATTTCTCCGGTCCA-3′ (jaz10F) and 5′-ACTTTCTCCTTGCGATGGGAAGA-3′ (jaz10R). *LOX3* (At1g17420) transcripts were quantified using primers 5′-AACACAACCACA TGGTCTTAAACTC-3′ (lox3F) and 5′-GGAGCTCAGAGTCTGTTTTGATAA G-3′ (lox3R).

Plasmid Construction and Transformation

Vectors were based on MultiSite Gateway Technology (www.invitrogen.com). Promoters were amplified from wild-type genomic DNA with indicated oligonucleotides for: the 2-kb upstream region directly preceding the first ATG of SCR (At3g54220; Malamy and Benfey, 1997), LOX6 (At1g67560; 5′-CGGGGT ACCGGTTGTTGAAATTTCTGATGCT-3′ and 5′-TTCCCCCCCGGGTTTTGT TTGGAGTTTGGCAGT-3′), and the 4-kb upstream region directly preceding the first ATG of SUC2 (At1g22710; 5′-CGGGGTACCCTGCTAAAACTATTC CATTTCAAAATG-3′ and 5′-TTCCCCCCCGGGATTTGACAAACCAAGAAA GTAAG-3′). After amplification, these sequences were verified and cloned via restriction digestion with *XmaI* and *KpnI* into a modified pUC57 (Chauvin et al., 2013) to create pEN-L4-promoter-R1 clones. The open reading frame of TPC1 (At4g03560) and TPC1D454N was amplified from cDNA from wild-type and fou2 plants (5′-ACAAAAAGCAGGCTTAATGGAAGACCC-3′ and 5′-AGAAA GCTGGGTTGTGTCAGAAGTGGAACACT-3′). Amplification products were recombined into pDONR221 (Invitrogen) to produce pEN-L1-gene-L2 clones. To generate promoter fusion with proteins under the control of endogenous promoters, pEN-L4-promoter-R1 plasmids were recombined with pEN-L1-CDS-L2 into pEDO097pPR7m24GW by double Gateway Technology to obtain SUC2pro-TPC1D454N, SCRpro-TPC1D454N, LOX6pro-TPC1D454N, and SUC2pro-TPC1 clones. All constructs were introduced into Arabidopsis backgrounds by floral dip *Agrobacterium*-mediated transformation. For promoter fusions, transformed seeds expressing red fluorescence protein in T1, T2, and T3 lines were selected by fluorescence microscopy. TPC1ΔCai (Guo et al., 2017) was synthesized by GenScript. The following mutations were introduced into the TPC1 coding sequence: Asp (GAC) 240-Ala (GCC), Asp (GAT) 454-Ala (GCT), and Glu (GAA) 528-Ala (GCA). The synthetic gene was cloned into the Entry vector pDONR/Zeo and recombined with pUC57 carrying the SUC2 promoter for plant transformation. From multiple transformants with similar phenotypes, a minimum of two independent transgenic lines for individual each construct was used in experiments.

JA and JA-Ile Analyses

JA and JA-Ile measurements were performed as described by Glauser et al. (2014). Plants were 5 weeks old and had not been wounded. The internal standards used were JA-d5 for JA and JA-Ile-$^{13}C_6$ for JA-Ile. Limits of quantifications for JA and JA-Ile were 0.4 and 0.15 pmol g^{-1} fresh weight, respectively.

Statistical Analysis

Statistical significance in pairwise comparisons was evaluated by Student's *t* test. Multiple comparisons using ANOVA followed by Tukey's honestly significant difference (HSD) test were performed in the software R 3.2.2 (www.r-project.org).

Accession Numbers

Sequence data TPC1 can be found in the GenBank/EMBL data libraries under accession numbers 825655/ NP_567258.1.

Supplemental Data

The following supplemental materials are available.

Supplemental Figure S1. Effect of serial leaf wounding on rosette growth of *lox* mutants.

Supplemental Figure S2. Expressing $TPC1^{D454N}$ in phloem companion cells of *tpc1-2* phenocopies *fou2*.

Supplemental Figure S3. Independent transformants show similar phenotypes and fresh weights to those used for Figure 4 in the main text.

ACKNOWLEDGMENTS

Archana Kumari (University of Lausanne) gave us critical advice and Marion Ribault (University of Lausanne) provided valuable technical help.

Received April 29, 2020; revised July 9, 2020; published July 15, 2020.

LITERATURE CITED

Acosta IF, Laparra H, Romero SP, Schmelz E, Hamberg M, Mottinger JP, Moreno MA, Dellaporta SL (2009) *Tasselseed1* is a lipoxygenase affecting jasmonic acid signaling in sex determination of maize. Science **323:** 262–265

Ballaré CL, Austin AT (2019) Recalculating growth and defense strategies under competition: Key roles of photoreceptors and jasmonates. J Exp Bot **70:** 3425–3434

Beyhl D, Hörtensteiner S, Martinoia E, Farmer EE, Fromm J, Marten I, Hedrich R (2009) The *fou2* mutation in the major vacuolar cation channel TPC1 confers tolerance to inhibitory luminal calcium. Plant J **58:** 715–723

Bonaventure G, Gfeller A, Proebsting WM, Hörtensteiner S, Chételat A, Martinoia E, Farmer EE (2007a) A gain-of-function allele of TPC1 activates oxylipin biogenesis after leaf wounding in Arabidopsis. Plant J **49:** 889–898

Bonaventure G, Gfeller A, Rodríguez VM, Armand F, Farmer EE (2007b) The *fou2* gain-of-function allele and the wild-type allele of Two Pore Channel 1 contribute to different extents or by different mechanisms to defense gene expression in Arabidopsis. Plant Cell Physiol **48:** 1775–1789

Browse J (2009) Jasmonate passes muster: A receptor and targets for the defense hormone. Annu Rev Plant Biol **60:** 183–205

Caldelari D, Wang G, Farmer EE, Dong X (2011) Arabidopsis *lox3 lox4* double mutants are male sterile and defective in global proliferative arrest. Plant Mol Biol **75:** 25–33

Campos ML, Yoshida Y, Major IT, de Oliveira Ferreira D, Weraduwage SM, Froehlich JE, Johnson BF, Kramer DM, Jander G, Sharkey TD, et al (2016) Rewiring of jasmonate and phytochrome B signalling uncouples plant growth-defense tradeoffs. Nat Commun **7:** 12570

Chauvin A, Caldelari D, Wolfender JL, Farmer EE (2013) Four 13-lipoxygenases contribute to rapid jasmonate synthesis in wounded *Arabidopsis thaliana* leaves: A role for lipoxygenase 6 in responses to long-distance wound signals. New Phytol **197:** 566–575

Chauvin A, Lenglet A, Wolfender JL, Farmer EE (2016) Paired hierarchical organization of 13-lipoxygenases in Arabidopsis. Plants (Basel) **5:** 16

Chehab EW, Yao C, Henderson Z, Kim S, Braam J (2012) Arabidopsis touch-induced morphogenesis is jasmonate mediated and protects against pests. Curr Biol **22:** 701–706

Chini A, Gimenez-Ibanez S, Goossens A, Solano R (2016) Redundancy and specificity in jasmonate signalling. Curr Opin Plant Biol **33:** 147–156

Fernández-Milmanda GL, Crocco CD, Reichelt M, Mazza CA, Köllner TG, Zhang T, Cargnel MD, Lichy MZ, Fiorucci AS, Fankhauser C, et al (2020) A light-dependent molecular link between competition cues and defence responses in plants. Nat Plants **6:** 223–230

Gasperini D, Chauvin A, Acosta IF, Kurenda A, Stolz S, Chételat A, Wolfender JL, Farmer EE (2015) Axial and radial oxylipin transport. Plant Physiol **169:** 2244–2254

Gfeller A, Baerenfaller K, Loscos J, Chételat A, Baginsky S, Farmer EE (2011) Jasmonate controls polypeptide patterning in undamaged tissue in wounded *Arabidopsis* leaves. Plant Physiol **156:** 1797–1807

Glauser G, Dubugnon L, Mousavi SAR, Rudaz S, Wolfender JL, Farmer EE (2009) Velocity estimates for signal propagation leading to systemic jasmonic acid accumulation in wounded Arabidopsis. J Biol Chem **284:** 34506–34513

Glauser G, Vallat A, Balmer D (2014) Hormone profiling. In JJ Sanchez-Serrano, and J Salinas, eds, Arabidopsis Protocols. Humana Press, Totowa, NJ, pp 597–608

Grebner W, Stingl NE, Oenel A, Mueller MJ, Berger S (2013) Lipoxygenase6-dependent oxylipin synthesis in roots is required for abiotic and biotic stress resistance of Arabidopsis. Plant Physiol **161:** 2159–2170

Guo Q, Major IT, Howe GA (2018) Resolution of growth-defense conflict: Mechanistic insights from jasmonate signaling. Curr Opin Plant Biol **44:** 72–81

Guo J, Zeng W, Jiang Y (2017) Tuning the ion selectivity of two-pore channels. Proc Natl Acad Sci USA **114:** 1009–1014

Hafke JB, van Bel AJE (2013) Cellular basis of electrical potential waves along the phloem and impact of coincident Ca2+ fluxes. In GA Thompson, and AJE van Bel, eds, Phloem: Molecular Cell Biology, Systemic Communication, Biotic Interactions. Wiley, New York, pp 122–140

Hedrich R, Mueller TD, Becker D, Marten I (2018) Structure and function of TPC1 vacuole SV channel gains shape. Mol Plant **11:** 764–775

Hedrich R, Salvador-Recatalà V, Dreyer I (2016) Electrical wiring and long-distance plant communication. Trends Plant Sci **21:** 376–387

Howe GA, Major IT, Koo AJ (2018) Modularity in jasmonate signaling for multistress resilience. Annu Rev Plant Biol **69:** 387–415

Huot B, Yao J, Montgomery BL, He SY (2014) Growth-defense tradeoffs in plants: A balancing act to optimize fitness. Mol Plant **7:** 1267–1287

Jewell JB, Browse J (2016) Epidermal jasmonate perception is sufficient for all aspects of jasmonate-mediated male fertility in Arabidopsis. Plant J **85:** 634–647

Jimenez-Aleman GH, Almeida-Trapp M, Fernández-Barbero G, Gimenez-Ibanez S, Reichelt M, Vadassery J, Mithöfer A, Caballero J, Boland W, Solano R (2019) Omega hydroxylated JA-Ile is an endogenous bioactive jasmonate that signals through the canonical jasmonate signaling pathway. Biochim Biophys Acta Mol Cell Biol Lipids **1864:** 158520

Klepikova AV, Kasianov AS, Gerasimov ES, Logacheva MD, Penin AA (2016) A high resolution map of the *Arabidopsis thaliana* developmental transcriptome based on RNA-seq profiling. Plant J **88:** 1058–1070

Lenglet A, Jaślan D, Toyota M, Mueller M, Müller T, Schönknecht G, Marten I, Gilroy S, Hedrich R, Farmer EE (2017) Control of basal jasmonate signalling and defence through modulation of intracellular cation flux capacity. New Phytol **216:** 1161–1169

López-Salmerón V, Cho H, Tonn N, Greb T (2019) The phloem as a mediator of plant growth plasticity. Curr Biol **29:** R173–R181

Major IT, Yoshida Y, Campos ML, Kapali G, Xin XF, Sugimoto K, de Oliveira Ferreira D, He SY, Howe GA (2017) Regulation of growth-defense balance by the JASMONATE ZIM-DOMAIN (JAZ)-MYC transcriptional module. New Phytol **215:** 1533–1547

Malamy JE, Benfey PN (1997) Analysis of SCARECROW expression using a rapid system for assessing transgene expression in Arabidopsis roots. Plant J **12:** 957–963

Nguyen CT, Kurenda A, Stolz S, Chételat A, Farmer EE (2018) Identification of cell populations necessary for leaf-to-leaf electrical signaling in a wounded plant. Proc Natl Acad Sci USA **115:** 10178–10183

Noir S, Bömer M, Takahashi N, Ishida T, Tsui TL, Balbi V, Shanahan H, Sugimoto K, Devoto A (2013) Jasmonate controls leaf growth by repressing cell proliferation and the onset of endoreduplication while maintaining a potential stand-by mode. Plant Physiol **161:** 1930–1951

Ozalvo R, Cabrera J, Escobar C, Christensen SA, Borrego EJ, Kolomiets MV, Castresana C, Iberkleid I, Brown Horowitz S (2014) Two closely related members of Arabidopsis 13-lipoxygenases (13-LOXs), LOX3 and LOX4, reveal distinct functions in response to plant-parasitic nematode infection. Mol Plant Pathol **15:** 319–332

Park J, Halitschke R, Kim HB, Baldwin IT, Feldmann KA, Feyereisen R (2002) A knock-out mutation in allene oxide synthase results in male sterility and defective wound signal transduction in Arabidopsis due to a block in jasmonic acid biosynthesis. Plant J **31:** 1–12

Peiter E, Maathuis FJM, Mills LN, Knight H, Pelloux J, Hetherington AM, Sanders D (2005) The vacuolar Ca^{2+}-activated channel TPC1 regulates germination and stomatal movement. Nature **434:** 404–408

Pottosin I, Dobrovinskaya O (2018) Two-pore cation (TPC) channel: Not a shorthanded one. Funct Plant Biol **45:** 83–92

Poudel AN, Holtsclaw RE, Kimberlin A, Sen S, Zeng S, Joshi T, Lei Z, Sumner LW, Singh K, Matsuura H, et al (2019) 12-Hydroxy-jasmonoyl-L-isoleucine is an active jasmonate that signals through CORONATINE INSENSITIVE 1 and contributes to the wound response in Arabidopsis. Plant Cell Physiol **60:** 2152–2166

Sheard LB, Tan X, Mao H, Withers J, Ben-Nissan G, Hinds TR, Kobayashi Y, Hsu FF, Sharon M, Browse J, et al (2010) Jasmonate perception by inositol-phosphate-potentiated COI1-JAZ co-receptor. Nature **468:** 400–405

Sibaoka T (1962) Excitable cells in Mimosa. Science **137:** 226

Truernit E, Sauer N (1995) The promoter of the *Arabidopsis thaliana* SUC2 sucrose-H^+ symporter gene directs expression of beta-glucuronidase to the phloem: Evidence for phloem loading and unloading by SUC2. Planta **196:** 564–570

Wysocka-Diller JW, Helariutta Y, Fukaki H, Malamy JE, Benfey PN (2000) Molecular analysis of SCARECROW function reveals a radial patterning mechanism common to root and shoot. Development **127:** 595–603

Xie DX, Feys BF, James S, Nieto-Rostro M, Turner JG (1998) COI1: An Arabidopsis gene required for jasmonate-regulated defense and fertility. Science **280:** 1091–1094

Yan Y, Stolz S, Chételat A, Reymond P, Pagni M, Dubugnon L, Farmer EE (2007) A downstream mediator in the growth repression limb of the jasmonate pathway. Plant Cell **19:** 2470–2483

Zhang Y, Turner JG (2008) Wound-induced endogenous jasmonates stunt plant growth by inhibiting mitosis. PLoS One **3:** e3699

Supplemental Data for:

Yang and Lenglet-Hilfiker et al. LOX3 and LOX4 control wound-response growth restriction in *Arabidopsis*

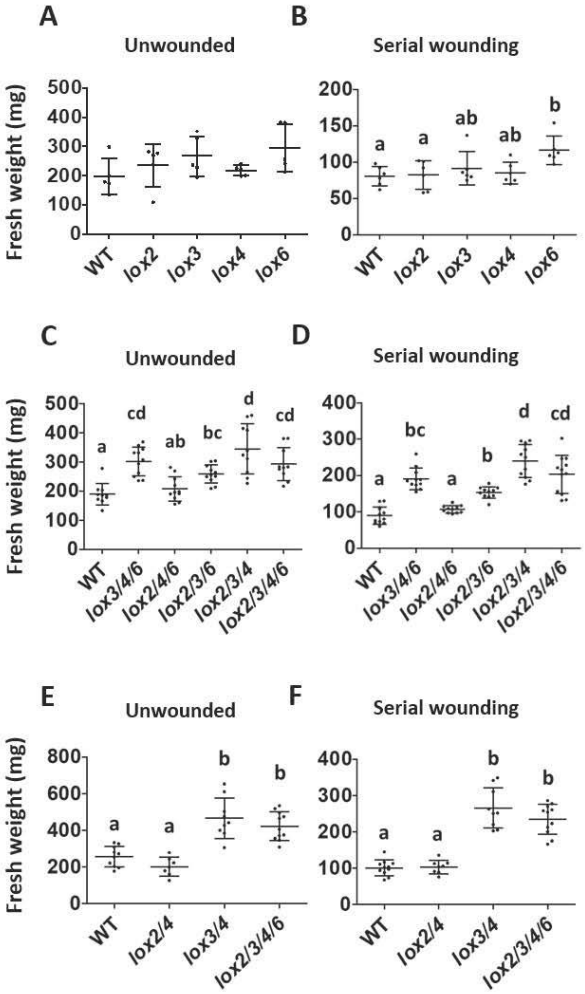

Supplemental Figure S1. Effect of serial leaf wounding on rosette growth of *lox* mutants. (A) and (B), fresh weights of unwounded and serially wounded WT and *lox* single mutants. For the unwounded group, n=5. For the serially wounded group, n = 6. (C) and (D), fresh weights of unwounded and serially wounded WT, *lox* triple mutants and the *lox* quadruple mutant. For each group, $n \geq 10$. (E) and (F), fresh weights of unwounded and serially wounded WT, *lox* double mutants and the *lox* quadruple mutant. For each group, $n \geq 7$. Bars represent the mean of fresh weight (± SD). Letters indicate statistically significant differences, Tukey's HSD test ($p<0.05$). Bars sharing the same letters indicate no statistically significant differences. The dataset used in this figure was the same as that used for Fig. 2 in the main text.

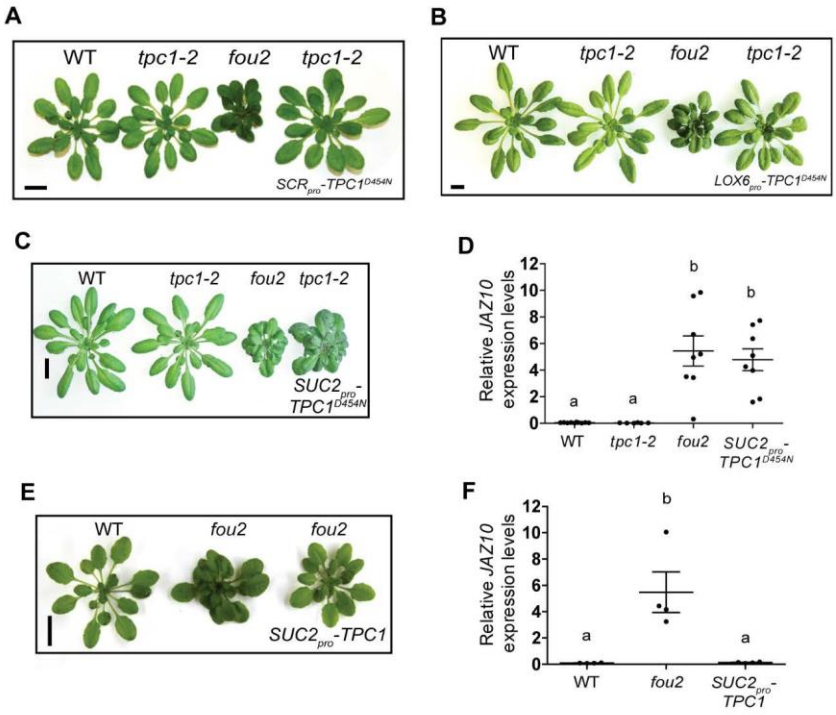

Supplemental Figure S2. Expressing *TPC1*^{D454N} in phloem companion cells of *tpc1-2* phenocopies *fou2*. All plants were 5 weeks-old. (A) Rosette morphology of WT, *tpc1-2*, *fou2* and *LOX6pro-TPC1*^{D454N} in *tpc1-2*. Scale bar = 1 cm. (B) Rosette morphology of WT, *tpc1-2*, *fou2* and *SCRpro-TPC1*^{D454N} in *tpc1-2*. Scale bar = 1 cm. (C) Morphology of WT, *tpc1-2*, *fou2* and *SUC2*$_{pro}$*-TPC1*^{D454N} expressed in *tpc1-2*. Scale bar = 1 cm. (D) *JAZ10* transcript levels in leaf 8 of unwounded WT, *fou2*, *tpc1-2* and *SUC2*$_{pro}$*-TPC1*^{D454N} in the *tpc1-2* background. *JAZ10* transcripts

were normalized to those of *UBC21* and displayed relative to the expression in the WT control. Error bars are from the mean of 2 combined experiments (n≥3 biological replicates per experiment; ±SEM). Letters indicate significant differences, Tukey's HSD test ($p<0.0001$). (E) Rosette morphology of WT, *fou2* and $SUC2_{pro}$-*TPC1* in the *fou2* background. Note the partial suppression of the *fou2* phenotype. Scale bar = 1 cm. (F) *JAZ10* transcript levels in leaf 8 of unwounded WT, *fou2* and $SUC2_{pro}$-*TPC1* in the *fou2* background. Error bars are mean of 4 biological replicates (±SEM). Letters indicate significant differences, Tukey's HSD test ($p=0.001$).

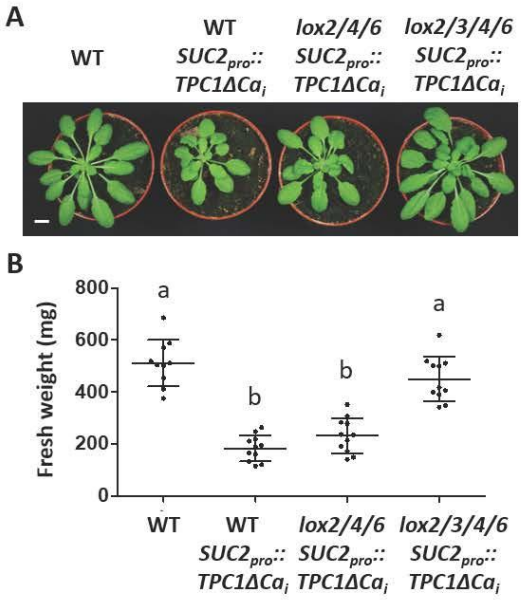

Supplemental Figure S3. Independent transformants show similar phenotypes and fresh weights to those used for Fig. 4 in the main text. In order to ensure that transgenic lines used in the main text were representative further independent transformant lines were analyzed. All plants were 5 weeks-old. (A) Rosette morphologies of WT, WT expressing *SUC2*$_{pro}$*::TPC1ΔCa*$_i$, *lox2/4/6* expressing *SUC2*$_{pro}$*::TPC1ΔCa*$_i$ and *lox* quadruple mutant expressing *SUC2*$_{pro}$*::TPC1ΔCa*$_i$. Scale bar = 1cm. (B) Fresh weights of the same lines. Data are means (± SD), n = 10 – 11. Letters indicate significant differences, Tukey's HSD test ($p<0.05$).

Chapter 3: MATERIALS AND METHODS FOR CHAPTERS 4 TO 7

Plant material and growth conditions. Arabidopsis thaliana (Col-0 accession) plants were grown in soil in 7 cm diameter pots in short days (10 h light, 120 µ Einsteins m^{-2} s^{-1}) at 22°C, and 14 h darkness at 18°C. Experiments were conducted at the 5-week (adult phase) stage. Col-0 or seeds collected from populations growing on the University of Lausanne, Dorigny campus were also grown in the laboratory or on the campus. For this, seeds from wild-grown *Arabidopsis* were collected and dried for 14 days, then seeds were stratified for 7 days before planting in the laboratory. To plant the laboratory Col-0 accession in the field on the UNIL campus, 7-day-old seedlings were transferred from short-day conditions into the field on 18 April 2019. Plants experienced light snow on 4 May, frost on 5 May, strong wind on May 13-5 and several dry periods prior to harvesting which took place during the period of May 20-24. *Mimosa pudica* plants were grown in soil in long days (16 h light, 25K lux) at 21-24 °C, and 8 h darkness at 18°C. Experiments were conducted with 7-week-old (for leaf 5) and 1-year-old (for adult leaves) *M. pudica* plants.

Cytosolic calcium imaging. 5-week-old *Arabidopsis* plants expressed *UBQ10pro::GcaMP3* signals were recorded with SMZ18 stereomicroscope (Nikon Instruments Europe BV, Amsterdam, Netherlands), ORCA-Flash4.0 (C11440) camera (Hamamatsu, Solothurn, Switzerland) and eGFP emission/excitation filter set (AHF analysentechnik AG, Tübingen, Germany). *Spodoptera littoralis* 5th instar larvae weight approximately 500 mg were used.

Surface potential measurements. Silver/silver chloride electrodes were placed on leaf 8 as described in Mousavi et al, (2013). The connection between the electrode and leaf were made with a drop of 10 mM KCl in 0.5 % (w/v) agar. The reference electrode was placed in the soil. Surface potential signals were recorded using LabScribe3 software (iWorx Systems, Inc., Dover, NH) and signals were analyzed for depolarization amplitude and duration as described

previously (Mousavi et al., 2013). Hollow columnar plastic supports (Maxi beads 10 mm #8571, Hama, Denmark) were placed underneath and in contact with the petiole at the lamina/petiole junction. After 2 h rest, borosilicate beads of 4 mm diameter weighing 84.8 ± 1.0 mg (n=12) (Z265934-1EA, Sigma-Aldrich, Steinheim, Germany) were dropped from 2 cm height onto the adaxial lamina/petiole junction. To facilitate bead dropping, markers were cut from toothpicks (Popstar, Ljubljana, Slovenia). These were marked at 1 cm intervals and inserted into soil so that one of the interval markers aligned with the upper surface of the target leaf. In other cases borosilicate beads of different weight (and diameters) were used: 5 mm diameter weighing 169.7 ± 2.2 mg (n=12) (Glaskugeln Nr. HH56.1, Carl Roth, Germany), 3mm diameter weighing 38.6 ± 1.9 mg (n=12) (Z143928-1EA, Sigma-Aldrich, Steinheim, Germany) and 2mm diameter weighing 7.1 ± 0.8 mg (n=12) (Z273627-1EA, Sigma-Aldrich, Steinheim, Germany).

Electrical penetration graph (EPG) recordings. The EPG system used for recording electrical signals from phloem sieve elements (SEs) was as described previously (Salvador-Recatalà et al., 2014; Kumari et al., 2019). Bead stimulation was conducted when aphids (*Brevicoryne brassicae* L.) were in the E2 feeding phase according to Tjallingii (1978; 1990). Using the same set-up we also recorded signals from xylem vessels. Xylem-specific aphid electrical activity (xylem-phase; Tjallingii, 1990) was used as a cue for these experiments. Experiments were carried out in a Faraday cage. The aphids were attached with gold wires (diameter 18 µm) using water-based silver glue (EPG Systems, Wageningen, Netherlands). Aphids were placed close to the lamina/petiole junction of leaf 8. The reference electrode was placed in the soil. Recordings were made with a Giga-4 EPG amplifier (EPG Systems, Wageningen, Netherlands). A calibration pulse (50 mV) was applied prior to each recording. During aphid feeding, borosilicate beads 5 mm diameter weighing 169.7 ± 2.2 mg (n=12) (Glaskugeln Nr. HH56.1, Carl Roth, Germany) were dropped onto the petiole from 2 cm height, approximately 5 mm

away from the aphid electrode. For quantification of the electrical signal the maximum amplitude was measured from the baseline. The signal duration was defined as the time from depolarization of half amplitude to repolarization of half amplitude.

Force calculation. Beads were dropped onto adaxial petiole/lamina junctions as described above. Serial images perpendicular to the fall path of the bead were captured with a USB 3.0 monochrome DMK 33UX174 camera (The Imaging Source, Bremen, Germany) at 1000 frames per second. These recordings were used to determine the duration of contact between the bead and the leaf. The force was calculated accordingly.

Fusicoccin treatment. Fusicoccin (1mg, Santa Cruz Biotechnology, Inc. Finnell, Dallas, SC-200754) was dissolved in 367 µl of 100% ethanol to prepare 4 mM stock solution. 5 µl of 4 mM stock solution was diluted with 995 µl of water for making 20 µM working solution. 6 weeks old plants were treated with 20 µM Fusicoccin or mock solution (0.5% ethanol) for 5 minutes using the Ricca factor assay developed by Gao et al, (submitted). The scalded petiole of leaf 13 was cut in the fusicoccin. 5 minutes later we tested the ability of leaf 8 to respond to 4 mm diameter beads. For this, electrodes were placed in position E2.

Trypan blue staining 5-week-old *Arabidopsis* leaves were stained with lactophenol-trypan blue (0.005 %, W/V) at 37°C and de-stained with 95 % (W/V) EtOH (Gouhier-Darimont et al., 2013; Alfonso et al., 2021). The trichomes and skirt cells were imaged with a VHX-6000 digital microscope (Keyence, Osaka, Japan).

Quantitative PCR Total RNA was isolated with DNA-free RNA isolation protocols (Oñate-Sánchez and Vicente-Carbajosa 2008). Total RNA 400 ng was used to synthesize complementary DNA with M-MLV Reverse Transcriptase, RNase H minus, (Promega) first-strand synthesis system. Quantitative PCR analysis was performed on 10 ng of cDNA with a

homemade master mix containing GoTaq polymerase (Promega) and 5X colorless GoTaq reaction buffer (Promega), 0.2 mM dNTPs, 2.5 mM $MgCl_2$, ROX dye and SYBR green in a final volume of 20 µl. Ubiquitin-conjugating enzyme (*UBC21*) At5g25760 was used as reference gene. *JAZ10* (At5g13220) and *AOS* (At5g42650) transcripts were displayed relative to *UBC21*.

Generation of transgenic lines. The four groups of AHAs chosen were: phloem expressed group AHA1, AHA3, AHA8, AHA11 (You et al 2019), mesophyll expressed group AHA1, AHA2, AHA5, AHA11 (Kim et al 2018), clade II group AHA5, AHA6, AHA8, AHA9 (Haruta et al 2010) and clade III group AHA4, AHA7, AHA10, AHA11 (Haruta et al 2010). Three guide RNAs per gene were designed using the Benchling website (https://benchling.com/editor). Guide RNAs (Table S1) were cloned using the oligo annealing technique (Fauser et al; 2014) and then ligated into Gateway-entry vectors (pRU41-pRU46) which had been linearized with BbsI (R3539S, New England BioLabs Inc.) according to Ursache et al, (2021). Six guide RNAs (three per target gene) were assembled into the intermediate vector pSF280 using Golden Gate cloning with BsaI (Eco31I, FD0294, Thermo Fisher Scientific). For simultaneously targeting four AHAs, two intermediate vectors, each containing six guide RNAs, were cloned into destination vectors (pRU051 and pRU052) with the *PcUBi4-2::SpCas9* and FastRed or FastGreen cassettes respectively (Shimada et al 2010; Ursache et al 2021). Wild-type plants were co-transformed with the two destination vectors. T1 transgenic seeds with both red and green fluorescence were planted and genotyped. Multiple CRISPR-mutated *aha* T1 lines were selected for the absence of Cas9 in the T2 generation and genotyped to exclude potentially non-heritable somatic mutations. Two independent *aha1aha11* double mutant lines were identified : A11 and A24. Line A11 has a 274T insertion and a deletion from 874G to 1298C in *AHA1*. Line A11 also has deletion from 275G to 287A and 6G, 687A insertion in *AHA11*. Line A24

has a 274A insertion and a deletion from 874G to 1299C in *AHA1* and insertion of 8T, deletion of 286G and 287A in *AHA11*. The A11 line was retransformed with *PcUBi4-2::SpCas9* vectors to target *AHA3* and *AHA8* so as to generate triple or quadruple mutants. Homozygous mutations in *aha3* were identified in the T1 CRISPR-mutated generation. To maintain *aha3* homozygous background, the homozygous plants (male sterile) were backcrossed with WT. Fluorescent seeds indicating the presence of Cas9 were kept as a backcross population. In such a population, Cas9 could independently mutate the single wild-type copy of *AHA3*, which increase the frequency of *aha3* homozygous mutations. A single heterozygous mutation in *aha8* was identified in the clade II group. This mutant was selfed but no homozygous *aha8* mutants were recovered.

Chapter 4: A NEW MECHANOSTIMULATION ASSAY

Introduction:

Mechanical stimulation triggers inducible defense responses in unwounded plants (Chehab et al., 2012; Moerkercke et al., 2019). Triggering surface calcium signals around trichomes is known to be related to defense activation in the touched leaves (Zhou et al., 2017; Matsumura et al., 2022). This is reflected in the behavior of insect herbivores. A caterpillar (*Pieris brassicae*) walking calmly over the leaf surface, does not trigger many cytosolic calcium signals in the epidermis as measured with intensometric calcium reporter GCaMP3 (Figure 4.1A). However when the caterpillar was stressed by poking it with a tooth pick, its behavior changed and the fleeing caterpillar triggered calcium responses in the plant (Figure 4.1B). This interesting behavior might be due to the long-term co-evolution of insect herbivores and plants. *Pieris brassicae* is a specialist meaning that it is fully adapted to a narrow range of hosts. Therefore, it may have coevolved in a way that doesn't trigger immunity while walking over its host plants.

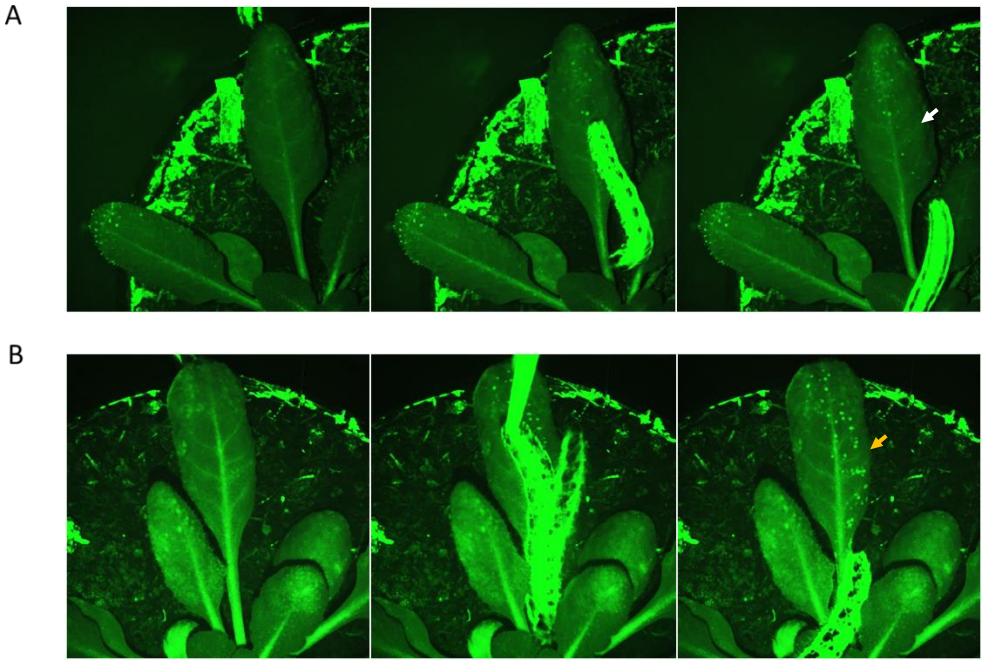

Figure 4.1 Caterpillar walking triggers calcium signals on the leaf surface. Cytosolic calcium signals were recorded from 5-week-old *Arabidopsis* expressing *UBQ10pro::GCaMP3.* (A) A caterpillar walking across a plant without any threat. (B) The caterpillar was poked on the posterior end with tooth pick while walking. The arrows indicate leaf areas over which caterpillars passed.

Results:

Quantification of force application

There are many interesting studies on touch-induced defense responses. For example, forceps touching the *Arabidopsis* inflorescence stem induced local transcription of the jasmonate pathway marker gene *JAZ10* (Sehr et al., 2010). Repeatedly bending rosette leaves by hand slowed down the vegetative-to-reproductive stage transition and increased defense against both herbivores and pathogens (Chehab et al., 2012). Additionally, water-spraying up-regulated MYC2/MYC3/MYC4-dependent gene expression and jasmonate synthesis in *Arabidopsis* leaves (Moerkercke et al., 2019). Recent work has shown that brushing the leaf surface induced defense-related cytosolic calcium increases surrounding the trichomes (Matsumura et al., 2022). The observation that came out of these studies was the diversity of mechanostimulation methods used by different research groups. Some of these methods (e.g. Matsumura et al. 2022) were semi-quantitative in terms of input forces used to stimulate plants. However, none of the present methods can be reproduced exactly. Leaf bending is one mechanostimulation method that has been used (Lee et al., 2005; Chehab et al., 2012). For example, how does one hold the leaf while bending it, how far is the leaf to be bent from the horizontal plane? Therefore, the first aim in this thesis was to establish a new mechanostimulation method allowing robust and quantitative stimulation. In order to minimize interlaboratory variation, our approach was to drop a glass bead from a set elevation. The energy

input came from the velocity of the falling bead (Figure 4.2). For example at 2 cm elevation, a bead would fall for about 64 milliseconds (t_1) to reach its target. At this time, the bead will have obtained a final velocity (V_2) of about 0.63 meters per second. Its momentum determines the total energy input from this bead. Therefore, dropping an 85 mg borosilicate bead from a 2 cm altitude could give about 53.22 µNs of momentum.

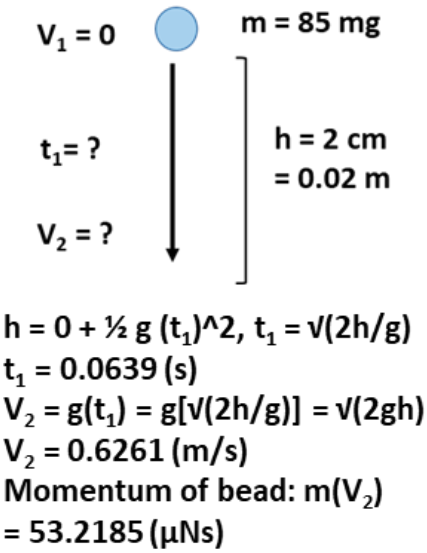

Figure 4.2. Force quantification for bead stimulation. Beads accelerate from $V_1 = 0$ to $V_2 = 0.6261$ m/s.

When the bead reaches the leaf surface, its momentum is transferred into the target causing a conformational change of the leaf. At the returning (rebound) point (t_2), the velocity of the bead is zero (Figure 4.3). A plastic support was used to stabilize the petiole of the stimulated leaf. The time duration (t_2) from reaching the leaf surface until rebounding determined the acceleration to the bead ($a = \Delta V/t$). It also determined the force application by the bead to the stimulated leaf petiole ($F = m\ a$). Thus, the force application could be calculated. For example, 1-millisecond duration and an 85 mg bead would give about 53 mN force

application to the petiole. Under ideal conditions, if the time duration was shortened to half, the force application would then double.

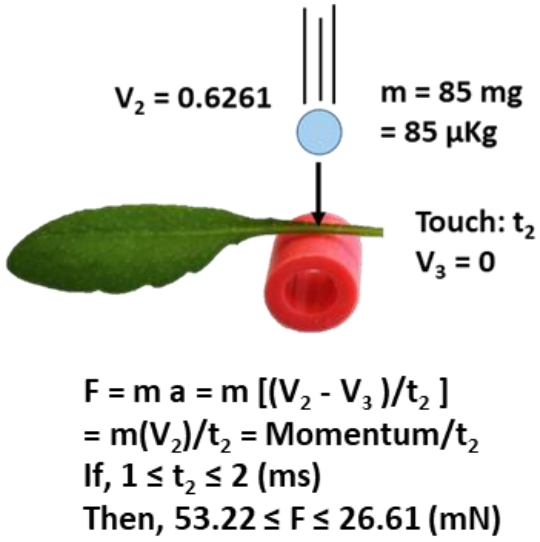

Figure 4.3 Force quantification for bead stimulation. Beads decelerate to reach $V_3 = 0$. A 1 millisecond impact time will result in 53 mN force applied to the leaf. A 1.5 millisecond impact time results in an applied force of approximately 38 mN.

In order to quantify the force, contact duration was recorded with a high-speed camera (1000 frames per second) (Figure 4.4). Each frame recorded during the contact represented 1 millisecond. Under ideal conditions, the returning point (t_2) of a perfectly elastic collision is exactly half of the entire duration ($2t_2$). An example recording showed that it took three frames for the duration of the entire contact. In such a case, half of the entire time (1.5 milliseconds) was taken as the returning point (t_2) (Figure 4.4 A, B). The experiment was repeated 12 times with 12 independent, 5-weeks-old *Arabidopsis* and 12 independent 85 mg borosilicate beads (Figure 4.4 C). We found an average of 1.5 milliseconds for the t_2 for this new

mechanostimulation assay. It indicated, that within 1.5 milliseconds, a 37.7 ± 10.1 mN force was applied to the leaf petiole. This allowed us to perform the mechanostimulation more robustly and more quantitatively than with existing methods (brushing, bending, water spraying, etc).

A

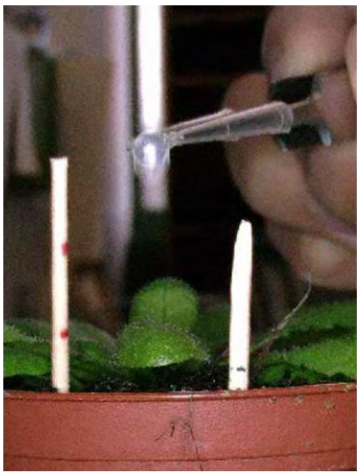

B

C

	$2t_2$ (ms)	t_2 (ms)	force (mN)
No.1	3	1,5	35,48
No.2	3	1,5	35,48
No.3	4	2	26,61
No.4	2	1	53,22
No.5	4	2	26,61
No.6	3	1,5	35,48
No.7	4	2	26,61
No.8	2	1	53,22
No.9	3	1,5	35,48
No.10	3	1,5	35,48
No.11	2	1	53,22
No.12	3	1,5	35,48
AVG	3	1,5	37,70
SD	0,74	0,37	10,10

Figure 4.4 Force quantification for bead stimulation. (A) Bead dropping distances are marked on posts set in the soil. (B) The representative frames showing a bead making contact with the leaf/petiole junction. (C) The contact time from which the bead hits the leaf until it decelerates to $V_3 = 0$ was estimated by video photography. The average impact time until V_3 was estimated to be 1.5 milliseconds for a 85 mg bead.

This new mechanostimulation method was developed with the goal of reducing interlaboratory artifacts. Taking advantage of the force quantification, we then employed a collection of borosilicate beads each having different diameters and weights. The smallest borosilicate bead was 2 mm in diameter and had 7.1 ± 0.8 mg (N=12) weight on average. Thus, the average force application through these 2 mm beads was estimated as 3 mN (Figure 4.5). This means, that by simply switching the sizes of the borosilicate beads and extrapolating our calculations, we could apply forces ranging from 3 mN up to 76 mN. We can to some extent relate these forces to wind speeds using Wind force = impact area x air density x wind speed^2. A 3 mN wind force at an air density of 1.229 Kg/m^3 on an a 2 cm^2 leaf surface would give an estimated wind speed of 3.49 meter per second (12.56 km/hr), which corresponds to Beaufort scale 3 (12-19 Km/hr).

diameter	weight	force
2 mm	7.1 ± 0.8 mg	3 mN
3 mm	38.6 ± 1.9 mg	17 mN
4 mm	84.8 ± 1.0 mg	38 mN
5 mm	169.7 ± 2.2 mg	76 mN

Figure 4.5 Force estimation for each size of borosilicate beads. Weight was measured from 12 independent borosilicate beads.

Characterizing mechanostimulation-induced electrical signals

We successfully developed a new mechanostimulation method to apply forces in a more quantitative manner than many existing assays. With this new method, a plastic support was used to stabilize the stimulated petiole. This stabilized stimulation allowed us to test whether mechanostimulation triggers electrical signals or not. To date, the only study which showed

that mechanostimulation could trigger electrical signals in *Arabidopsis* leaf was from Degli-Agosti (2014). That study used leaf brushing. However, stimulation with a paint brush was a concern since it is difficult to standardize the strength and speed of brushing. Also, that work used invasive electrodes which made the results more complicated to interpret. We thus used our new method coupled with the non-invasive surface electrodes to measure touch-induced electrical signals in *Arabidopsis* petiole (Figure 4.6A).

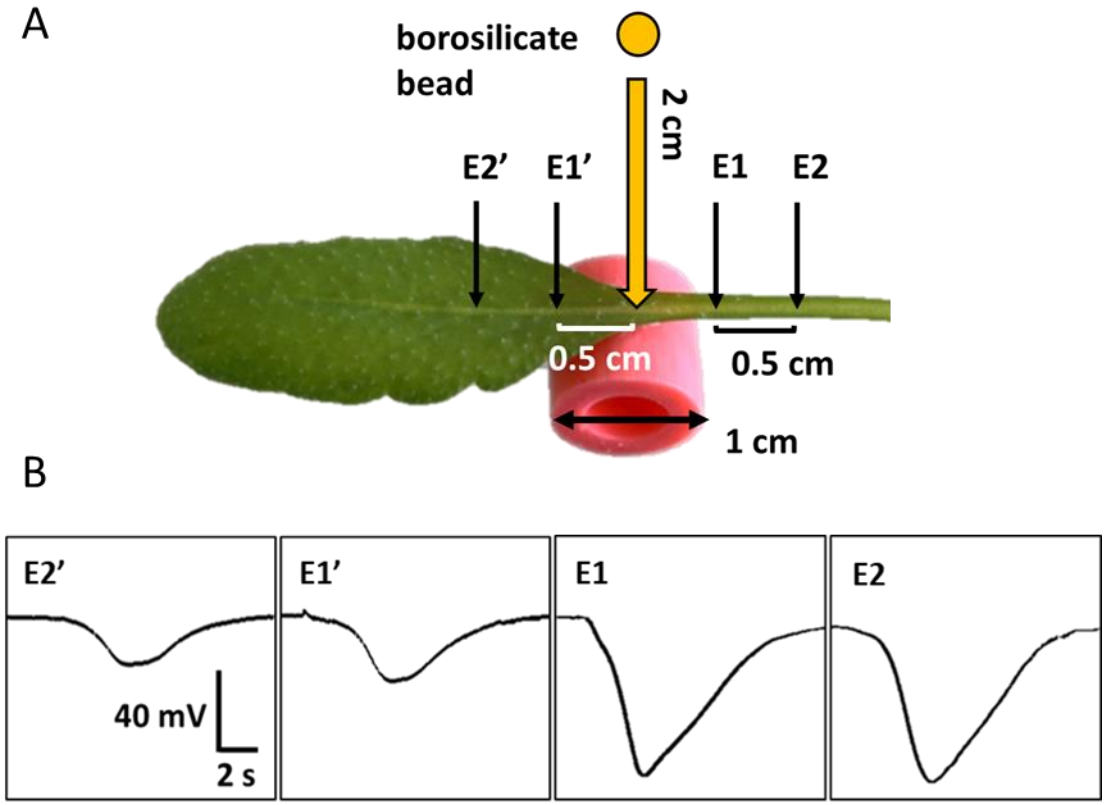

Figure 4.6 Experimental design. (A) Surface potential changes were recorded on the stimulated leaf in response to dropping an 85 mg bead from an elevation of 2 cm onto the blade/petiole junction. The calculated force applied was 38 mN. E1, E2, E1' and E2' represent the positions of surface electrodes. (ZT = 6-8) (B) Representative surface potentials at the different electrode positions.

Four positions were recorded in two combined experiments. One experiment was recorded with two electrodes placed on the petiole (E1 and E2) and another experiment was performed with two electrodes placed on the lamina (E1’ and E2’). Each electrode was placed at a distance of 5 mm from another electrode in order to record the signal propagation. Mechanostimulation-induced electrical signals were characterized with non-invasive surface electrodes in 5-week-old Arabidopsis leaves (Figure 4.6B). In the experiments leaves 8 were stimulated. The mechanostimulation-induced electrical signals that we observed had quite a short duration (time from half amplitude of depolarization phase till half amplitude of repolarization phase). Their architectures were more similar to the action potential in Venus flytrap (Stuhlman and Darden, 1950) than to the slow wave potential in *Arabidopsis* (Mousavi et al., 2013). Secondly, the signal measured from E1 and E1’ appeared instantly after bead-stimulation. Mechanostimulation-induced electrical signals then propagated bi-directionally to E2 and E2’. There were clear differences between signals measured from electrodes on the petiole and electrodes on the lamina. The signals appeared to decrease in amplitude (voltage difference from maximum to minimum) from E1’ to E2’ on the lamina. But the amplitudes were rather similar between E1 and E2 along the petiole.

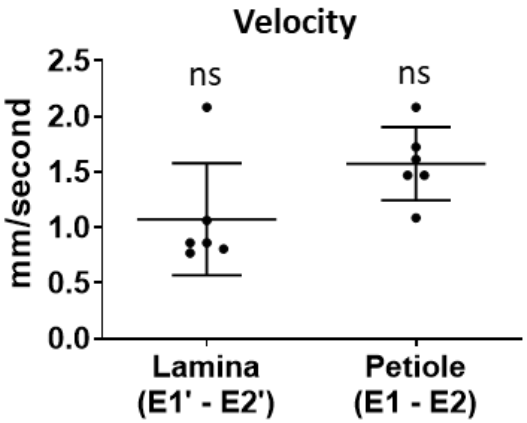

Figure 4.7 Velocities of electrical signal between electrodes. Beads (85 mg) were dropped

onto the leaf/petiole junction to produce a force calculated to be 38 mN. ZT = 6-8. Bars are means ± SD. (n = 6). Student t-test: $P<0.05$. ns = not significant.

The velocity of the mechanostimulation-induced electrical signals was calculated according to the peak-to-peak time (e.g., E1-E2). On average, the signals propagated with speeds of 1-1.5 mm per second in both directions (Figure 4.7). This is similar to the velocities of slow wave potentials and sieve element wound signals (Mousavi et al., 2013; Salvador-Recatala et al., 2014). No significant difference was found between the velocity in petiole (E1-E2) and lamina (E1'-E2'). This velocity is much slower than the velocity of the action potential reported in the Venus flytrap (Sibaoka, 1966), and much faster than the velocity of touch-induced calcium waves in *Arabidopsis* trichomes (Matsumura et al., 2022). Our results suggested the mechanostimulated surface potential might be a new type of signal.

To better investigate the properties of these electrical signals we conducted further experiments and noted that the signal amplitudes had a trend of decreasing towards leaf tips (Figure 4.6B). Because of this trend, a portion of the signals didn't propagate to the E2' position successfully (Figure 4.8). Four data points revealed signals measured in the E1' position, but electrical signals failed to reach E2' position. Quantification of these mechanostimulation-induced electrical signals showed that the difference in amplitude between signals in the petiole and signals in the lamina was significantly different (Figure 4.8A). The amplitudes were decreased from E1' to E2', but were not statistically significant. There were almost no differences in amplitude between the E1 and E2 positions. Furthermore, no statistically significant difference was found in signal duration among all the measuring positions (Figure 4.8B). Despite the data points failing to reach the E2' position, all the measured mechanostimulation-induced electrical signals showed a high similarity in the duration. This

might suggest that these electrical signals share similar depolarization and repolarization kinetics. No matter how much the voltage was changed, the time durations from start to the end were similar. In summary, no large differences in electrical signal duration existed in the cells responding to the mechanostimulation.

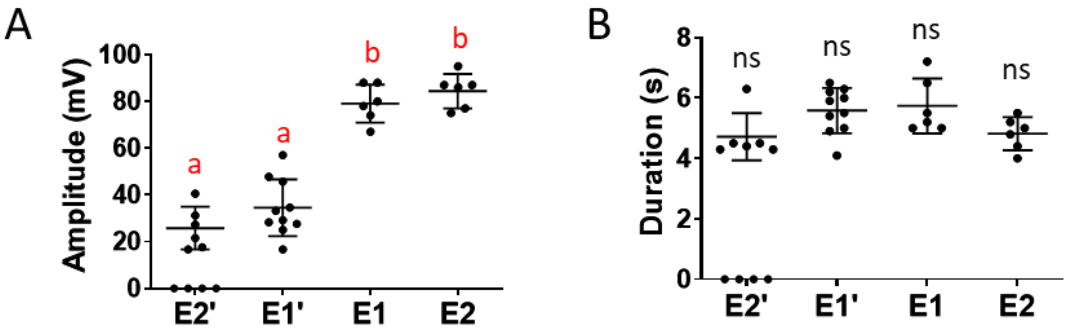

Figure 4.8 Quantification of mechanostimulation-induced electrical signals. The bead used were 4 mm diameter; calculated force 38 mN. ZT = 6-8. (A) Amplitude, voltage changes from the maximum to the minimum. (B) Duration, the time between half amplitude of depolarization and repolarization. Bars are means ± SD. (n = 6-10). Letters indicate significant differences, ns = not significant, Tukey HSD test: $P<0.05$. Data were from 2 combined experiments (one for E1'/E2' and one for E1/E2).

In our experiments, mechanostimulation-induced electrical signals were successfully recorded and quantified with non-invasive surface electrical signals. In our first experiment, we found that electrode positions on the petiole gave the most pronounced amplitude. The E2 position was chosen for further characterizing the electrical signals. We then stimulated *Arabidopsis* leaves with each bead size from 2 cm elevation to find what was the critical force threshold for triggering the mechanostimulation-induced electrical signal. Strikingly, the smallest bead we tested could trigger the electrical signal in a small portion of individuals

(Figure 4.9A). This observations strongly suggested that a 3 mN force applied is the threshold of triggering the mechanostimulation-induced electrical signal.

Surprisingly we found that the 3 mN force triggered electrical signals which showed an all-or-nothing feature. The all-or-nothing feature in threshold is a well-known property of action potentials (Bear et al., 2020). Together with the sharp-peaked amplitude and a rather short duration, the mechanostimulation-induced electrical signal therefore appeared to be the action potential. Also, there was no dose-dependent feature in the strength of force application (Figure 4.9A and B). That is, the amplitudes and durations were quite similar up to 76 mN force application (Figure 4.9B). These experiments indicated that our new mechanostimulation method allowed quantification, reproducibility, and flexibility compared to methods using brushing or bending. Stimulations were consistent while dropping the same size of borosilicate beads from the same elevation (Figure 4.8 and Figure 4.9), and there were very limited variations between experiments. In order to standardize the mechanostimulation assay, the 38 mN force (4 mm, 85 mg borosilicate bead) was then chosen for further experiments.

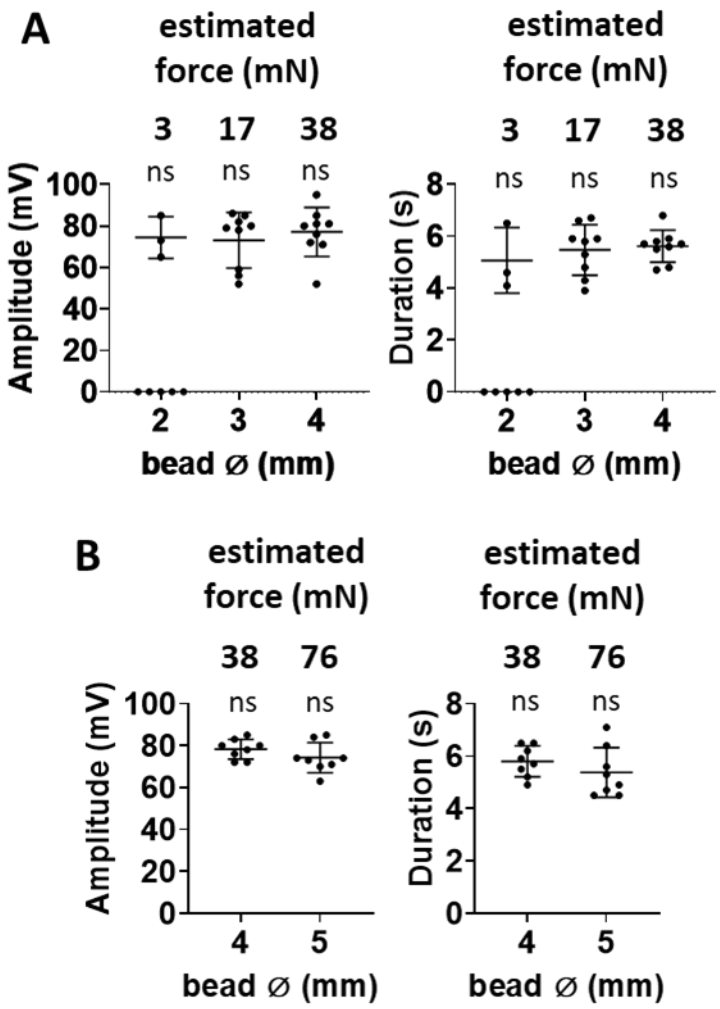

Figure 4.9 Characterizing the threshold of mechanostimulation-induced electrical signals. (A) 3mN, 17mN and 38mN estimated force were applied through dropping 7 mg (2mm ∅), 39 mg (3mm ∅) and 85 mg (4mm ∅) borosilicate beads 2 cm onto lamina/petiole junctions. ZT = 6-8 Bars are means ± SD. (n = 8-9). Letters indicate significant differences, Tukey HSD test: $P<0.05$. (B) 38mN and 76mN estimated force were applied through dropping 85 mg (4mm ∅) and 170 mg (5mm ∅) borosilicate beads 2 cm onto lamina/petiole junctions. ZT = 6-8. Bars are means ± SD. (n = 8). Student t-test: ns = not significant.

Electrical signals triggered by single mechanostimulations showed all-or-nothing features. Moreover, increasing force dosages did not increase the signal amplitudes and durations. The next characteristic to be investigated was the refractory period. The refractory

period is the time duration (length of the recovery period) that allows a second response after the first response. As mentioned, the 38 mN force application and E2 measuring position were chosen for these experiments. Three different time intervals between two consecutive stimulations were tested. Consistently, the first stimulation triggered the typical mechanostimulated electrical signal at the 0-minute time point (Figure 4.10A). Surprisingly, 30 minutes after the first stimulation, a second response could be stimulated. This response was weak in amplitude. But only about half of the stimulations could trigger the second response at 30 minutes time point, while the other half did not trigger electrical signalling (Figure 4.10B). Furthermore, at the 60-minute time point, the mechanostimulated electrical signal had almost recovered its responsiveness (Figure 4.10A). The amplitudes were half-recovered on average but the duration was already fully recovered (Figure 4.10B). Then, 90 minutes after the first stimulation, electrical signals identical to the initial signal were stimulated (Figure 4.10A and B). No statistically significant difference in amplitude and duration compared to single mechanostimulations were found. In summary, responsiveness was almost recovered 60 minutes after stimulation, but the strength of response required 90 minutes for recovery.

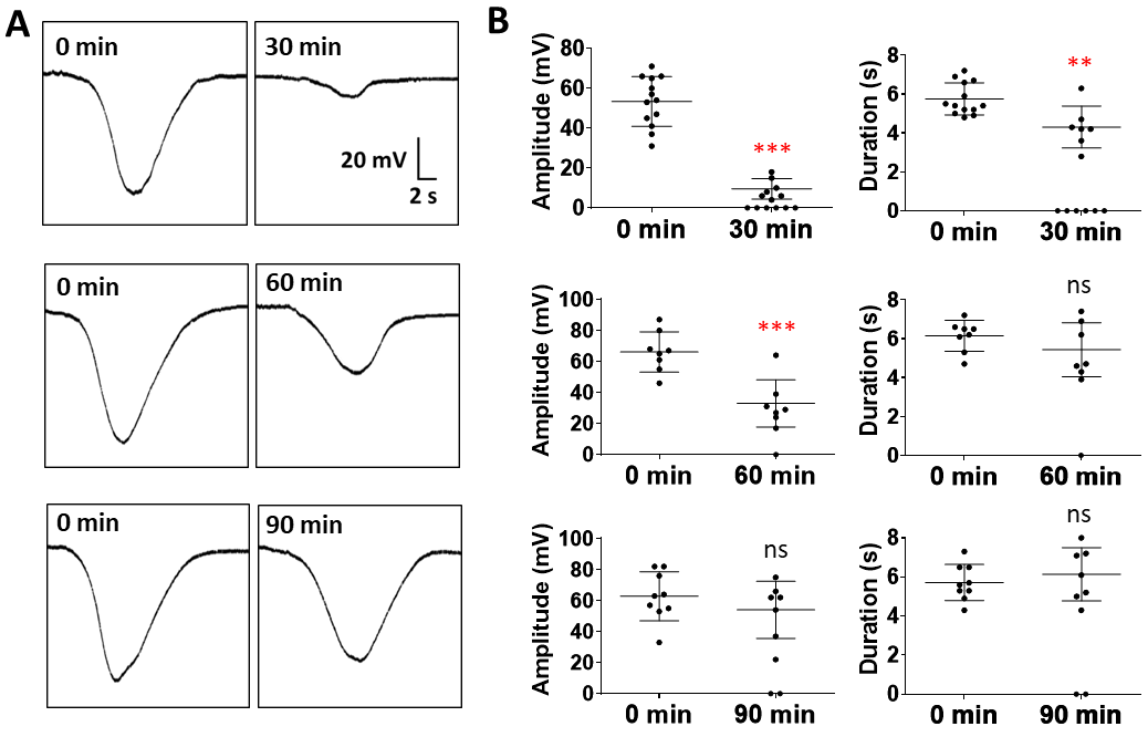

Figure 4.10 The refractory period of mechanostimulation-induced electrical signals. (A) Representative surface potential changes of two consecutive bead (85 mg; 38 mN) stimulations on the same plant with 30, 60 and 90 min intervals. ZT = 6-8 (B) Quantification of amplitude and duration. Bars are means ± SD. (n = 8-13). Student t-test: *** P<0.001. ns = not significant. All the recordings were measured at electrode position E2.

In summary, we successfully standardized a new mechanostimulation method. The novel method allowed us to measure mechanostimulated electrical signals non-invasively. The signals could propagate bi-directionally along the mid-vein. The petiole produced the most pronounced electrical signals measured. Taking the advantage of the assay's robustness, we further identified the threshold of mechanostimulated electrical signals. That showed an all-or-nothing feature in the force threshold. Neither amplitude nor duration correlated with the strength of stimulation. The sharp depolarization, short duration, and all-or-nothing response seemed similar to action potentials. However, the intermediate amplitude signals formed prior

to refraction differed from action potentials. Responsiveness at 30 minutes after the first stimulation was restored, but not fully recovered in the strength of response. It took at least 90 minutes to attain an amplitude like which was stimulated by the first stimulation.

Trichomes are not necessary for leaf mechanosensation

The bead mechanostimulation method was able to generate surface potential changes that were measured from four positions (E1, E2, E1' and E2') on the leaf surface. *Arabidopsis* leaf surfaces have specialized defensive hair cells named trichomes which can sense environmental stimuli (Zhou et al., 2017). Trichomes can concentrate mechanical forces from stimuli and can transmit forces to adjacent skirt cells (Zhou et al., 2017). In that study, compression forces activated cytosolic calcium changes and apoplastic pH changes in the skirt cells around the stimulated trichome. A more recent study found that touch-induced cytosolic calcium changes are not limited to the surrounding skirt cells (Matsumura et al., 2022). Ring-shaped calcium signal waves diffused away from the mechanostimulated trichome with a velocity of approximately 1 μm per second (Figure 4.11)(Matsumura et al., 2022).

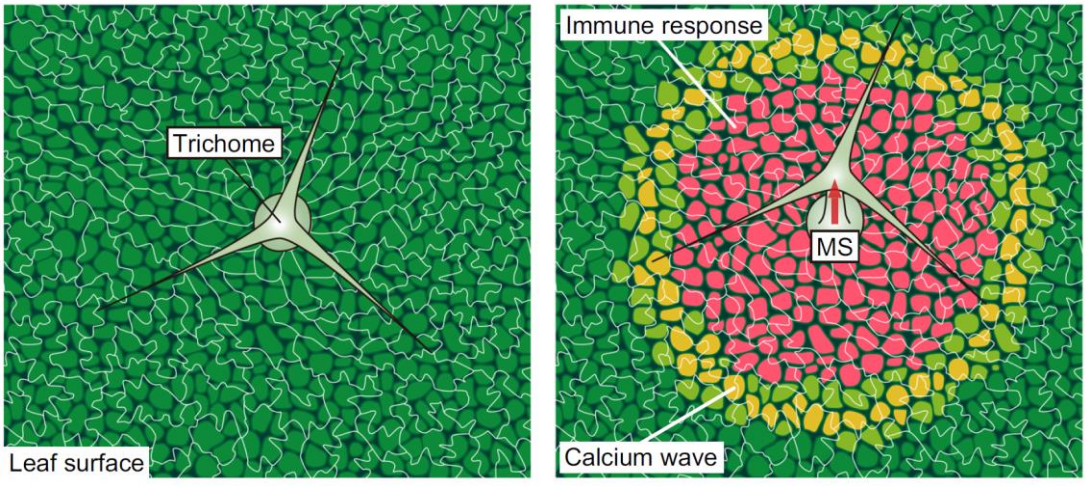

Figure 4.11 Mechanical stimulations trigger calcium waves and immune responses around mechanosensory trichomes (Figure from Matsumura et al., 2022).

Matsumura et al. (2022) showed that the calcium signals induced CAMTA3-dependent immune responses around touched trichomes. Both the touch-induced calcium signals and immune responses were attenuated in the *gl1* mutant which has almost no trichomes on leaf surfaces (Oppenheimer et al., 1991; Matsumura et al., 2022). Therefore, we tested if the mechanostimulation-induced surface potential depended on trichomes. In these experiments, a surface electrode was placed on the E2 position on the stimulated leaf (Figure 4.12A). Interestingly, 38 mN force stimulations triggered similar responses in the WT and in *gl1-1* mutants (Figure 4.12B). The amplitudes and durations were not affected in the *gl1-1* mutant.

This experiment indicated that trichomes do not play an important role in sensing bead-stimulation and in triggering the mechanostimulated surface potentials measured. The mechanostimulation-induced surface potential was different from the mechanostimulation-induced calcium wave. If trichomes were not necessary for sensing mechanostimulation, how are mechanical force transmitted? Also, the velocity of diffusing calcium waves (1 μm per second) was much slower than the velocity of surface potential propagation (1-1.5 mm per second) (Figure 4.7). It is unlikely that transmitting mechanostimulation-induced surface potential relied on the chemical diffusion pathway proposed by Matsumura et al. (2022). If it was not due to chemical diffusion through cell-to-cell connections such as plasmodesmata, would vasculature connections be necessary for this signal propagation? Moreover, could vascular tissues be the mechanical force sensors rather than just a signal transmitting path? Thus, we next investigated the role of vascular tissues in mechanostimulation-induced electrical signals.

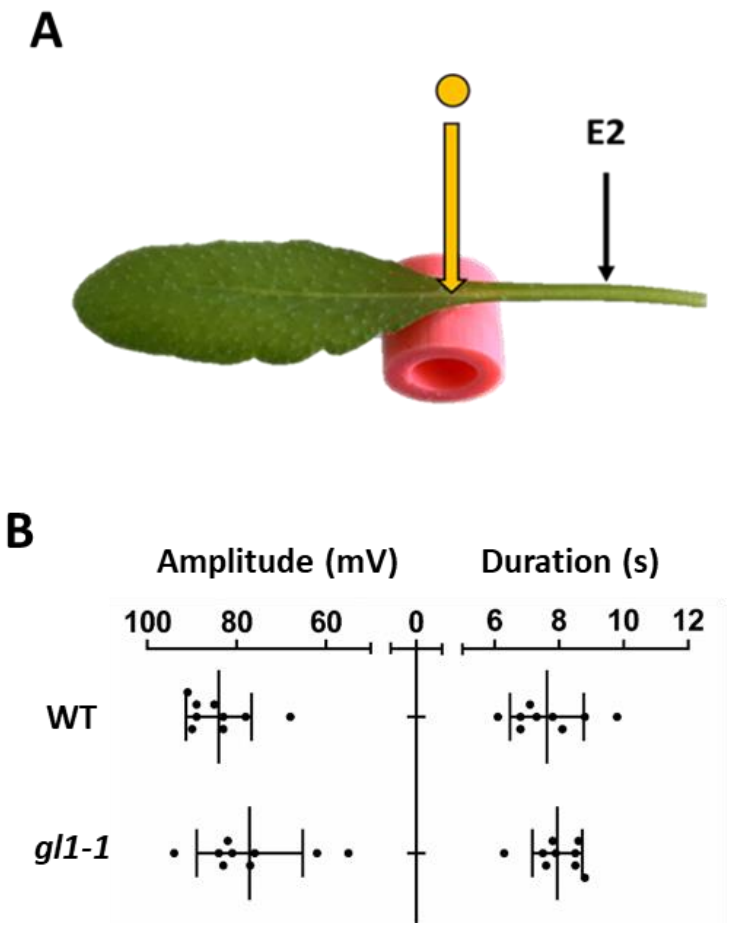

Figure 4.12 Mechanostimulation-induced surface potentials in WT and *gl1*. (A) Experimental design. (B) Surface electrical signals in WT and *gl1-1* elicited in response to 85 mg beads dropped from an elevation of 2 cm (38 mN force) and monitored at electrode position E2. ZT = 6-8. Bars are means ± SD (n = 9). Student t-test: not significant.

Mechanostimulation-triggered electrical signals in the phloem

Mechanostimulation-induced electrical signals had the ability to propagate bi-directionally from E1 to E2 and from E1' to E2' (Figure 4.7). Surface electrodes placed on the center of the leaf lamina and the leaf petiole measured the velocities of electrical signal propagation (6-9 cm per minute). These velocities are similar to the velocities of wound-response slow wave potentials (approximately 8.5 cm per minute; Mousavi et al., 2013) and sieve element wound signals (6 cm per minute; Salvador-Recatala et al., 2014). Regarding the characteristics of the slow wave potential, its long-distance propagation relies heavily on vascular connections between leaves (Mousavi et al., 2013; Nguyen et al., 2018). The amplitudes of the mechanostimulation-induced electrical signals were smaller on the lamina than on the petiole. In theory, the center of the leaf lamina has relatively less concentrated vascular tissues than the petiole. This suggests the mechanostimulated electrical signals are possibly associated with the vascular tissues within the stimulated leaf. More concentrated vascular tissues in the petiole produce a bigger response than the lamina. We then investigated the correlation of mechanostimulated electrical signals with the vascular tissues. Taking advantage of non-invasive recording, surface electrodes could be placed at any position on the leaf surface without the artifacts caused by invasive wounding.

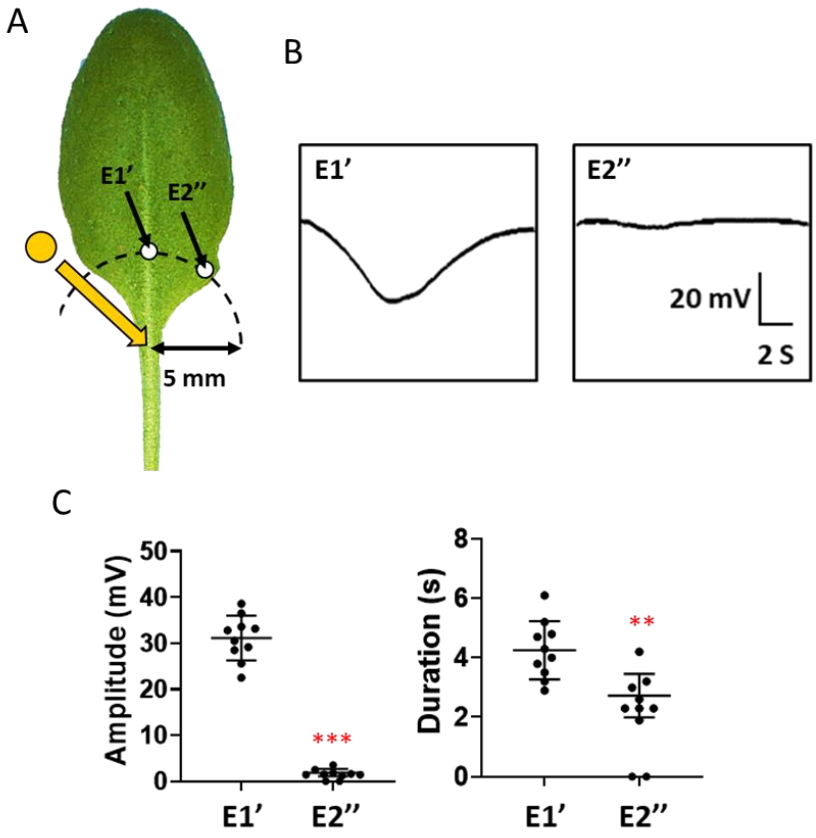

Figure 4.13 Mechanostimulation-induced surface electrical signals are more pronounced at the midvein than at the lamina. (A) Experimental design: E1' and E2'' are the positions of surface electrodes. Electrodes were 5 mm distant from the stimulation site. The support below the stimulation site is not shown. (B) Representative surface potential changes recorded on the stimulated leaf in response to dropping an 85 mg bead from an elevation of 2 cm onto the blade/petiole junction. The force applied was estimated to be 38 mN. ZT = 6-8. (C) Amplitude and duration. Bars are means ± SD. (n = 10). Student t-test: ** P<0.01, *** P<0.001.

Two electrodes, one on the center (E1') and one on the edge (E2''), were placed on the stimulated leaf (Figure 4.13A). Although the edge of the lamina should have some smaller veins still, its vascular cell population must be less than the mid-vein area. Mechanostimulation triggered a ring-shaped calcium wave which diffused out to the surrounding area from the stimulated trichome (Matsumura et al., 2022). Although there was almost no difference found

in the *gl1-1* mutant, the mechanostimulation-induced surface potential could still, in theory, propagate by a similar diffusion pathway (Figure 4.12B). Two electrodes were placed in a 5-mm-distance radius away from the bead mechanostimulation site (Figure 4.13A). If the mechanostimulated signal depended on the diffusion pathway, like the surface calcium waves, the measured signal would be similar in strength within these two electrodes. Strikingly, mechanostimulated electrical signals appeared to be more associated with propagation in vascular tissues than by diffusion (Figure 4.13B). Although there were weak signals measured from the edge of the leaf (E2’’), they did not compete with the stronger signals measured from the center of the leaf lamina (E1’) (Figure 4.13C). When quantified, mechanostimulation-induced electrical signals from E1’ were ten times stronger in amplitude than signals from E2’’. Moreover, the time durations were approximately twice longer compared E1’ and E2’’. These experiments suggested that the mechanostimulation-induced electrical signal was highly associated with the main vasculature. A very weak electrical signal was measured from E2’’, which might be a signal similar to the mechanostimulated surface calcium wave (Matsumura et al., 2022). But the signal found in E2’’ was much weaker than the signal found in E1’. Therefore, the mechanostimulated surface potential found in our new mechanostimulation method was most likely not related to calcium diffusion waves on the leaf surface. In conclusion, these data suggested that the grouped vascular tissues in veins appeared to be the major factor controlling the strength of mechanostimulated surface potentials (Figure 4.8 and Figure 4.13C).

Mechanostimulation-triggered electrical signals (surface potentials) were associated with the main vasculature. The velocity of mechanostimulated electrical signals was similar to the velocities of wound-induced slow wave potentials and sieve element wound signals (Mousavi et al., 2013; Salvador-Recatala et al., 2014). Since our new mechanostimulation method was robust and flexible enough, we were tempted to apply it with living-aphid

electrodes to probe phloem sieve-element specific electrical signals (Salvador-Recatala et al., 2014). Because aphids preferred to feed in the lamina, an electrode placement close to E1' position was chosen (Figure 4.6 and Figure 4.14). The bead stimulation site was approximately 1 cm away from the aphid to avoid interference (Figure 4.14A). A gold wire was glued to the back of the aphid to connect with the measuring electrode (Figure 4.14B). Since any touch might possibly trigger mechanostimulated responses, the aphid electrode was gently placed back to the measuring site while it moved away. The aphids then settled to feed. By reading the signatures of the electrical signal, it was possible to distinguish that the aphid was feeding on the sieve element or on other cell types (Figure 4.15) (Tjallingii, 1990). Occasionally, the aphid might feed on the xylem but this occurred much more rarely than phloem feeding. Sieve element wound signals were measured during the phloem-feeding phase (Salvador-Recatala et al., 2014).

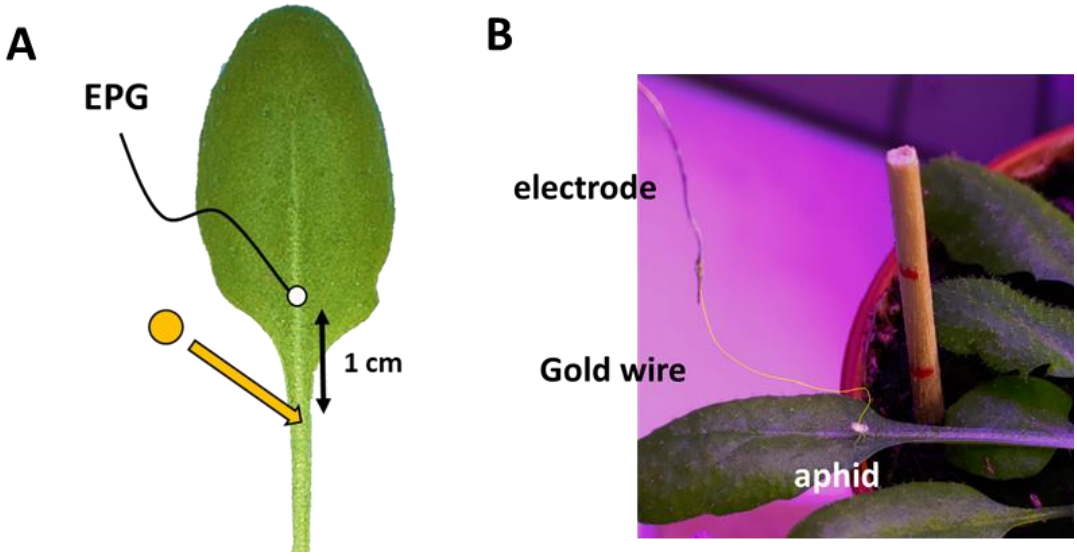

Figure 4.14 Measurement of the mechanostimulation-triggered electrical signal with living aphids. (A) Experimental design: the aphid electrode was feeding on the mid-vein in the lamina, which corresponding to the E1' position (Figure 4.13). A 170 mg bead was used to stimulate the petiole 1 cm away from the feeding aphid. Note that no support was placed under the leaf. (B) Photo of an aphid electrode.

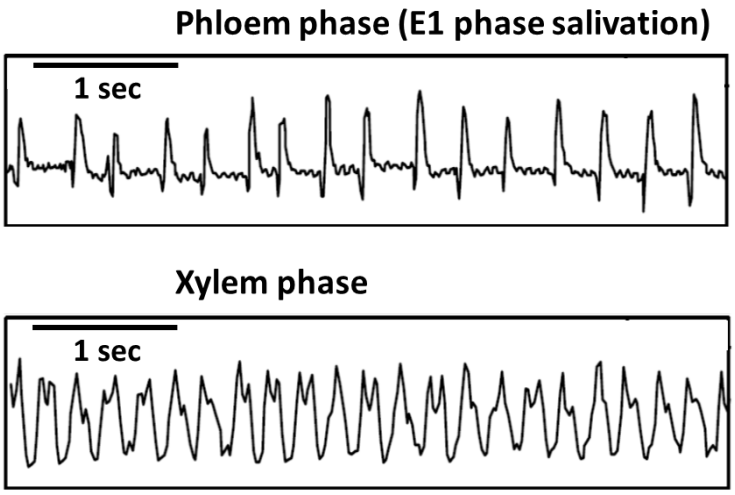

Figure 4.15 The EPG electrical signal signature in phloem feeding phase. (Figure from Tjallingii, 1990.)

Fortunately, aphids were not very sensitive to the movement of mechanostimulated leaves. Even if 170 mg (5 mm) beads were used, mechanostimulation didn't disrupt the feeding behavior and sieve element mechanostimulated signals were recorded successfully (Figure 4.16A). This is the first time that a touch-induced electrical signal has been measured from vascular tissues. Black arrowheads in Fig. 4.16A and B indicate the touch artifact during bead mechanostimulation. Compared with the sieve element wound signal, the mechanostimulated signal had only a sharp depolarization peak, without a slow phase (Salvador-Recatala et al., 2014). The shape of the mechanostimulated signal from the sieve element was similar to that of the mechanostimulated surface potential (Figure 4.16B). However, we found that the sieve element signal was shorter in time duration than the surface potential. These two types of measurement from approximately similar E1' positions were similar in the amplitude but different in the duration. There was no statistically significant difference in the amplitude. This was consistent with the other two experiments, in which the height of amplitude depended on the position of measuring (Figure 4.8 and Figure 4.13). In summary, those data clearly showed

that the duration of surface potentials was more than two times longer compared to the duration of the sieve element signal (Figure 4.17). This difference in duration suggests the sieve element mechanostimulated signal was a novel signal, which may not have been described previously. Considering the surface potential might be the summation of electrical potential changes captured with the surface electrode on its measuring position, the mechanostimulated sieve element signal could be a component of mechanostimulated surface potential. In this scenario, additional cell types to sieve elements within the vascular bundle would be responsive to bead mechanostimulations.

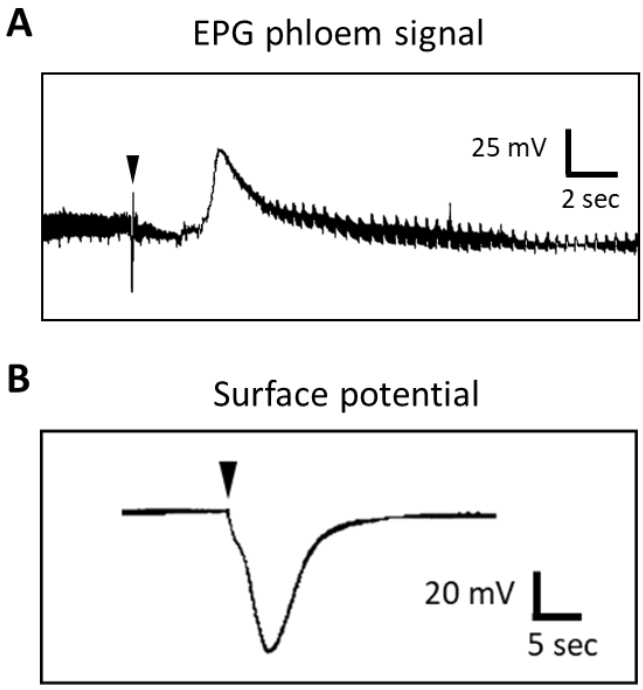

Figure 4.16 Two types of mechanostimulation-induced electrical signal. (A) Electrical signals from phloem SEs were recorded with living aphid electrodes. (B) Surface potentials recorded with surface electrodes. In both cases, a 170 mg bead was dropped 2 cm onto the petiole of the measured leaf. For surface potential measurements, leaves are supported, however leaves were unsupported for EPG measurements. Black arrowheads indicate the moment of stimulation. Note that the upward direction of the sieve element signal was due to intracellular recording. The downward direction of surface potential was due to extracellular recording.

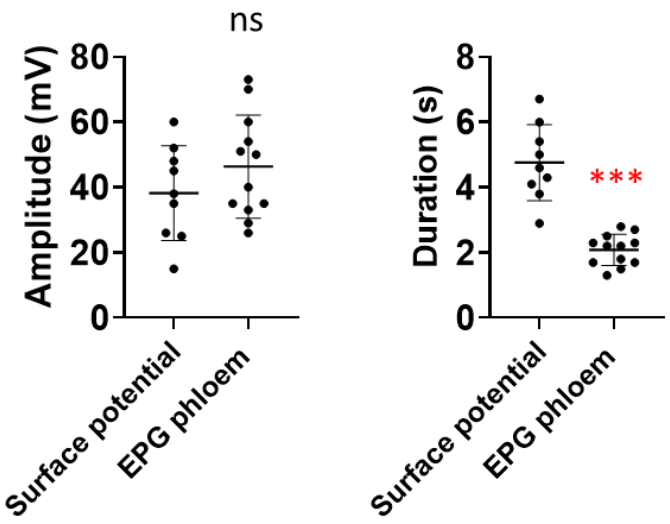

Figure 4.17 Quantification of amplitude and duration of mechanostimulation-induced electrical signals. In both cases, a 170 mg bead was dropped 2 cm onto the petiole of the measured leaf. For surface potential measurements, leaves are supported, however leaves were unsupported for EPG measurements. Surface electrode: n=9; phloem: n=12. Error bars are mean ± SD. Student t test: *** P<0.001, ns = not significant.

In this study, mechanostimulation triggered electrical signals in the vascular tissue were investigated for the first time. Experiments using surface electrodes showed that the mechanostimulated surface potential is heavily dependent on the main vein (Figure 4.13). This indicated that the surface potential was not similar to the epidermal touch-triggered diffusing calcium wave reported by Matsumura et al. (2022). However, the diffusing calcium wave could be similar to the mechanostimulated surface potential found in the leaf edge (E2’’). The amplitudes measured from E1’ position are much bigger than E2’’. Using the living aphid electrode, a unique mechanostimulation-triggered sieve element signal was successfully recorded. The sharp-peak shape of the sieve element mechanostimulated signal was similar to mechanostimulated surface potential. The duration of the sieve element signal was quite different from the surface potential. Moreover, in both cases, the surface potential and the sieve

element signal, we found that the vascular tissues are very important in sensing and responding to mechanical stimulations.

Time – an extra dimension

Mechanostimulation-induced surface potentials differed in the amplitudes within different electrode positions (E1, E2, E1', E2' and E2''; Figure 4.8 and Figure 4.13). Among these experiments, approximately 20-50 % of the plants didn't respond to our mechanostimulations. We found that the experiments conducted in the early afternoon would have more insensitive plants than experiments conducted in the later afternoon. Also, in our experiments, no mechanostimulation-induced electrical signals were ever successfully measured in the morning. This was a very strong hint which suggested an undiscovered factor underlying such a characteristic: the time of day.

Would that be the reason why the plants were more sensitive in the later afternoon? To investigate this, we measured the mechanostimulations-induced surface potentials at 11:00, 12:00, 14:00, and 16:00 along the time of day. In the short-day growth room, lights were on from 8:00 (Zeitgeber Time) until 18:00. The time points tested represented 3 hours, 4 hours, 6 hours, and 8 hours after Zeitgeber Time. Electrode position E2 on the leaf petiole was used to monitor the most pronounced response (Figure 4.8). Strikingly, we found the responsiveness of mechanostimulated surface potentials does depend on the time of day (Figure 4.18). Consistent with the previous impression, no mechanostimulated surface potential was measured at 11:00. Few plants (2 out of 7) began to be sensible at 12:00, but the mechanostimulated signals were small in amplitude. The responsiveness then increased up to 75 % (6 out of 8) of plants at 14:00. Until 16:00, all the plants were able to respond to the bead mechanostimulation. The amplitudes and durations were similar between 14:00 and 16:00.

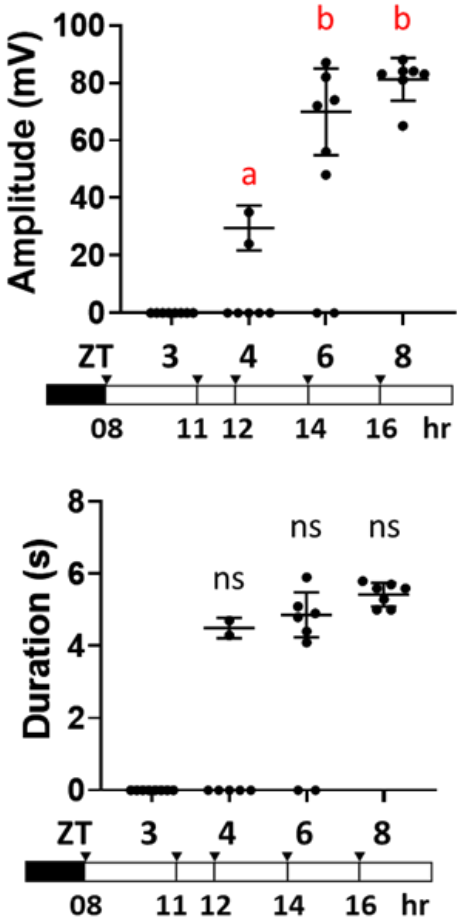

Figure 4.18 Responsiveness to mechanostimulation depends on the time of day. Amplitude and duration of mechanostimulation-induced surface potential changes at 11:00, 12:00, 14:00, and 16:00 which represent the time points of 3hr, 4hr, 6hr, and 8hr after Zeitgeber Time (ZT). Bars are means ± SD (n = 7-8). Letters indicate significant differences, Tukey HSD test: $P<0.05$. Data were from 2 combined experiments (one for 11:00/14:00 and one for 12:00/16:00). Plants were stimulated with 85 mg borosilicate beads dropped from 2 cm elevations onto lamina/petiole junctions of leaf 8 producing estimated forces of 38 mN. Electrical signals were monitored at electrode position E2.

Conclusion and Discussion:

In this chapter, we firstly developed a new mechanostimulation method. The new method was more quantitative than brushing, spraying, and bending (Chehab et al., 2012; Moerkercke et al., 2019; Matsumura et al., 2022). Mechanostimulated surface potentials were

recorded with non-invasive electrodes. The signal we observed could be propagated bi-directionally along the mid-vein. The most pronounced signals were found on the basipetal midvein at the E1 and E2 positions on the petiole. Towards the leaf tip, from the E1' to the E2' positions in the lamina, mechanostimulated surface potentials had a trend of decreasing in amplitude. Trichomes had almost no role in this signal. Mechanostimulated surface potentials were tightly associated with the mid-vein vasculature. Tiny signals were found at the leaf edge, which might correlate to the calcium wave diffusion (Matsumura et al., 2022). Sieve element mechanostimulated signals were measured with the EPG system. Their amplitudes were similar to mechanostimulated surface potentials at a similar measuring position, but the durations were significantly shorter. These results suggest that vascular tissues, especially phloem, have an essential role in sensing and responding to mechanostimulations.

Taking advantage of this new mechanostimulation method, we investigated the threshold of mechanostimulated surface potentials with 2 mm, 3 mm, 4 mm, and 5 mm diameter borosilicate beads. 3 mN estimated force applied from 2 mm beads reached the threshold to trigger mechanostimulated surface potential. This signal required at least 30 minutes to be able to respond weakly for the second time. For a full response, 90 minutes of rest was needed. Also, we found the responsiveness of mechanostimulated surface potential heavily depends on the time of day. No signal could be triggered at 11:00 (3 hours after Zeitgeber Time). In short-day growth conditions, *Arabidopsis* became sensible to mechanostimulation at 12:00. The response at 12:00 was as weak as the 30 minutes time point after first stimulation. Responsiveness to mechanostimulation continued to increased up to 100 % after 14:00. Surface potentials recorded at 14:00 and 16:00 were similar in both amplitude and duration.

Our results suggest that vascular tissues might have a touch-sensitive physiology which is associated with the time of day. Whether or not this special physiology correlated to circadian

rhythm needed to be investigated. It has been found that low temperature-induced increases in free cytosolic calcium in *Arabidopsis* guard cells correlated with circadian rhythms (Dodd et al., 2006). Furthermore, a more recent study showed circadian modulation of dark-induced free calcium in the chloroplast and cytosol of *Arabidopsis* (Marti et al., 2020). These studies suggested that circadian rhythms might have a role in gating cation movement in plant cells. To depolarize a membrane, neutralizing the charge transfer across the membrane was required. The resting plasma membrane has more positive charges on the outside (apoplast) and more negative charges on the inside (cytosol) (Sze et al., 1999). There are many ways to neutralize membrane potentials, for example, positive charges (eg. protons) could either cross the plasma membrane or negative charges (eg. Cl^- or NO_3^-) could be released from cellular compartments to the cytosol or expelled from the cell. The major mechanism driving the depolarization of plasma membrane in the vascular tissues is not yet known. The vasculature-dependent, mechanostimulation-induced electrical signal which was characterized in this chapter might have potential to address such questions. Moreover, the 3 mN force was the threshold of the mechanostimulation-induced electrical signal. It was similar to the force of a wind of Beaufort scale 3 applied to a 2 cm^2 leaf area. A windy environment repeatedly triggered mechanostimulation-induced responses might delay the inflorescence development like repeat leaf bending (Chehab et al., 2012; Darwish et al., 2022). Therefore, the threshold of mechanostimulation-induced responses would be critical for determining if an environment was ideal for *Arabidopsis* growth. Also, the caterpillar (*Pieris brassicae*) walking-induced GCaMP3 signals on the leaf surface but not in the vasculature (Figure 4.1). That suggested the walking behavior exceeds the threshold sensitivity of the leaf surface but not in the vascular tissue. These thresholds might be able to distinguish if the aggressor was passing by on the surface or if the aggressor was approaching the vascular tissues. Vascular tissues are the key for the

jasmonate-dependent growth regulation (Yang et al., 2020). Thus, the plant could better control the balance of growth and defense with an appropriate mechanosensitivity threshold. These would be the reasons why the threshold of mechanostimulation-induced responses is important.

Chapter 5: MECHANOSTIMULATED ELECTRICAL SIGNALS DEPEND ON PROTON PUMPS

Introduction:

Among the well-known mechanosensitive plants, Venus flytrap (*Dionaea muscipula*) has sensory hairs on the inside of its traps. Touching the sensory hairs induces traps closure that captures insects for nutrient supply (Figure 5.1 from Hedrich and Neher, 2018). This mechanism was known for more than a hundred years to be triggered by two consecutive mechanical stimulations to the sensory hairs (Forterre et al., 2005; Hedrich and Neher, 2018). To excite trap closure, these two touches should be applied within a 30 second interval. A recent study models Venus flytrap with the electrochemical charge buildup and predicts the closure movement of traps could be possibly triggered with a single stimulation (Burri et al., 2020). Additionally, mechanostimulation firstly triggers an action potential prior to inducing the trap closure (Stuhlman and Darden, 1950; Forterre et al., 2005). However, the location of sensory hairs is difficult to access with borosilicate beads. Therefore, the Venus flytrap would not be an ideal plant to examine with our bead mechanostimulation method.

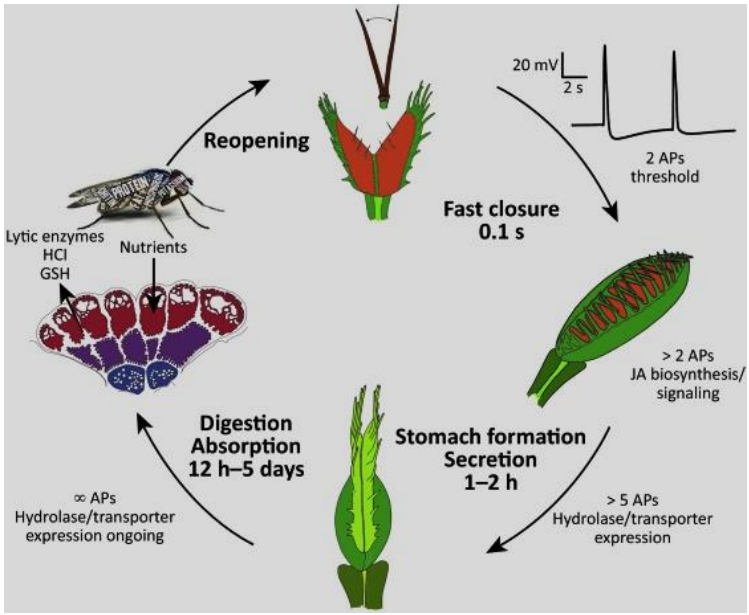

Figure 5.1 Closure and reopening cycle of the Venus flytrap. Two consecutive action potentials trigger trap closure. After the digestion and absorption process, the trap slowly reopens (Figure from Hedrich and Neher, 2018).

Another famous mechanosensitive plant is *Mimosa pudica*. Its leaves have many leaflets connected to the petiole with pulvini (Figure 5.2). Touching leaflets and petioles can induce leaflet closure and downward movements of petioles. Subsequently, it undergoes a slow recovery phase until reopening the leaflets and lifting up the petioles (Bose, 1927). This movement is thought to avoid herbivory by reducing visibility (Bose, 1926). Similar wound-induced movements of *Arabidopsis* leaf petioles were observed recently by Kurenda et al. (2019). Like many other plants, *Mimosa* leaves open in the morning and close at night, based on circadian rhythms (Ueda and Nakamura, 2007). Testing the mechanostimulated movements in *Mimosa* might provide new insights into the time-associated responsiveness. Therefore, prior to studying *Arabidopsis* in more detail, we applied bead mechanostimulations to *Mimosa pudica* plants.

Figure 5.2 A greenhouse grown *Mimosa pudica* plant over 1-year old.

Mechanostimulation-induced surface potentials in *Arabidopsis* were characterized and standardized in Chapter 4. Using *Mimosa pudica* we investigated whether mechano-responsiveness depended on the time of day. The best characterized mechanism regulating the time or light-dependent physiologies is the circadian clock (Nohales and Kay, 2016). It is controlled by transcriptional regulators such as MYB-like transcription factors (Alabadi et al., 2001). The day-night cycle is regulated with transcription factors negatively regulating each other and evening complex proteins repressing the transcription factors (Zhu et al., 2022). Mutations affecting the circadian clock lead to clock arrhythmia (Alabadi et al., 2001). Investigating mechanostimulated responses in circadian clock mutants might reveal the time dependent feature further.

Results:

Mechanostimulated movement in *Mimosa pudica*

In order to test bead mechanostimulations in *Mimosa*, newly germinated seedlings were grown in the greenhouse until 7 weeks old (Figure 5.3). The 7-week-old *Mimosa* plants were much smaller than the 1-year-old *Mimosa* shown in Figure 5.2. Considering the effect of juvenile-to-adult transition, juvenile and adult leaves might have different sensitivities to touch. In *Arabidopsis*, leaf 7 is the first adult leaf which shaped differently from the juvenile leaves. We found the shape of leaves 1-5 differed from leaf 7 in *Mimosa pudica* as well (Figure 5.3). Thus, leaves emerged after leaf 7 we named as adult leaves. Both leaf 5 and adult leaf were tested with bead mechanostimulation accordingly (Figure 5.4 A and B). Strikingly, a 4 mm (85 mg) borosilicate bead dropped from 2 cm elevation at 16:00 (ZT=8) could trigger leaflets closure in both leaf 5 and in adult leaves (Figure 5.5 A and B). However, the movement of the

petiole was not consistent among stimulated leaves. We therefore focused on mechanostimulation-triggered leaflet closure in the following experiments.

Figure 5.3 A greenhouse grown 7-week-old *Mimosa pudica* plant.

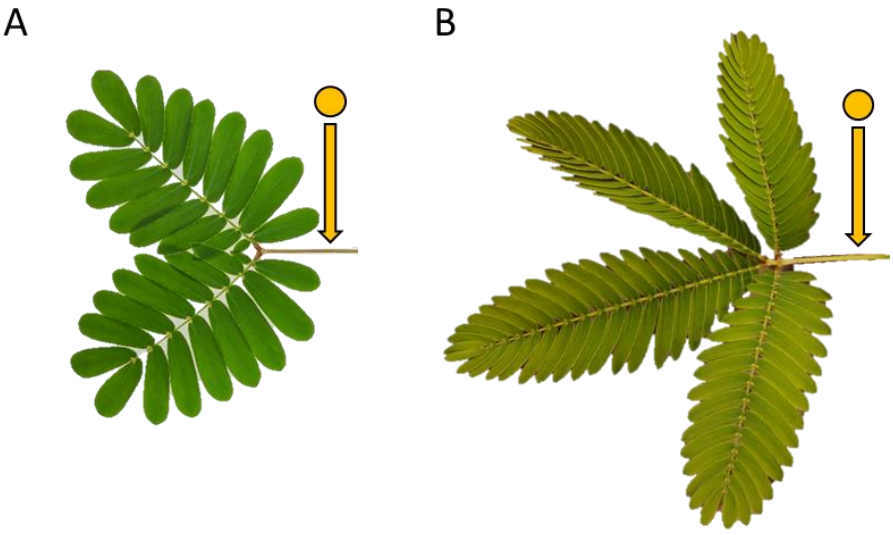

Figure 5.4 Experimental design of mechanostimulation in *Mimosa*. 85 mg beads were dropped from 2 cm onto the unsupported petioles of (A) Leaf 5 of a 7-weeks old plant (B) A leaf of 1-year-old plant.

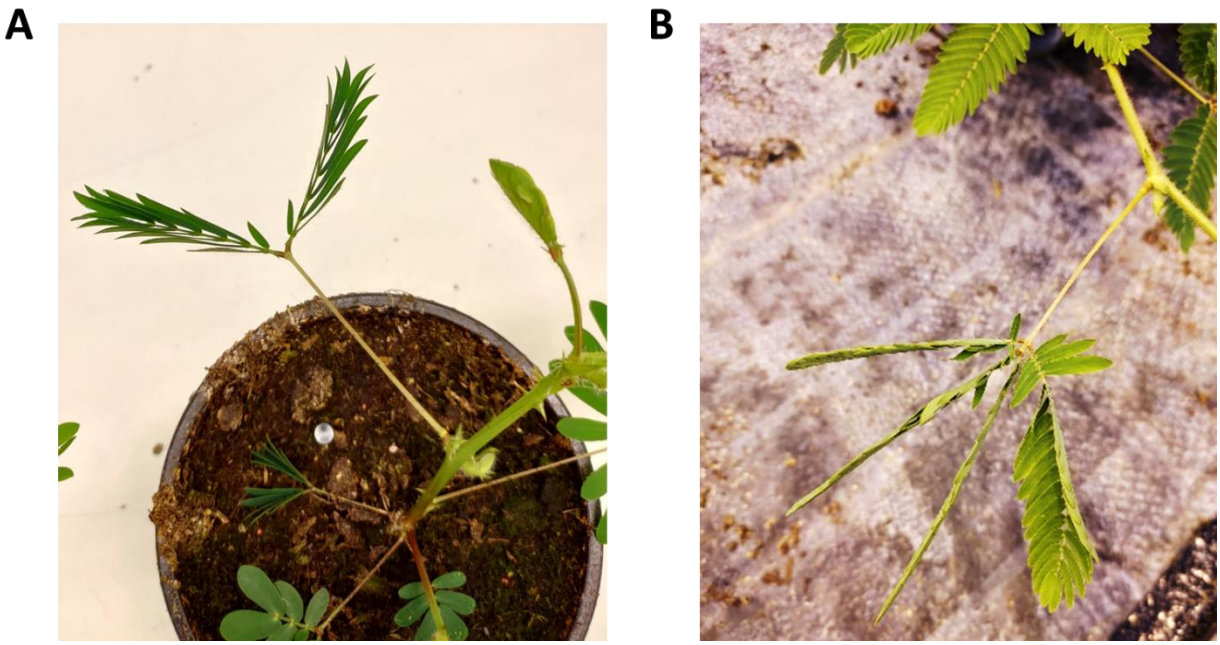

Figure 5.5 Mechanosimulation-induced leaflets closure in *Mimosa pudica*. The petioles of (A) leaf 5 (B) adult leaf was stimulated with 4 mm (85 mg) borosilicate beads in the afternoon. These experiments were performed in the greenhouse.

We first compared mechanostimulation-induced leaflet movements in leaves 5 of 7-week-old *M. pudica* plants. Strikingly, the responses in the morning were significantly different from the responses in the afternoon (Figure 5.6 A and B). On average, we found around 60 % of leaflets were mechanosensitive in the morning whereas more than 80 % of leaflets moved in the afternoon (Figure 5.7). This observation was replicated and on two plants showed all the leaflets on the same leaf were triggered by single stimulation in the afternoon. The folded leaflets can be quantified easily. This is an advantage of using *Mimosa* in mechanostimulation experiments. In summary, these data indicated that the responsiveness to mechanostimulation in the young *M. pudica* leaf is depended on the time of day.

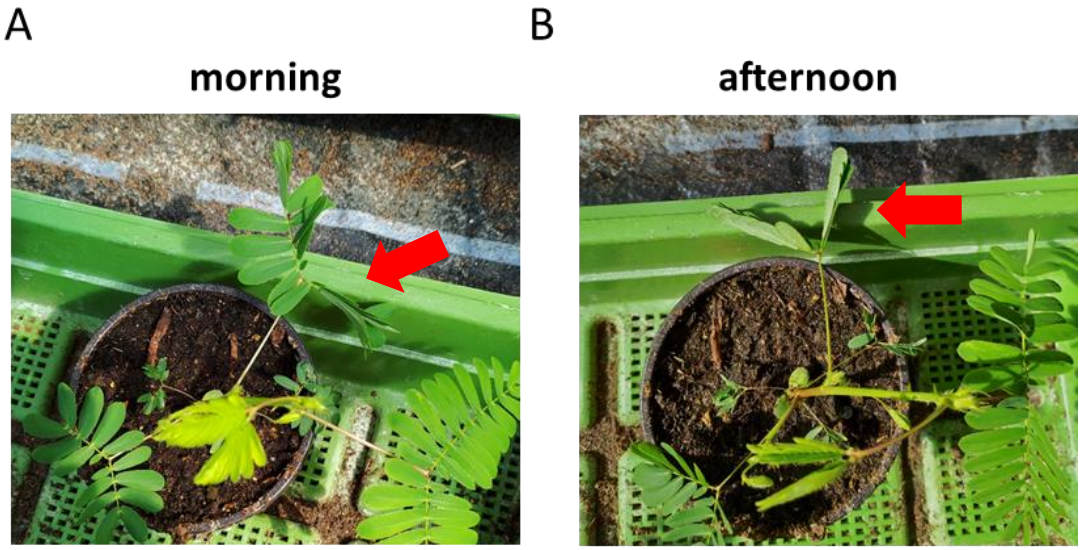

Figure 5.6 Mechanostimulated leaflet movement in 7-weeks old *Mimosa pudica*. (A) leaf 5 mechanostimulated in the morning (B) leaf 5 mechanostimulated in the afternoon.

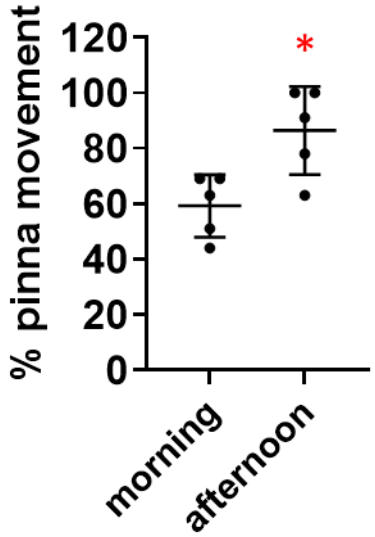

Figure 5.7 Quantification of mechanostimulated leaflet movement in 7-week-old *M. pudica*. 4 mm diameter bead weighing on average 85 mg were dropped onto petioles. The moved leaflets were calculated by excluding the unmoved leaflets from the total leaflets. Percentage of moved by total leaflets were shown. Bars are means ± SD (n = 5). Student *t*-test: * $P<0.05$ (n = 5).

We next investigated whether mechanostimulation responses were similarly affected by the time of day in older plants. Three independent leaves in the 1-year-old *Mimosa* were tested on two independent days. Each independent leaf stimulated in one day was counted as one

biological replicate. Consistently, more leaflets were mechanosensitive in the afternoon than in the morning (Figure 5.8A and B). About 20 % of leaflets responded in the morning and 70 % of leaflets responded in the afternoon (Figure 5.9). This difference was statistically significant. However, the responding-leaflet percentages were less compared to leaves 5 of the younger plants. This might be because the adult leaves have thicker and stiffer petioles. The stiffness and thickness of the petiole might increase the threshold (resistance) of mechanostimulation-triggered responses. Collectively, the findings in *Mimosa* showed that mechanostimulation-induced responses are affected by the time of day and are likely to independent of the juvenile-to-adult transition because similar responses were found in young and old plants.

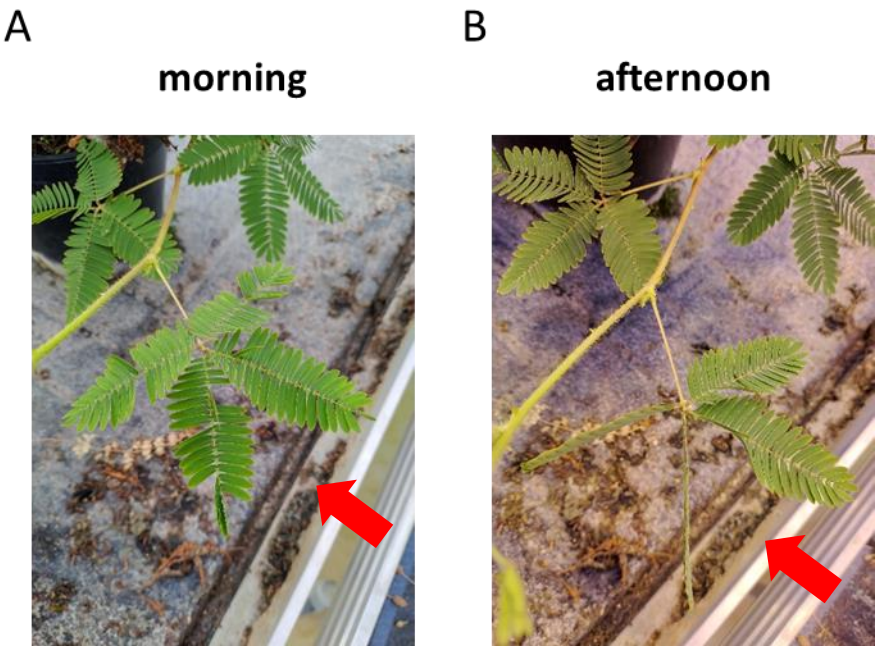

Figure 5.8 Mechanostimulated leaflet movement in 1-year-old *Mimosa pudica*. The mechanostimulated leaf (A) in the morning (B) in the afternoon.

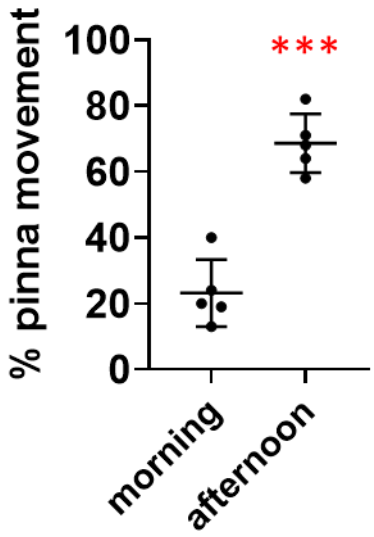

Figure 5.9 Quantification of mechanostimulated leaflet movement in 1-year-old *Mimosa*. The moved leaflets were calculated by excluding the unmoved leaflets from the total leaflets. Percentage of moved by total leaflets were shown. Bars are means ± SD (n = 5). Student *t*-test: *** P<0.001 (n = 5).

Arabidopsis elf3 mutants have increased mechano-responsiveness:

Mechanostimulated responses were consistently associated with the time of day both in *Arabidopsis* and *Mimosa*. Since the circadian clock is a crucial mechanism controlling day-night physiology, we investigated whether this clock has a role in time-dependent mechanostimulated responses. Mutation of the evening complex protein, EARLY FLOWERING 3 (ELF3), lead to the loss of circadian rhythm (McWatters et al., 2000). The *elf3* mutant plants under continuous light have an early flowering phenotype and increased hypocotyl elongation relative to the WT (Zagotta et al., 1992; Hicks et al., 1996). We hypothesized that the *elf3* mutant would either lose mechano-responsiveness due to the no night-loop building up, or increase in responsiveness throughout the daytime due to a continuous day-loop. All of the 5-week-old *elf3* mutants had long and thin petioles in short-day condition (Figure 5.10). Besides the petiole, *elf3* had only a few fully expanded leaves at 5-weeks old. It was not possible to do mechanostimulation on leaf 8 like in WT. Furthermore,

many of the 5-week-old *elf3* plants developed inflorescence stems, which make experiments difficult.

Figure 5.10 5-week-old WT and *elf3-1* plants grown under short-day conditions.

For better handling of the flowering *elf3* plants, inflorescence stems were carefully fixed to pipette tips a day prior experiments (Figure 5.11A). Because the *elf3* plants didn't develop as the many leaves as WT under short-day conditions, fully expanded leaves were used for mechanostimulations. Surprisingly, more than half of *elf3* plants (five out of eight) were able to respond to mechanostimulations in the morning (Figure 5.11C). WT plants, however, were consistently completely insensitive to mechanostimulation at this time. This showed that, compared to the WT, mechano-responsiveness was much increased in *elf3*. Interestingly, at 16:00, all the *elf3* and WT plants responded to mechanostimulation (Figure 5.11D), but WT plants had higher amplitudes than *elf3* in the afternoon. However, no difference was found in signal durations. Signal amplitudes at both time points (ZT = 3 and 8) in *elf3* were rather similar (Figure 5.11C and D). This suggested that the strength of mechanostimulated-response was not

altered by the time of day in *elf3*. *elf3* mutants were able to give a full-strength mechanostimulated response in the morning. Furthermore, mechano-responsiveness was increased in *elf3* in the afternoon. This indicated that, although the circadian clock was partially arrhythmic in *elf3*, the responsiveness to mechanostimulation was still regulated by the time of day.

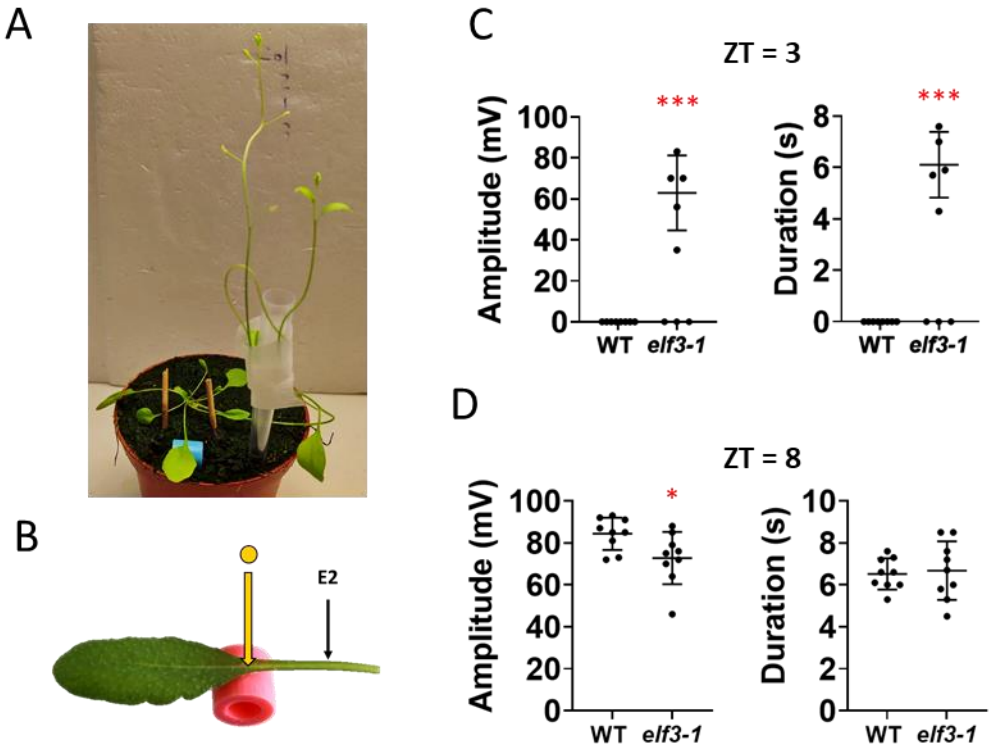

Figure 5.11 The responsiveness to mechanostimulation-triggered electrical signal is increased in *elf3-1*. (A) A fixed 5-week-old *elf3-1* plant. (B) Experimental design. Mechanostimulation-induced surface potential recorded at (C) 11:00 (ZT=3) (D) 16:00 (ZT=8) time points. The force exerted by the 4 mm bead was estimated to be 38 mN. Bars are means ± SD (n = 8-9). Student t-test: * P<0.05; *** P<0.001.

The constitutively active proton pump mutant *ost2-2D* attenuated mechanostimulated signals:

Mechano-responsiveness associated with the time of day was found in both *Arabidopsis* and *Mimosa pudica.* Plasma membrane proton pumps (H^+-ATPases) in *M. pudica* are thought to regulate leaf movements and proton/ion fluxes. Pulvinar motor cells in this plant have high proton pump expression levels and high transmembrane potentials (Fleurat-Lessard et al., 1997). Also, pulvinus phloem companion cells and parenchyma cells have a high density of plasma membrane proton pumps. Pulvinar cells are important in regulating leaf positions. Plasma membrane proton pumps can help motor cells to recover the ionic gradient across the plasma membrane. Furthermore, proton pump activities were found to differ during circadian leaflet movements in *Samanea* (Lee and Satter, 1987).

In *Arabidopsis*, the *elf3* mutation which causes circadian clock dysregulation increases mechano-responsiveness in the morning. This indicates that the circadian clock has a significant effects on mechano-responsiveness. Besides its circadian clock, *elf3* can also restore plasma membrane proton pump activities in the phototropin mutant background (*phot1 phot2*) (Kinoshita et al., 2011). *phot1 phot2* lacks the blue light receptor kinases which phosphorylate the C-terminus of plasma membrane proton pumps under blue light stimulation (Kinoshita et al., 2001). Phosphorylations of plasma membrane proton pumps allow 14-3-3 proteins binding to the auto-inhibitory domain which is important for proton pump activation (Kinoshita and Shimazaki, 1999). The phosphorylation of plasma membrane proton pumps is much increased in *phot1 phot2 elf3* relative to the WT (Kinoshita et al., 2011). This leads to stomata opening which reverses the stomata closure phenotype in *phot1 phot2.* This evidence suggested that the underlying proton pump activity might be associated with the phenotype in *elf3.*

The plasma membrane proton pump AHA1 is a major proton pump which is most strongly expressed in the vasculature (Kumari et al., 2019). A constitutively active mutant of AHA1, *open stomata2* (*ost2-2D*), increases AHA1 activity (Merlot et al., 2007). We thus used the *ost2-2D* mutant to test whether the activity of plasma membrane proton pump is important for mechanostimulated electrical signals. Firstly, we observed no strong phenotype of the rosette of 5-week-old *ost2-2D* (Figure 5.12A). Mechanostimulations were applied to leaves 8 of the WT and *ost2-2D* (Figure 5.12B). Interestingly, constitutively active AHA1 did not increase the responsiveness to mechanostimulation in the morning (Figure 5.12 C). All of the WT and *ost2-2D* plants were completely insensitive at 11:00 (ZT=3). These results suggested that either the increased responsiveness in *elf3* is not due to proton pump activity or the constitutively active proton pump form is different from the phosphorylated form.

To further test the importance of plasma membrane proton pumps in mechanostimulated electrical signals, we then examine the responses at the other time points. Surprisingly, in the afternoon, mechanostimulated electrical signals were hugely decreased in *ost2-2D* (Figure 5.12 D and E). Signal amplitudes in *ost2-2D* were below 20 mV on average at 14:00 and below 40 mV on average at 16:00, while WT had normally 60-80 mV amplitudes in the afternoon. Also, durations were statistically significantly decreased in *ost2-2D*. This indicates that plasma membrane proton pump activities are important for mechanostimulation-induced electrical signalling. Plasma membrane proton pumps are under tight regulation. The phosphorylated C-terminal auto-inhibitory domain recruits 14-3-3 binding which activate the proton pump (Kinoshita and Shimazaki, 1999). Dephosphorylation releases the auto-inhibitory domain from 14-3-3 proteins and this reduces the activity of the proton pump (Spartz et al., 2014). The fact that *ost2-2D* did not change mechano-responsiveness in the morning might be because of the difference between this constitutively active mutation and increased phosphorylation. That is,

phosphorylations could be further regulated by dephosphorylations but the constitutively active mutation could not be regulated by phosphorylations (Haruta et al., 2015).

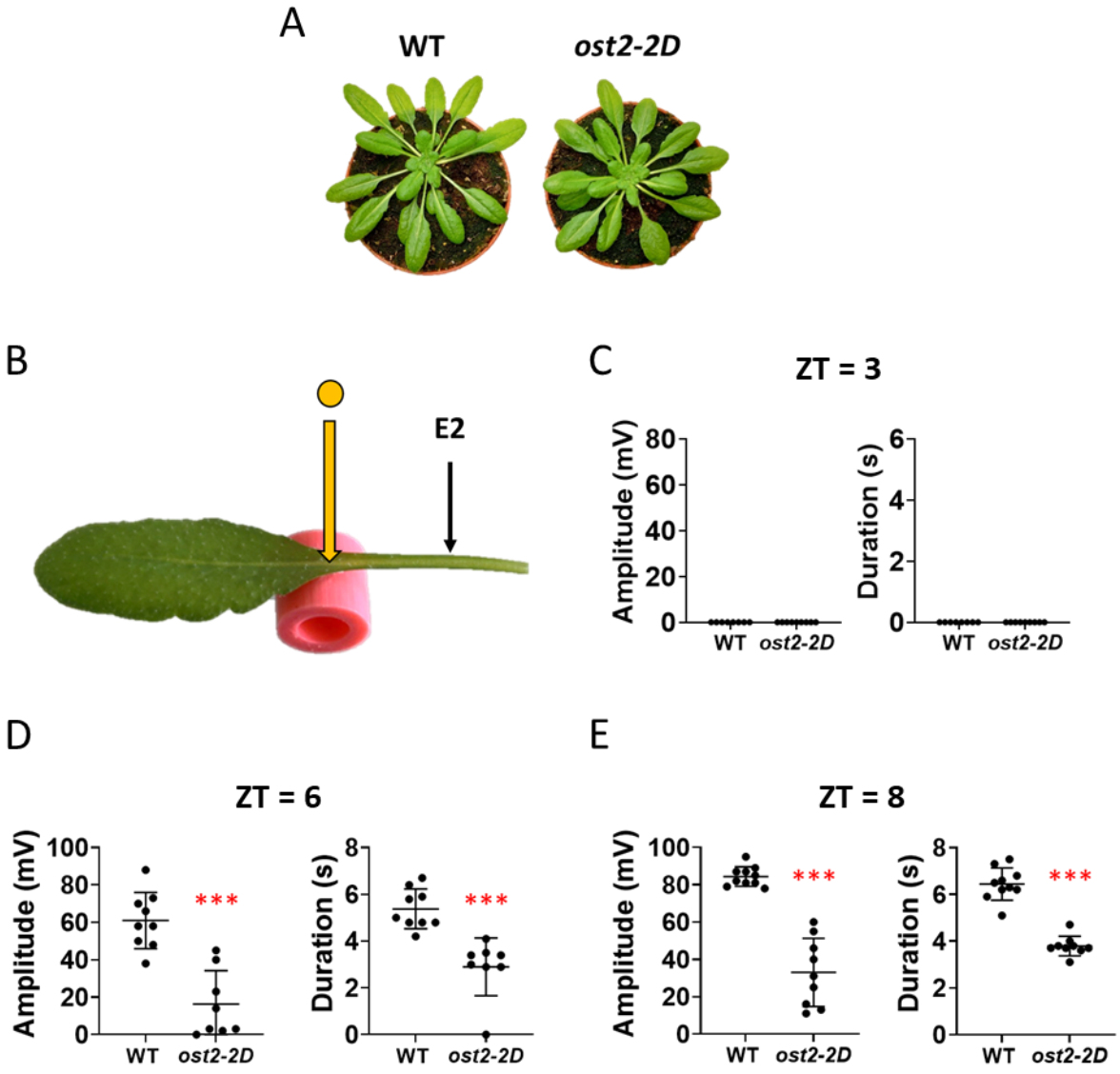

Figure 5.12 Mechanostimulation-triggered electrical signals are reduced in *ost2-2D*. (A) Rosette phenotypes of 5-weeks old WT and *ost2-2D*. (B) Experimental design. Mechanostimulation-induced surface potentials were recorded at (C) 11:00 (ZT=3) (D) 14:00 (ZT=6) (E) 16:00 (ZT=8) time points. The force exerted by the 4 mm diameter bead was estimated to be 38 mN. Bars are means ± SD (n = 8-9). Student t-test: *** P<0.001.

Fussicoccin treatment eliminated the mechanostimulated signal:

Constitutively mutated AHA1 in the *ost2-2D* mutant attenuated mechanostimulation-induced surface potentials by about 50 %. In Arabidopsis, the AHA family consists of 11 members (Haruta et al., 2010). Most of the AHAs are suggested to be localized on the plasma membrane and to have a H^+-ATPase activity (Rodrigues et al., 2014; Hoffmann et al., 2019; Hoffmann et al., 2020). Genes belonging to the same family with shared similar functions are often associated with gene redundancy. In order to investigate whether gene redundancy had an effect on mechanostimulated responses, we pharmaceutically activated AHAs using fusicoccin. Fusicoccin is a fungal toxin which stabilizes the interaction of 14-3-3 proteins with the C-terminal auto-inhibitory domain of plasma membrane H^+-ATPases (Kinoshita and Shimazaki, 1999; Würtele et al., 2003). Thus, fusicoccin can activate all the plasma membrane proton pumps at the same time. Fusicoccin treatment through the exposed veins was shown to reduce wound-induced electrical signals (Kumari et al., 2019). However, vein-exposure surgeries would be problematic for our non-invasive measurements.

Chemicals from damaged tissues can induce wound responses. The most famous story of chemical signals is the "Ricca's Factor" (Ricca, 1926). Ricca Factors fed through the xylem can induce distal leaf movements in *Mimosa pudica*. Ricca's assay was further developed by Gao et al., (submitted) to study wound-released elicitors. In this method, the petiole on the distal leaf is killed with boiled water. Xylem vessels in the killed petiole can serve as a chemical delivery tunnel to the distant leaf. Therefore, we reasoned that we might be able to deliver fusicoccin from the distal leaf to the local leaf through the connection of xylem. In theory, fusicoccin delivered through the xylem might diffuse within the bundle sheath. Vascular tissues within the bundle sheath were potentially the most responsive tissues to mechanostimulations

(Chapter 4). Thus, Ricca's assay would be an ideal method to test fusicoccin treatments on mechanostimulation-induced electrical signals in unwounded local leaves.

Leaf 13 petioles were treated with boiling water at least 3 hours before mechanostimulations. Measurements and stimulations on leaf 8 were identical to prior experiments. After 3 hours of rest, the dead zones of the petioles were cut in 20 µM fusicoccin (Gao et al., submitted) (Figure 5.13 A). Mechanostimulation experiments on leaf 8 were done at the 16:00 time point (ZT=8) when mechanostimulation-induced surface potentials had the most pronounced signals. Mock and fusicoccin treatments were treated for 5 minutes prior to mechanostimulation. Both treatments did not induced electrical signals before bead stimulations (Figure 5.13 B). The following mechanostimulations triggered electrical signals in the mock condition. (Figure 5.13 B). Basal mechanostimulated responses were not affected by mock treatments.

Strikingly, fresh fusicoccin treatments almost eliminated mechanostimulation-induced electrical signals (Figure 5.13 B). This finding indicated two things. First, fusicoccin treatments effectively reached the vascular tissues in the stimulated leaf and second, that the activity of plasma membrane proton pumps was necessary for mechanostimulation-induced electrical signals. Among fusicoccin treated plants, mechanostimulated signals were completely eliminated in three cases (Figure 5.13 C). Signal amplitudes were reduced to 4.3 ± 5.9 mV by fusicoccin treatments, which was less than 10 % of the control level (77 ± 9.4 mV). Also, durations were reduced to about half after fusicoccin treatments. This was consistent with previous experiments: No matter how small the amplitude was, durations were less affected (Figure 4.10, Figure 4.13, and Figure 5.12). This experiment suggested mechanostimulation-induced electrical signals depended on the activities of plasma membrane proton pumps. In summary, dysregulation of plasma membrane proton pumps eliminated mechanostimulated electrical signals almost completely.

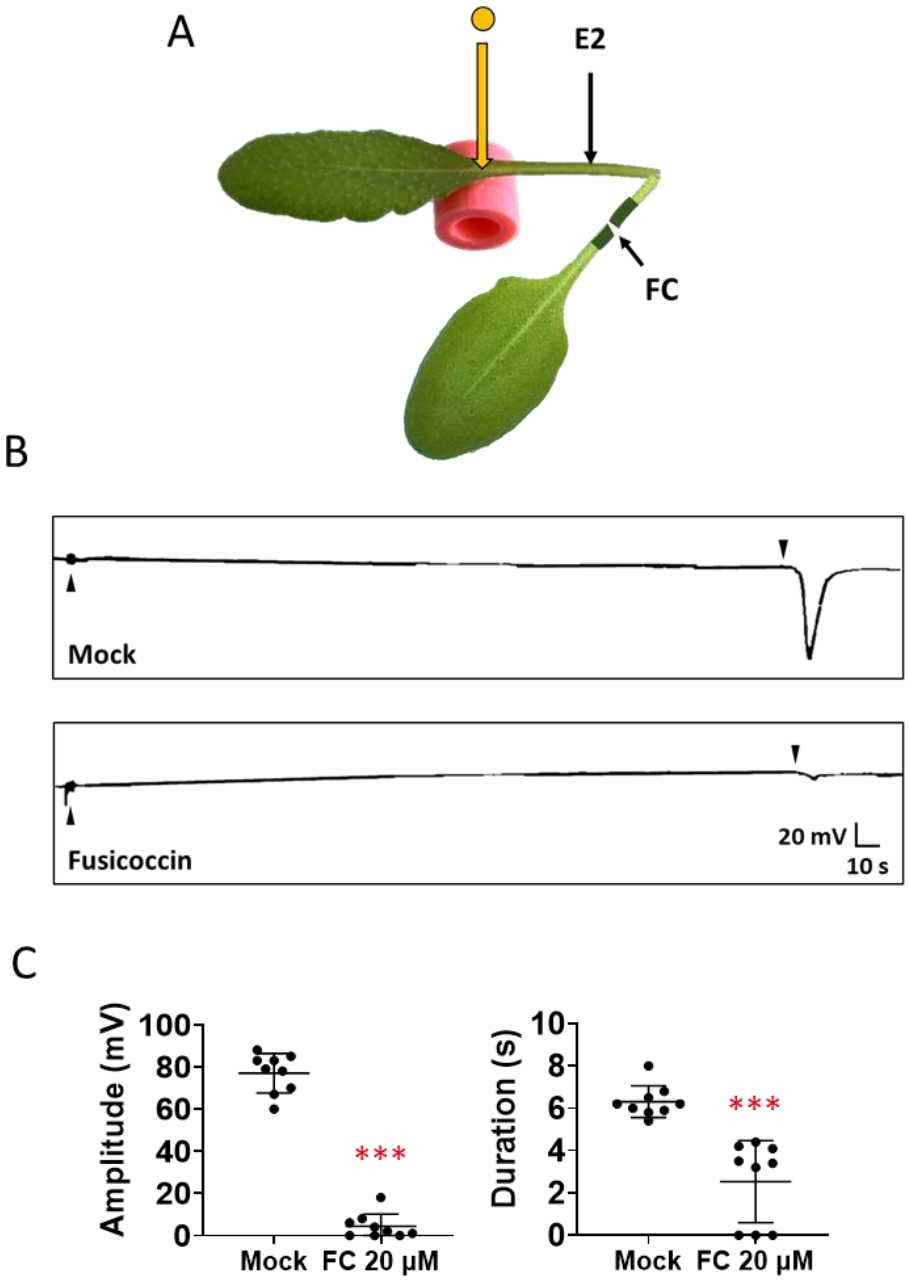

Figure 5.13 Fusicoccin treatment attenuates mechanostimulation-induced electrical signals. (A) Experimental design. The force exerted by the 4 mm bead was estimated to be 38 mN. (B) Example of mechanostimulation-induced electrical signal recorded 5 minutes after mock or fusicoccin treatment. The triangle on the left represents the timing of treatment. The triangle on the right represents the timing of mechanostimulation. (C) Amplitude and duration. (ZT = 8) Bars are means ± SD (n = 9). Student t-test: *** P<0.001.

Conclusion and Discussion:

The well-known mechanosensitive plant *Mimosa pudica* was stimulated with 4 mm (85 mg) borosilicate beads. Mechanostimulation successfully triggered leaflet closure in young and old leaves. Surprisingly, the responsiveness of mechanostimulated leaflet movements increased depending on the time of day. Mechanostimulations could trigger more leaflet movements in the afternoon than in the morning. The time of day somehow controlled the mechano-responsiveness in both *Mimosa* and *Arabidopsis*. In order to investigate whether mechano-responsiveness is linked with circadian rhythm, *elf3* circadian clock mutant was used. Due to the loss of the night complex, *elf3* plants were under a continuous light loop (McWatters et al., 2000). Strikingly, under short-day conditions, mechanostimulation triggered surface potentials in most of the *elf3* plants in the morning. Mechano-responsiveness was further increased in the afternoon. 100 % of WT and *elf3* plants responded to mechanostimulations in the afternoon. These data suggested that the circadian rhythm is important for mechano-responsiveness. However, the arrhythmic circadian clock in *elf3* mutant didn't abolish the relationship between time (light) and mechano-responsiveness completely. It might be something that is regulating the time (light) dependent mechano-responsiveness other than ELF3.

The plant endogenous clock has been shown to be important for the activation of jasmonate-mediated defenses. When the day-night cycle of *Arabidopsis* plants and caterpillars of cabbage looper (*Trichoplusia ni*) are synchronized, the plants are better defended (Goodspeed et al., 2012). Specifically, plant tissues remained after a 72 hours of caterpillar feeding. The caterpillars also grow slower while the clocks are synchronized. However, an out-of-phase day-night cycle between plants and caterpillars results in more damage to the plants. Caterpillars gained approximately three times more weight under those conditions than with synchronized day-night cycles. Day-night cycle-associated defense regulation depends on

jasmonate. *Allene oxide synthase* mutants which cannot produce jasmonate, and circadian arrhythmic mutant *lux2* showed no differences in defense in the clock-synchronization experiments. This suggests that the circadian rhythm positively correlates with jasmonate-dependent defenses. Many studies show that mechanostimulations trigger defense responses (Chehab et al., 2012; Moerkercke et al., 2019; Matsumura et al., 2022). The circadian rhythm regulated mechano-responsiveness might be a possible cause of the day-night cycle-associated defense regulation.

The *elf3* mutant had increased phosphorylation levels of plasma membrane proton pumps (Kinoshita et al., 2011). Plasma membrane proton pump AHA1 regulates wound-induced electrical signals in *Arabidopsis* (Kumari et al., 2019) and the activity of proton pumps is associated with leaves circadian movements in *Samanea* (Lee and Satter, 1987). Also, the expression pattern of plasma membrane proton pumps is associated with the motor cells in *Mimosa* (Fleurat-Lessard et al., 1997). This evidence suggested that plasma membrane proton pump activities might be an underlying factor in mechanostimulated responses. To investigate the role of plasma membrane proton pumps in mechanostimulation-induced electrical signals, the dominant gain-of-function mutant *ost2-2D* was tested. Unexpectedly, mechano-responsiveness was not increased in *ost2-2D* in the morning. This might be because of the difference between increased phosphorylations in *elf3* and the constitutive mutation in *ost2-2D*. Phosphorylated proton pumps could be dephosphorylated upon stimulation, but the constitutive mutation would completely dysregulate the proton pump (Merlot et al., 2007; Haruta et al., 2015). Furthermore, amplitudes and durations of mechanostimulation-induced electrical signals were significantly decreased in *ost2-2D*. Considering gene redundancy of AHA family members, we thus activated all the plasma membrane proton pumps by exogenous treatments with fusicoccin. Fusicoccin was applied from the distal leaf to the tested leaf through the xylem connections. Due to fusicoccin effectively activating all the plasma membrane proton pumps,

mechanostimulation-induced electrical signals were almost eliminated. We interpret this to mean that membranes did not depolarize successfully after bead stimulation. In summary, genetically and pharmaceutically manipulated plasma membrane proton pump activities attenuated mechanostimulation-induced electrical signals significantly, showing that the activity of the plasma membrane proton pump was crucial to the mechanosensation.

We noted that in our experiments the durations of mechanostimulation-induced electrical signals were less affected than amplitudes. *ost2-2D* attenuated durations to half of WT levels. When fusicoccin treatments eliminated signal amplitudes, durations were also reduced to half of control levels. In Chapter 4, there are more examples where durations are less varied than amplitudes: 1) Surface potentials measured on laminas (Figure 4.8); 2) Surface potentials stimulated 30 minutes post first stimulations (Figure 4.10); 3) Surface potentials measured on the edges of leaves (E2'') (Figure 4.13) and 4) Surface potentials stimulated at 12:00 (ZT=4) (Figure 4.18). If signal amplitude corresponded to the change of electrical charges across the plasma membrane, the duration would be related to the kinetic of these changes (Hodgkin and Huxley, 1952). That is, in other words, related to the opening and closing of ion channels or pores, which allow ionic charges to travel through the plasma membrane. Manipulated proton pumps decreased the levels of ion movement, which attenuated signal amplitudes. However, manipulating proton pump activities did not influence the opening and closing of the channels completely since the signal durations were less affected. This might suggest that only limit amount of channels are involved in the depolarization and repolarization of mechanostimulation-induced electrical signals. As long as the channels were stimulated, the time required during the opening and closing of these channels is similar.

Chapter 6: MECHANOSTIMULATION AND JASMONATE PATHWAY ACTIVATION

Introduction:

Mechanostimulation with 2 mm (7 mg) borosilicate beads dropped from an elevation of 2 cm applied an estimated 3 mN force to leaves. A 3 mN force application would be similar to the wind force applied by a Beaufort scale 3 (12-19 Km/hr) wind blowing against a 2 cm^2 leaf surface. Repeated leaf bending triggers growth inhibition of the rosette leaves and the inflorescence stems in *Arabidopsis* (Chehab et al., 2012; Darwish et al., 2022). However, plants that were grown in nature and not under laboratory conditions would be expected to receive multiple environmental stimulations per day. Those stimuli, such as wind and rain drops, would have the potential to continuously trigger mechanostimulated responses. We found that, *Arabidopsis* grown under non-laboratory conditions often have smaller rosettes than *Arabidopsis* grown in the laboratory (Figure 6.1). Both wild accession plants from seeds collected in Dorigny (Vaud, Switzerland) and Col-0 plants showed severe growth retardation while growing in the field.

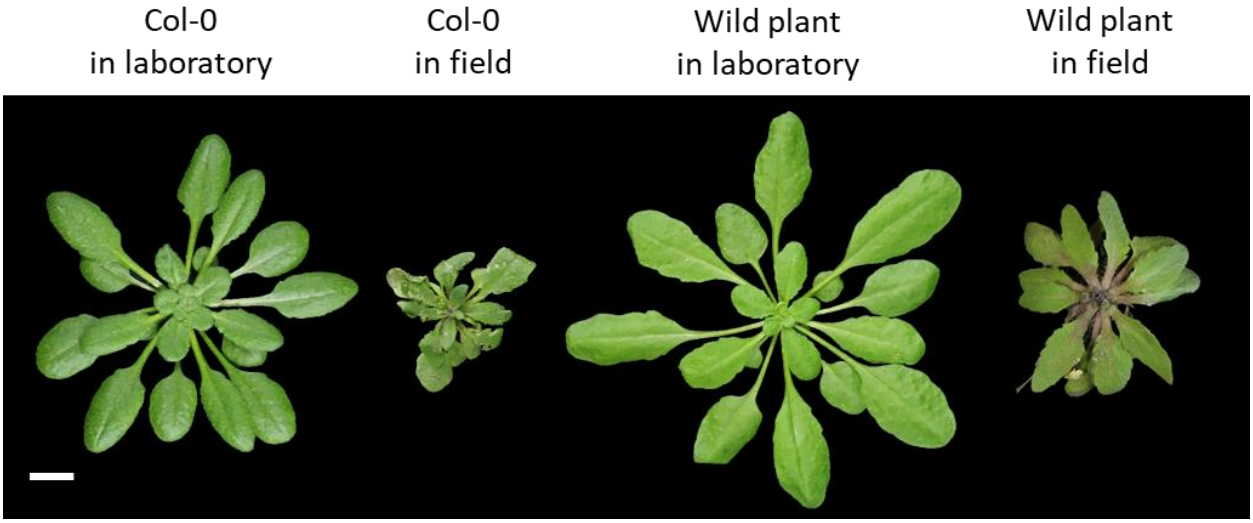

Figure 6.1 Arabidopsis grown in nature displays small rosette phenotypes. Rosette morphology of *Arabidopsis* growing in laboratory under short-day conditions used for all experiments compared with *Arabidopsis* plants in nature. The figure was assembled from four separate images. Scale bar = 1 cm.

Jasmonate is an essential hormone for wound-induced defense responses in leaves (Acosta and Farmer 2010). Studies on wounding leaves found four 13-lipoxygenases (LOX2, LOX3, LOX4, and LOX6) contributed to rapid jasmonate biosynthesis (Chauvin et al., 2013). LOX2 and LOX6 were important for jasmonate production close to the wound and in the distal leaf, respectively (Glauser et al. 2009; Gasperini et al. 2015). *lox3* and *lox4* double mutation caused male sterility and loss of wound-associated growth inhibition in *Arabidopsis* (Caldelari et al., 2011; Yang et al., 2020). Activation of *LOX2* and *LOX6* by wounding induced *LOX3* and *LOX4* gene expression suggested regulation between pairs of LOXs (Chauvin et al., 2016). Furthermore, touch-induced inflorescence development and defense responses also depend on jasmonate synthesis (Chehab et al., 2012). Leaf bending-induced responses are abolished in the *allene oxide synthase* mutants (*aos*) which cannot produce jasmonate. The transcription factors MYC2, MYC3, and MYC4 are required for water spraying-induced jasmonate-response gene expression (Moerkercke et al., 2019). However, it is not clear which LOXs are involved in touch-induced jasmonate responses. Therefore, in this chapter, we investigated which LOXs were required for mechanostimulation-induced jasmonate biosynthesis in *Arabidopsis* leaves.

Results:

Jasmonate precursor biosynthetic enzymes LOX2 and LOX6.

To investigate which LOXs were required for mechanostimulation-induced jasmonate production, we chose to stimulate the center of the lamina. LOX2 is mostly expressed in the

soft tissues and not in mature vascular tissues (Chauvin et al., 2016). LOX3, LOX4, and LOX6 were all predominantly expressed in vascular tissues (Chauvin et al., 2016). Mechanostimulation in the center of the leaf lamina could stimulate both the soft tissues (LOX2) and the vascular tissues (LOX3, LOX4, and LOX6). Hence, we performed stimulations at the lamina center to compare the contributions of each LOX in mechanostimulation-induced responses. Firstly, we investigated whether the trichome skirt cells and vascular tissues could be stimulated by mechanostimulations. 3 mm borosilicate beads (38.6 ± 1.9 mg) and 3 mm stainless steel beads (209.7 ± 2 mg) were dropped from 2 cm elevations onto the center of the unsupported leaf lamina (Figure 6.2). Mechanostimulation triggered cytosolic calcium signals (monitored with GCaMP3) in cells surrounding the trichomes and in the veins (Figure 6.3). Trypan blue staining suggested that our mechanostimulation method did not produce wounds (Figure 6.4). Thus, this method was suitable for further investigating mechanostimulation-induced jasmonate production.

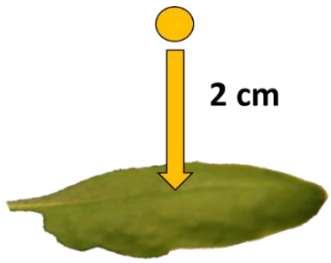

Figure 6.2 Experimental design. 3 mm (38.6 mg) bead stimulation at the lamina center. The leaf was unsupported and still attached to a 5-week-old plant.

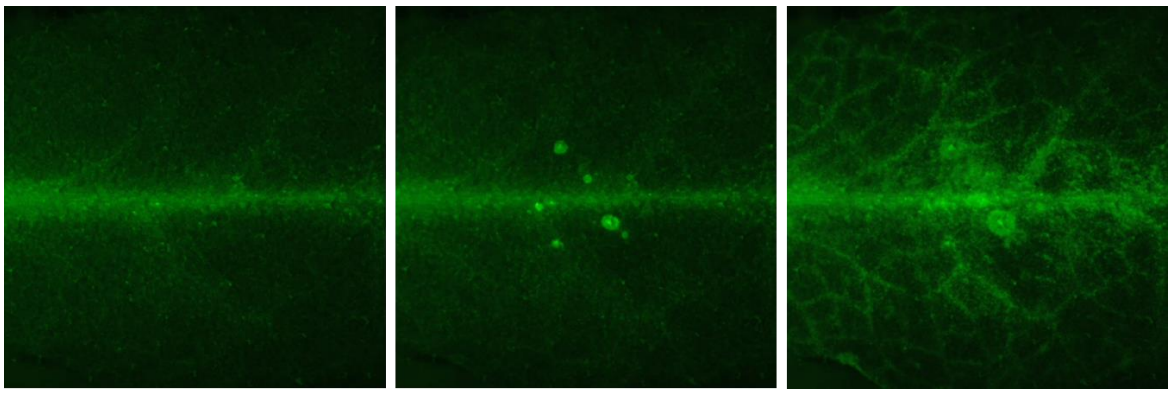

Figure 6.3 4 mm (85 mg) bead stimulation at the lamina center. Calcium signals were recorded from 5-week-old *Arabidopsis* expressing *UBQ10pro::GCaMP3.*

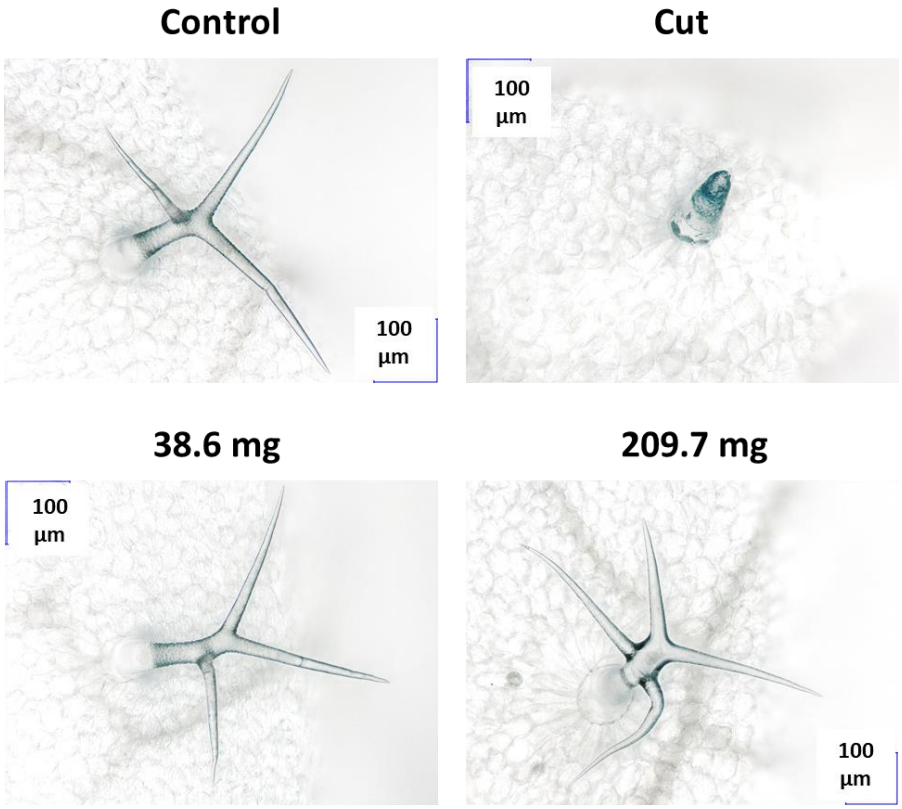

Figure 6.4 Mechanostimulation did not wound the leaf surface. 5-week-old *Arabidopsis* leaves were stained with trypan blue after bead (3 mm, 38.6 mg borosilicate; 3 mm, 209.9 mg stainless steel) mechanostimulations.

Next, we stimulated the lamina center with four consecutive bead (3 mm) mechanostimulations. The expression of *JAZ10*, a jasmonate-responsive marker gene, was investigated using Q-PCR with samples harvested at 30 minutes, 60 minutes, and 90 minutes after mechanostimulation. Strikingly, the expression of *JAZ10* was induced 10-40 fold at 60-90 minutes after mechanostimulation (Figure 6.5). Such a high level of transcript induction allowed us to further investigate the mechanostimulation-induced responses in *lox* mutants. Triple *lox* mutants were created by Chauvin et al. (2013). Only one of the four jasmonate

precursor-producing LOXs remained in each of the triple mutants. For example, testing the *lox2/3/4* triple mutant would reveal the contribution of the remaining LOX6 in response to mechanostimulation.

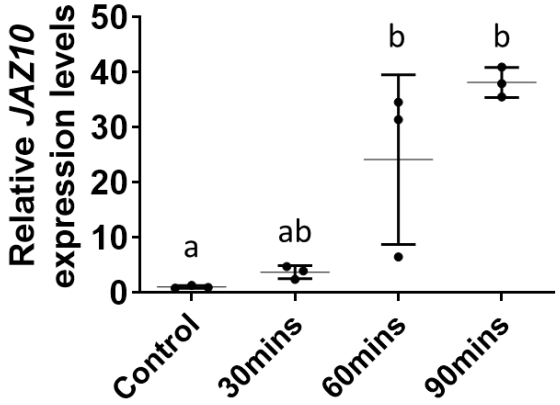

Figure 6.5 Mechanostimulation-induced *JAZ10* expression in leaves. Samples were harvested 30 minutes, 60 minutes, and 90 minutes after four consecutive mechanostimulations. 3 mm diameter (38 mg) borosilicate beads were dropped from an elevation of 2 cm. *JAZ10* transcriptions were normalized to *UBC21* and displayed relative to the expression in the WT control. Bars are means ± SD. (n = 3). Letters indicate significant differences, Tukey HSD test: $P<0.05$. Note that leaves were not supported therefore forces exerted by the beads are not given.

The 90-minute time point was chosen for the most stable mechanostimulation-induced *JAZ10* expression levels. All four *lox* triple mutants were tested and the *lox2/3/4/6* quadruple mutant was used as a negative control. Interestingly, mechanostimulation induced significant *JAZ10* expression in the *lox3/4/6* and *lox2/3/4* triple mutants (Figure 6.6A). No clear induction was found in the *lox2/4/6* and *lox2/3/6* triple mutants (Figure 6.6B). This indicated that the *LOX2* and *LOX6* are the major 13-LOXs required for mechanostimulation-induced rapid jasmonate production. Although the transcription of *LOX3* and *LOX4* in leaves could be

induced by touching (Darwish et al., 2022), *JAZ10* transcripts were not clearly induced in the *lox2/4/6* and *lox2/3/6* triple mutants. Thus, the induction of *LOX3* and *LOX4* transcriptions might be a secondary response induced by rapid touch-induced jasmonate production.

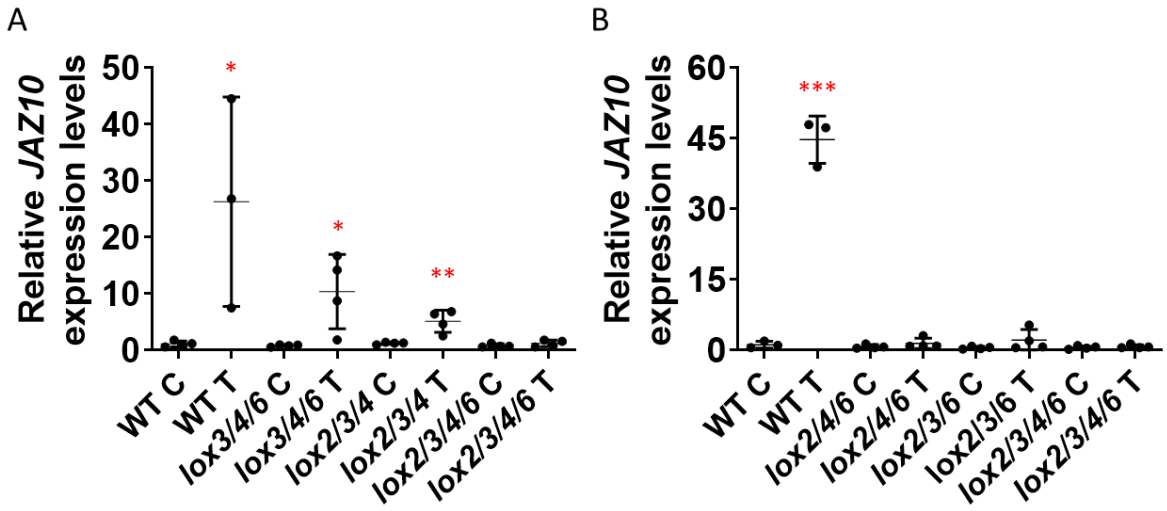

Figure 6.6 Mechanostimulation-induced *JAZ10* expression levels in 5-week-old *Arabidopsis*. 3 mm diameter (38 mg) borosilicate beads were dropped from an elevation of 2 cm. (A) Transcription levels of *JAZ10* in the WT, *lox3/4/6*, *lox2/3/4*, and *lox2/3/4/6*. (B) Transcription levels of *JAZ10* in the WT, *lox2/4/6*, *lox2/3/6*, and *lox2/3/4/6*. C = Control, T = Mechanostimulated. *JAZ10* transcriptions were normalized to *UBC21* and displayed relative to the expression in the WT control. Samples were harvest 90 minutes after mechanostimulations. Bars are means ± SD. (n = 3-4). Student *t* test: * P<0.05; ** P<0.01; *** P<0.001. Note that leaves were not supported therefore forces exerted by the beads are not given.

To further confirm these findings, the experiments were repeated with the leaf bending method at Chehab et al. (2012). Repeated leaf bending induces long-term responses such as thigmomorphogenesis (touch-regulated growth inhibition; Chehab et al., 2012). If the results were consistent with two mechanostimulation methods, then one can conclude that LOX2 and LOX6 jasmonate synthesis pathways respond to mechanostimulation. The stimulated leaf was repeatedly lifted up and down by 70 degrees from the horizontal plane 10 times (Figure 6.7).

Repeated leaf bending triggered a stronger cytosolic calcium signal (are measured with GCaMP3) than the bead stimulations (Figure 6.8). The whole leaf (lamina and petiole) was then sampled 90 minutes after stimulations.

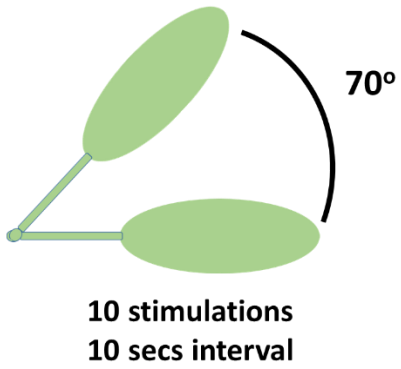

Figure 6.7 Experimental design for repeated leaf bending. Leaves were lifted by hand 10 times up and down from the horizontal plane.

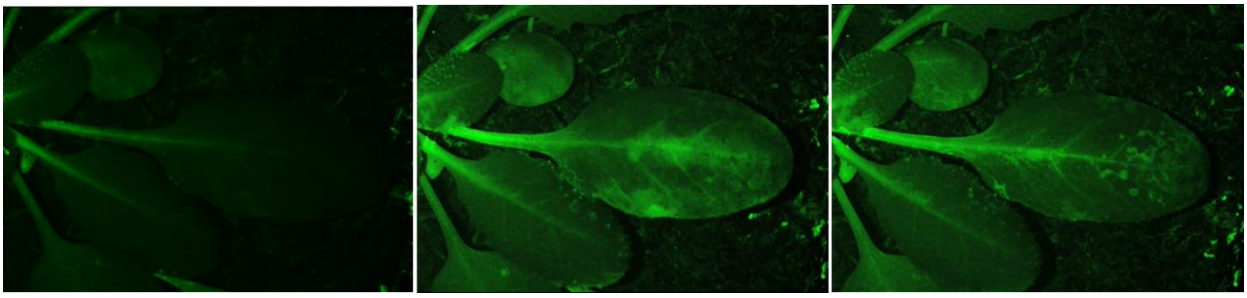

Figure 6.8 Repeated leaf bending triggered calcium signals. Leaves were bent as shown in fig. 6.7. Cytosolic calcium signals were recorded from 5-week-old *Arabidopsis* expressing *UBQ10pro::GCaMP3*.

WT plants had the highest levels of *JAZ10* transcripts following repeated leaf bending. Lower *JAZ10* transcript levels were found in the *lox3/4/6* and *lox2/3/4* triple mutants (Figure 6.9A). This was consistent with the previous experiments showing that LOX2 and LOX6 were the major mechanostimulation-responsive LOXs (Figure 6.6A). Surprisingly, *JAZ10* transcripts

were significantly induced in the *lox2/4/6* and *lox2/3/6* triple mutants (Figure 6.9B). We noted a lower basal level of *JAZ10* transcripts found in mechanostimulated *lox2/4/6* and *lox2/3/6*. The induced *JAZ10* transcript levels in *lox2/4/6* and *lox2/3/6* were similar to the control (basal) levels in the WT. This finding suggested that *LOX3* and *LOX4* could also contribute to mechanostimulation-induce jasmonate production. However, the contributions of *LOX3* and *LOX4* were minor compared to those of *LOX2* and *LOX6*.

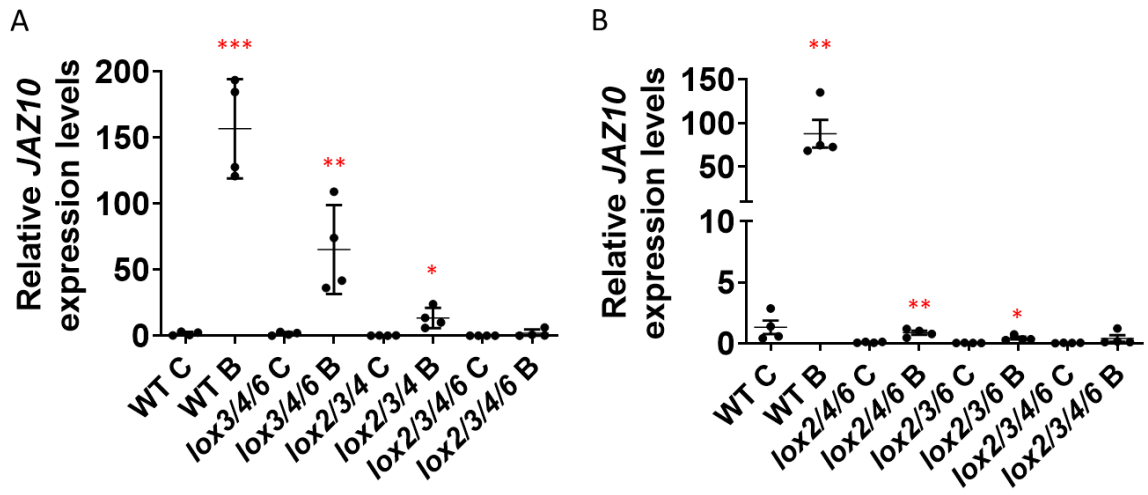

Figure 6.9 Bending-induced *JAZ10* expression levels in the leaves of 5-week-old *Arabidopsis*. Leaves were bent as shown in fig. 6.7. (A) Transcription levels of *JAZ10* in the WT, *lox3/4/6*, *lox2/3/4*, and *lox2/3/4/6*. (B) Transcription levels of *JAZ10* in the WT, *lox2/4/6*, *lox2/3/6*, and *lox2/3/4/6*. C = Control, B = bent. *JAZ10* transcripts were normalized to *UBC21* transcripts and displayed relative to expression in the WT control. Samples were harvest 90 minutes after mechanostimulations. Bars are means ± SD. (n = 4). Student *t* test: * P<0.05; ** P<0.01; *** P<0.001.

Mechanostimulation induced *AOS* transcription

We found that bead dropping mechanostimulation as well as repeated leaf bending induced *JAZ10* transcript accumulation in the lamina. The major LOXs responsive to

mechanostimulation were LOX6 (expressed chiefly in xylem contact cells) and LOX2 (expressed throughout soft tissues). We therefore investigated whether our bead mechanostimulation method, which was used in all the mechanostimulation-induced electrical signal experiments, could induce local jasmonate-responsive gene expression (Figure 6.10A). An *AOS::NLS-3xVenus* reporter (Marhavý et al., 2019) was chosen for visualizing spatial responses. Images were taken 4 hours after mechanostimulation. Strikingly, bead mechanostimulation induced clear reporter signals on the stimulated leaves (Figure 6.10B). The stimulation sites had the highest reporter signals. In order to further confirm the activation of the native *AOS* promoter more quantitatively, mechanostimulated petioles were analyzed with Q-PCR (Figure 6.10C). Consistently, *AOS* transcript levels were significantly induced with bead mechanostimulations in the stimulated petioles. In this experiment, mechanostimulation-induced *AOS* expression was investigated. These findings indicated that mechanostimulation with borosilicate beads not only triggered vasculature-associated electrical signals but also induced jasmonate-responsive gene transcriptions in the stimulated leaves.

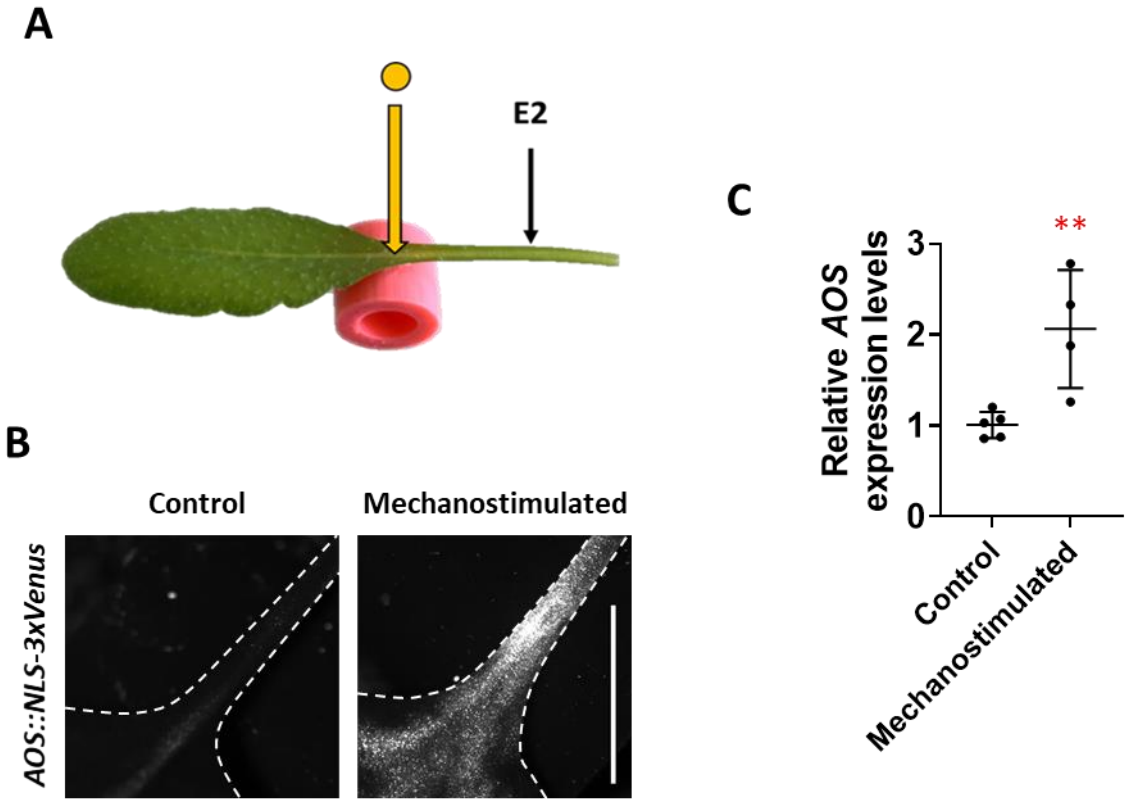

Figure 6.10 Mechanostimulation-induced *AOS* expressions in the 5-week-old *Arabidopsis*. (A) Experimental design. Plants were stimulated with 85 mg borosilicate beads dropped from 2 cm elevations onto lamina/petiole junctions of leaf 8 producing estimated forces of 38 mN. (B) Mechanostimulation-induced *AOS::NLS-3xVenus* signals. Both images are 4h after treatments. (C) Transcription levels of *AOS* in the control and mechanostimulated WT. *AOS* transcripts were normalized to those of *UBC21* and displayed relative to expression in the WT control. The petioles including the stimulation sites were sampled 90 minutes after mechanostimulation. Bars are means ± SD. (n = 4-5). Student *t* test: ** P<0.01.

Mechanostimulation-induced electrical signals do not depend on jasmonate

Bead mechanostimulation induced jasmonate-response gene expression in plants. Touch/bending-induced jasmonate induced short-term responsive gene expression, increased mid-term defenses against herbivory, and triggered long-term thigmomorphogenesis (Chehab et al., 2012; Moerkercke et al., 2019; Darwish et al., 2022). The induction of jasmonate-

responsive gene expression was investigated with several assays. If the mechanostimulation-induced electrical signal is an upstream signal activating jasmonate production, the loss of jasmonate producing ability should not affect the electrical signals. We therefore tested whether the ability of plants to produce jasmonate had an effect on the mechanostimulation-induced electrical signals. For this, the *aos* mutant which cannot produce jasmonate was used (Figure 6.11A). Interestingly, mechanostimulation triggered similar electrical signals in the WT and the *aos* mutants (Figure 6.11B). No statistically significant differences were found in signal amplitudes and durations. These results indicate that mechanostimulation-induced electrical signals didn't depend on jasmonate. Therefore, mechanostimulation-induced electrical signals are most likely to be an upstream signal for jasmonate-dependent touch responses.

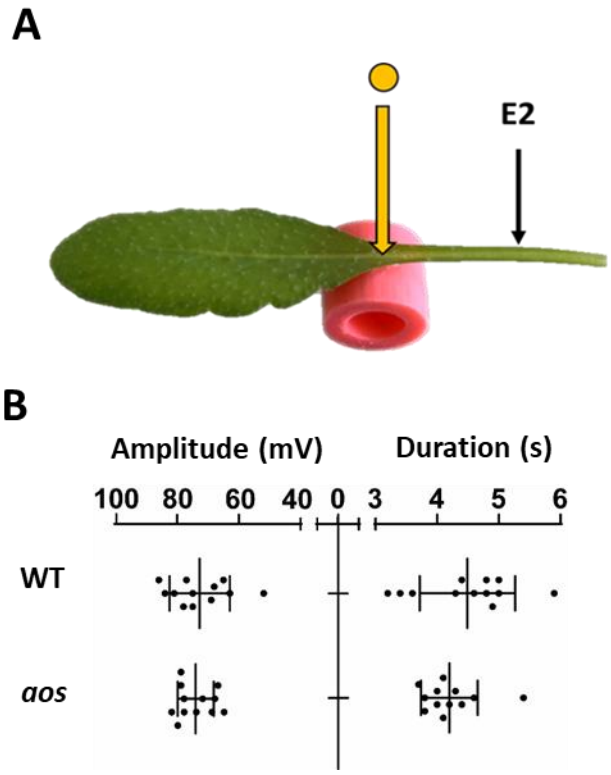

Figure 6.11 Mechanostimulation-induced surface potentials in the WT and *aos* mutants. (A) Experimental design. Plants were stimulated with 85 mg borosilicate beads dropped from 2 cm elevations onto lamina/petiole junctions of leaf 8 producing estimated forces of 38 mN. ZT =

6-8. (B) Quantification of mechanostimulation-induced surface electrical signals in WT and *aos*. Bars are means ± SD (n = 12). Student t-test: not significant.

Conclusion and Discussion:

Repeated mechanostimulation induces thigmomorphogenesis, slowing inflorescent stem development in a jasmonate-dependent manner (Chehab et al., 2012; Darwish et al., 2022). Mutants that cannot produce jasmonate (eg. *aos*) and which cannot induce proper jasmonate signalling (eg. *myc2 myc3 myc4*) both abolished thigmomorphogenesis (Chehab et al., 2012; Darwish et al., 2022). In the first step of jasmonate biosynthesis, four enzymes (LOX2, LOX3, LOX4, and LOX6) generate jasmonate precursors prior to the AOS action (Wasternack and Hause, 2013). Each of these LOXs had different expression patterns, for example, LOX3, LOX4, and LOX6 expressed mostly in the vasculature and LOX2 is not expressed in the mature vasculature (Chauvin et al., 2016). LOX2 and LOX6 are crucial for rapid jasmonate production induced by wounding. LOX3 and LOX4 had minor roles in rapid wound responses but were required for male fertility and wound-associated growth regulation (Caldelari et al. 2011; Yang et al., 2020).

In this Chapter, we investigated which LOXs contributed to touch-induced jasmonate production. Two mechanostimulation methods were used, the bead dropping method described previously (Chapter 4) and a repeated leaf bending method. Both methods induced cytosolic calcium signals (as monitored with GCaMP3) in the stimulated leaves. With trypan blue staining, we confirmed that bead stimulation did not wound the stimulated leaves. Interestingly, we found that both mechanostimulation methods induced *JAZ10* expression significantly in the *lox3/4/6* and *lox2/3/4* mutants. This suggested that LOX2 and LOX6 were the major jasmonate precursor producing gene products that respond to mechanostimulation. In parallel, repeated

leaf bending induced *JAZ10* expression weakly in the *lox2/4/6* and *lox2/3/6*. This might be because repeated leaf bending has a stronger effect than bead dropping. The induction of *JAZ10* in *lox2/4/6* and *lox2/3/6* was not detectable with the bead-stimulation method. Also, lower than WT basal levels of *JAZ10* transcripts were found specifically in the *lox2/4/6* and *lox2/3/6* mutant. The induction levels of *JAZ10* transcripts in the *lox2/4/6* and *lox2/3/6* were similar to the control levels in the WT. These findings suggested that LOX2 and LOX6 are the most responsive LOXs in mechanostimulation, and possibly to a minor extent, LOX3 and LOX4 also respond. This is similar to the finding of rapid wound-induced jasmonate production (Chauvin et al., 2013). Furthermore, repeated leaf bending triggered LOX3 and LOX4 activation might cause thigmomorphogenesis since LOX3 and LOX4 were shown to be the key to wound-associated growth regulations (Yang et al., 2020).

Mechanostimulation-induced jasmonate biosynthesis was investigated using experimental designs similar to those used for electrophysiology experiments. Using the genetically encoded fluorescence reporter GCaMP3, we found that stimulation sites showed the most pronounced reporter signals. The patterns of these signals were chiefly associated with the patterns of the vasculature. Also, qPCR experiments revealed that mechanostimulation-induced *AOS* expression. Furthermore, normal mechanostimulation-induced electrical signals were found in the *aos* mutants. These experiments showed that mechanostimulation can induce jasmonate-responsive genes and that mechanostimulation-induced electrical signals are not jasmonate-dependent. The mechanostimulation-induced electrical signal is likely to be an upstream signal which activates the jasmonate pathway. It might be similar to the wound-induced electrical signals that activated the jasmonate pathway in the distal leaves (Mousavi et al., 2013). Mutants (*glr3.3 glr3.6*) that abolished long-distance electrical signals and also eliminated the activation of the jasmonate pathway in the distal leaves. The proton pump *aha1*

mutation increased the durations of the long-distance electrical signals and also increased jasmonate responses (Kumari et al, 2019). Meanwhile, the *ost2-2D* mutant in which AHA1 is constitutively active attenuated wound-induced electrical signals and jasmonate production. It would be interesting to test if the reduced mechanostimulation-induced electrical signals affected jasmonate signalling in *ost2-2D* mutants. Whether *GLR3.3* and *GLR3.6* have roles in the production of mechanostimulated electrical signals and touch-induced jasmonate responses needs to be further addressed.

Chapter 7: SEARCHING FOR GENES UNDERLYING THE MECHANOSTIMULATION RESPONSE

Introduction:

The potential of the plasma membrane is regulated by proton pumps and ion channels (Sze et al., 1999). Distributions of ionic charges on the two sides of the membrane form the membrane potential. The resting plasma membrane has more positive charges on the apoplastic side and more negative charges on the cytoplasmic side. A polarized membrane is depolarized when the original charge distribution is neutralized. That might happen with anion channels releasing negative charges into the apoplast or for example, through positive charges entering the cell through proton channels. Giant algal cells such as those of *Chara* and *Nitella* have provided many valuable insights regarding the control of membrane potential. This work revealed that the membrane potentials of both the plasma membrane and endomembranes were responsive to chemical and physical stimuli (Tazawa et al., 1987; Kisnieriene et al., 2018). Mechanoperception has been studied, for example, in *Chara corallina*. Among many interesting findings was the potential involvement of outward-rectifying Cl^- channels in depolarizing touch-stimulated *C. corallina* cells (Shimmen, 2001). Moreover, depolarization might also occur due to charge transport between subcellular compartments and the cytoplasm. Thus, in this Chapter we tested the involvement of a variety of channels, transporters, and proton pumps in the mechanostimulation-induced electrical signal with T-DNA insertion mutants.

Results:

Aurore Chételat produced and genotyped all almt mutants used in this study.

Reverse genetic screening of ion channel mutants

Among anion channels, the aluminum-activated malate transporter (ALMT) family, chloride channel (CLC) family, voltage-dependent anion channel (VDAC) family, and two slow-type anion channels (SLAC1 and SLAH3) are examined for their responses to mechanostimulation. Roles of the ALMT family were first discovered in resistance to aluminum toxicity (Sasaki et al., 2004). Many roles of ALMTs beyond aluminum toxicity were found afterward (Sharma et al., 2016; Ramesh et al., 2015). ALMTs have ability to transport both organic (malate) and inorganic (chloride) anions (Barbier-Brygoo et al., 2011). The CLCs are found universally in both plants and animals (Jentsch T., 2008) Many of CLCs are anion-proton antiporters (Barbier-Brygoo et al., 2011). In theory, the activated antiporter CLCs can rapidly change the membrane potential which may cause rapid membrane depolarization. VDACs are localized on the outer membrane of mitochondria (Homble et al., 2012) and have important roles in controlling reactive oxygen species (ROS) release to the cytosol (Han et al., 2003). ROS is proposed to be important in electrical signalling in plants (Szechyńska-Hebda et al., 2022). The slow-type anion channels (SLAC) have preferences for transporting nitrate over other anions (Barbier-Brygoo et al., 2011). A recent study found that cytosolic pH decreases can activate the SLAC1 homolog 3 (Lehmann et al., 2021). If the slow-type anion channels are sensitive to cytosolic pH changes, the theoretical inhibition of plasma membrane proton pumps while the initiation of electrical signals might activate the slow-type anion channels (Farmer et al., 2020).

No spectacular differences in mechanostimulated electrical signalling were found in *almt* mutants, *clc* mutants, *vdac* mutants, *slac1,* and *slah3* (Table 7.1, Table 7.2, and Table 7.3). The significant decrease of amplitudes found in the *almt3 almt5* and *almt5 almt9* double mutants was not reproducible in the *almt3 almt5 almt9* triple mutants. Significant decreases of signal duration were found in the *almt6, almt11,* and *clcb,* but the reduction levels were

relatively small. Furthermore, mutants in the mechanosensitive channels *msl10* (Moe-Lange et al., 2021) and *piezo1* (Mousavi et al., 2021) mutants didn't show clear differences in signal amplitudes (Table 7.1 and Table 7.2). This indicates that these two mechanosensitive channels are not the major mechanosensors for mechanostimulation-induced electrical signals.

Two-pore channel 1 (TPC1) is a non-selective cation channel localized on the tonoplast (Bonaventure et al., 2007; Beyhl et al., 2009). The gain-of-function *tpc1* mutation *fou2* increases the activity of TPC1. Another more active form of TPC1 was produced and named *TPC1*ΔCa_i (Guo et al., 2017; Yang et al., 2020). The loss-of-function and gain-of-function *TPC1* mutants (*tpc1*, *fou2*, and *TPC1ΔCa*$_i$ from Yang et al., 2020) also didn't affect the amplitudes of the mechanostimulation-induced electrical signals (Table 7.1 and Table 7.2). However, electrical signal durations in *fou2* and *TPC1ΔCa*$_i$ were decreased by approximately 20 % relative to the WT level. It will be interesting for future studies to test if higher-order mutants of the above described lines could further shorten the duration and if the shortened duration could influence the touch-induced responses.

Glutamate receptor-like channels are necessary for the long-distance wound-induced electrical signals (Mousavi et al., 2013; Nguyen et al., 2018). *glr3.1glr3.3* and *glr3.3 glr3.6* double mutants reduced signal amplitudes by 30-50 % of the WT levels (Table 7.2). This was the greatest difference in amplitudes that we observed in T-DNA mutants. However, the effect of *glr* double mutants was not enhanced in the *glr3.1 glr3.3 glr3.6* triple mutants (Table 7.2). Instead, the amplitudes were merely reduced by 10-20 % in *glr* triple and quadruple mutants compared with WT. This suggested that the glutamate receptor-like channels might not have an essential role in mechanostimulation-induced electrical signals.

The sucrose transporter 2 (SUC2) is necessary for phloem loading. *Arabidopsis* homozygous *suc2* mutants show impaired rosette growth due to the disruption of phloem

loading (Gottwald et al., 2000). A heterozygous *suc2* mutant was tested with mechanostimulation. The durations of mechanostimulation-induced electrical signals were reduced in heterozygous *suc2* mutants (Table 7.2). The plasma membrane proton pump AHA3 is proposed to be necessary for phloem-loading (DeWitt and Sussman, 1995; Krysan et al., 1996; Robertson et al., 2004). Thus, we generated a heterozygous *aha3 suc2* double mutant. The heterozygous *aha3 suc2* double mutants reduced both electrical signal amplitudes and durations (Table 7.2). It differed from the *aha1* and *aha3* single mutants and *aha1 aha3* double mutants (Table 7.1 and Table 7.2). The *aha1* increased amplitudes and *aha1 aha3* increased durations of mechanostimulation-induced electrical signals. These findings suggested that the phloem-expressed AHA3 and SUC2 might be important for mechanostimulation-induced electrical signals. However, further studies are required to overcome the fact that homozygous loss-of-function suc2 mutants are extremely dwarfed and not usable in our experiments.

V-type proton pumps (V-ATPases) are large complexes localized on subcellular compartments (Frogac M., 2007; Lupanga et al., 2020). VHAs are responsible for pumping protons into the cytosol (which is different from AHAs). Theoretically, *vha* mutants would have more negative charges on the cytosolic side of the plasma membrane. This might have a similar effect to that of the constitutive active plasma membrane proton pump mutant *ost2-2D*, which constitutively pumps protons to the apoplast (Merlot et al., 2007). However, single *vha* mutants showed increased amplitudes after mechanostimulation (Table 7.3). This was quite different from the decreased amplitudes and durations found in *ost2-2D* (Table 7.1). Interestingly, a similar effect of the increasing in amplitudes has found in *aha1* mutant (Table 7.1). These results suggested that the p-type ATPase (AHAs) and v-type ATPase (VHAs) might contribute to mechanostimulation-induced electrical signals in different ways.

Table 7.1. Mechanostimulation triggered surface potentials

E1' position, 4mm bead, 2 cm elevation, ZT= 6-8

Values P<0.05 (Student *t* test) are colored in red, mean±SD

Gene	Amplitude (mV)	Duration (s)	N =
WT	40 ± 17	4.4 ± 0.8	12
almt1	33 ± 8	3.9 ± 0.8	7
almt6	29 ± 10	3.6 ± 0.6	8
almt8	36 ± 9	4.4 ± 0.6	8
almt11	36 ± 18	3.6 ± 0.8	8
almt14	37 ± 13	4.2 ± 0.5	8
WT	57 ± 12	6.3 ± 0.9	7
almt3 almt5	43 ± 4	6.4 ± 1.7	7
almt3 almt9	37 ± 9	5.3 ± 1	5
almt4 almt9	44 ± 8	7.1 ± 0.7	6
WT	42 ± 9	5 ± 0.8	9
almt5 almt9	44 ± 11	5.4 ± 0.6	10
WT	40 ± 17	5.8 ± 1.5	6
almt5 almt13	43 ± 14	5.5 ± 0.5	7
almt9 almt13	43 ± 17	4.8 ± 0.5	8
WT	33 ± 13	3.9 ± 0.6	10
almt4 almt5	41 ± 11	4.2 ± 0.6	11
almt4 almt13	28 ± 8	4.2 ± 0.9	9
WT	51 ± 10	5.1 ± 1.5	7
almt4 almt9	38 ± 11	6.1 ± 1.2	6
rbohd rbohf	37 ± 10	5.4 ± 0.9	4
WT	36 ± 14	4.3 ± 0.5	10
glr3.3 glr3.6	21 ± 9	4 ± 0.4	11
WT	29 ± 9	4.9 ± 1.1	7
SUC2::TPC1 ΔCa $_i$	25 ± 10	3.8 ± 0.4	6
WT	30 ± 12	4.7 ± 0.6	9
aha1-7	48 ± 9	4.3 ± 0.5	11
ost2-2D	22 ± 7	3.8 ± 0.6	10
WT	29 ± 16	4.4 ± 0.9	10
aha3f (+/-)	33 ± 11	4.4 ± 0.7	8
WT	41 ± 11	5.2 ± 0.7	6
tpc1	43 ± 15	5.6 ± 0.5	8
gl	38 ± 18	5.1 ± 1.3	8
msl10	42 ± 16	4.5 ± 0.5	7
WT	54 ± 12	6.1 ± 0.9	8
npf double	53 ± 15	5.5 ± 0.7	10
AHA3::AHA3Δ844	63 ± 16	5.7 ± 1.3	10

Col-2	38 ± 11	4 ± 0.4	8
clca	43 ± 11	3.9 ± 0.7	5
WT	49 ± 9	5.1 ± 0.8	9
clcd	42 ± 8	4.7 ± 0.3	8
clcg	43 ± 14	4.6 ± 0.8	9
vdac1	46 ± 12	5.3 ± 0.9	9
WT	47 ± 15	5 ± 1	10
clcb	43 ± 14	4.2 ± 0.5	8
vdac2	49 ± 14	4.3 ± 0.9	7
vdac3	48 ± 7	4.8 ± 0.5	8

Table 7.2. Mechanostimulation triggered surface potentials

E2 position, 4mm bead, 2 cm elevation, ZT= 6-8

Values P<0.05 (Student *t* test) are colored in red, mean±SD

Gene	Amplitude (mV)	Duration (s)	N =
WT	66 ± 15	5.4 ± 0.8	11
glr3.3	59 ± 19	5.1 ± 0.7	10
glr3.6	67 ± 17	5 ± 0.7	11
glr3.3 glr3.6	41 ± 16	4.9 ± 0.9	11
WT	70 ± 24	5.2 ± 0.5	6
glr3.1 glr3.3	36 ± 13	4.8 ± 0.9	9
WT	81 ± 9	6.5 ± 0.3	5
glr3.5	70 ± 14	6.6 ± 1.2	9
WT	71 ± 9	4.2 ± 0.9	12
glr3.4 glr3.5	84 ± 8	5 ± 0.8	12
WT	80 ± 10	5.6 ± 0.9	12
glr3.1 glr3.3 glr3.6	65 ± 11	5.4 ± 0.7	12
glr3.1 glr3.2 glr3.3 glr3.6	71 ± 10	5.3 ± 0.5	12
WT	78 ± 7	4.5 ± 0.6	9
almt3 almt5 almt9	82 ± 12	4.9 ± 0.7	9
WT	83 ± 11	5.6 ± 0.8	6
almt5 almt6	78 ± 11	4.7 ± 0.9	7
aca10	85 ± 7	4.9 ± 0.4	8
WT	79 ± 6	4.5 ± 0.6	10
almt12	73 ± 13	4.8 ± 0.8	10
fou2	86 ± 8	3.8 ± 0.8	8
WT	85 ± 8	5 ± 0.4	10
erd6	77 ± 13	5.4 ± 0.6	9
vdac4	86 ± 4	5.2 ± 0.5	10
WT	81 ± 14	6.5 ± 0.7	12
suc2-5(+/-)	75 ± 6	5.6 ± 1.2	11
suc2-5(+/-) aha3f(+/-)	63 ± 10	5.1 ± 0.6	6
WT	81 ± 8	4.5 ± 0.6	11
aha1-7 aha3f(+/-)	79 ± 3	5.4 ± 0.6	10
WT	75 ± 9	5.3 ± 0.7	10
irx5	67 ± 7	3.8 ± 0.5	8
WT	82 ± 8	4.6 ± 0.6	13
syt1-2	82 ± 7	4.1 ± 0.4	11
WT	87 ± 2	4.8 ± 0.4	9
piezo	84 ± 4	4.8 ± 0.6	9

Table 7.3. Mechanostimulation triggered surface potentials
E2 position, 4mm bead, 2 cm elevation, ZT= 6-8
Values P<0.05 (Student *t* test) are colored in red, mean±SD

Gene	Amplitude (mV)	Duration (s)	N =
WT	66 ± 13	5 ± 0.8	9
vha a2	82 ± 11	5.1 ± 0.5	9
vha a3	82 ± 11	5.2 ± 0.9	8
WT	79 ± 11	5.2 ± 1.2	10
cax1	76 ± 8	4.5 ± 0.6	10
cax3	80 ± 6	4.5 ± 0.3	8
WT	76 ± 14	5.2 ± 1	9
slac1	78 ± 5	5.4 ± 0.4	9
slah3	78 ± 11	4.6 ± 1.2	9
WT	74 ± 15	5.5 ± 0.9	7
Salk011449C	84 ± 8	5 ± 0.5	7
Salk021272C	76 ± 8	5.5 ± 0.9	8
SAIL_742_E05	62 ± 18	4.8 ± 0.6	7
WT	78 ± 13	5.4 ± 0.7	8
SAIL_272_E07	77 ± 14	5.2 ± 1	7

CRISPR-Cas9 mutation of the Arabidopsis H^+-ATPase family

The responsiveness of mechanostimulation-induced electrical signals is associated with the time of day (Chapter 4) and this finding was supported with the use of a circadian clock mutant. The *elf3* mutant grows as if it is under constant light conditions due to the loss of the night complex (McWatters et al., 2000). As detailed in Chapter 5, relative to the WT, its mechano-responsiveness was significantly increased in the morning. The phenotype of *elf3* seemed to be related to the activity of the plasma membrane proton pump (AHA), since an increased phosphorylation level of AHA had been identified in these plants by Kinoshita et al. (2011). However, the constitutively active proton pump mutant *ost2-2D* did not influence the responsiveness to mechanostimulation. Instead, the mechanostimulation-induced electrical signal was attenuated to almost half of the WT levels in the *ost2-2D*. Using fusicoccin treatment

through Ricca's assay (Gao et al., submitted), all the AHAs were activated which almost eliminated the mechanostimulation-induced electrical signals completely. These data from Chapter 5 indicated possible redundancy in the action of AHA family in this response. In *Arabidopsis*, the AHA family has 11 members (Figure 7.1 from Haruta et al., 2010). *AHA1* and *AHA2* are the most highly expressed genes of this family in most *Arabidopsis* tissues. The homozygous double mutant *aha1 aha2* is embryo lethal. *AHA1* and *AHA3* have the highest expression levels in the vascular tissues (You et al., 2019). However, the mutant *aha3* allele causes male gametophyte lethality. Therefore, only heterozygous T-DNA mutants are available for experiments (Robertson et al., 2004). AHA6, AHA8, and AHA9 are reported to be essential for pollen tube germination and fertility (Hoffmann et al., 2020). These issues make it difficult to mutate many redundant AHAs at a time. We therefore employed CRISPR-Cas9 approaches and used T-DNA insertion mutants to examine the importance of the phloem-expressed AHAs in the mechanostimulation-induced electrical signalling.

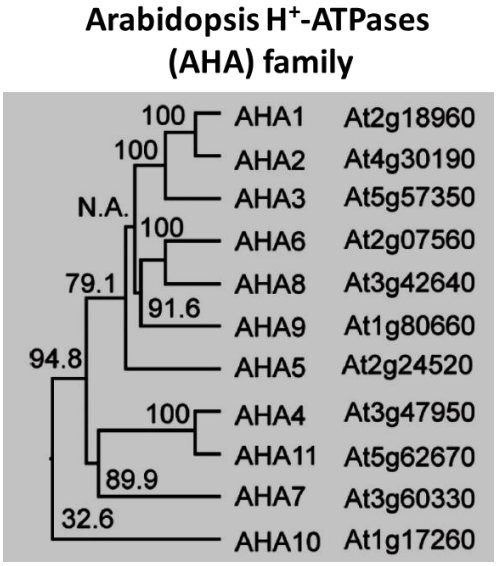

Figure 7.1 The 11 AHA family members in *Arabidopsis* (Figure from Haruta et al., 2010).

Firstly, we choose to target multiple AHAs with the CRISPR-Cas9 approach. The entire AHA family was divided into four groups: 1) phloem expressed group (based on You et al., 2019) *AHA1*, *AHA3*, *AHA8*, *AHA11*; 2) mesophyll expressed group (based on Kim et al., 2018) *AHA1*, *AHA2*, *AHA5*, *AHA11*; 3) clade II group *AHA5*, *AHA6*, *AHA8*, *AHA9*; 4) clade III group *AHA4*, *AHA7*, *AHA10*, *AHA11* (Haruta et al., 2010). Each *AHA* was targeted with three guide RNAs (Figure 7.2A) designed using the Benchling website (https://benchling.com/editor). Each destination clone had six guide RNAs for targeting two *AHA*s (Figure 7.2B). WT Arabidopsis were co-transformed with two destination vectors to generate mutations in four targeted *AHA*s at a time. Arabidopsis seeds were then selected according to red and green fluorescence in the T1 generation (Figure 7.2B). Yellow fluorescence indicated both the two constructs are co-transformed. In theory, co-transformed T1 individuals could produce up to quadruple *aha* mutations.

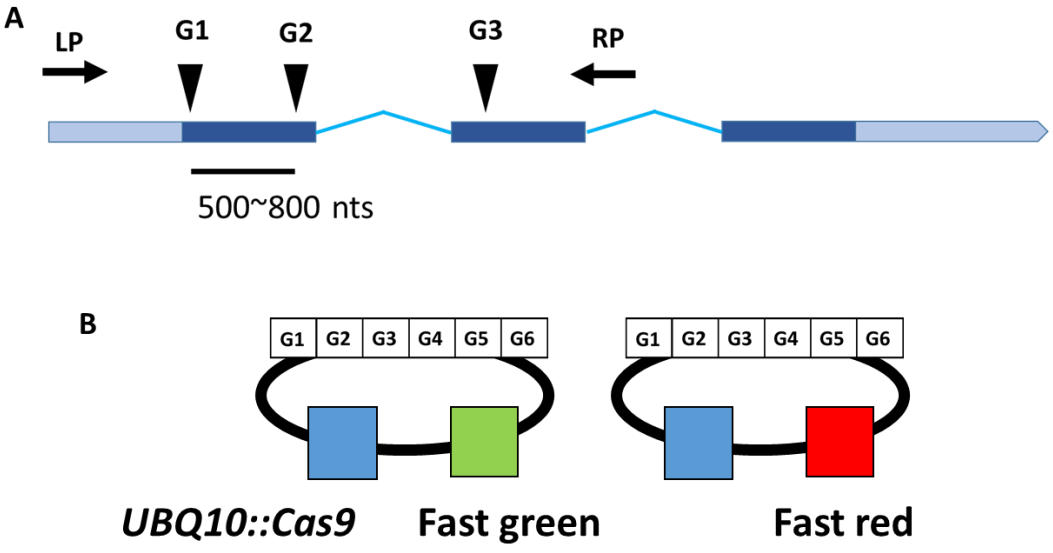

Figure 7.2 Scheme for guide RNA targeting of *AHA*s. (A) Each *AHA* was targeted by three guide RNAs at a 500-800 bp distance between the guide RNAs. (B) Six guide RNAs were assembled in one clone. Two clones, one with fast green and one with a fast red selection marker were co-transform into one WT plant.

Each T1 individual with clear CRISPR-deletions as detected using PCR genotyping was propagated to T2. Not many multiple mutations were found to be stable in the T2 generation, because the *UBQ10::Cas9* frequently produces somatic mutations. Two lines (#A11 and #A24) of *aha1 aha11* double mutant were found in the phloem targeting group (Figure 7.3). Both lines had early stop codons in the first few exons, which should stop translation. In the *AHA1* coding sequence, both lines had insertions in the third exon and deletions from the fourth to the sixth exons. In the *AHA11* coding sequence, both lines had an insertion in the first exon and a deletion in the fourth exon. Only line #A11 had an extra insertion on the sixth exon in *AHA11*. These stable mutations in lines #A11 and #A24 caused similar growth phenotypes to *aha1* T-DNA mutants (Kumari et al., 2019). That is, growth was similar to that of the WT

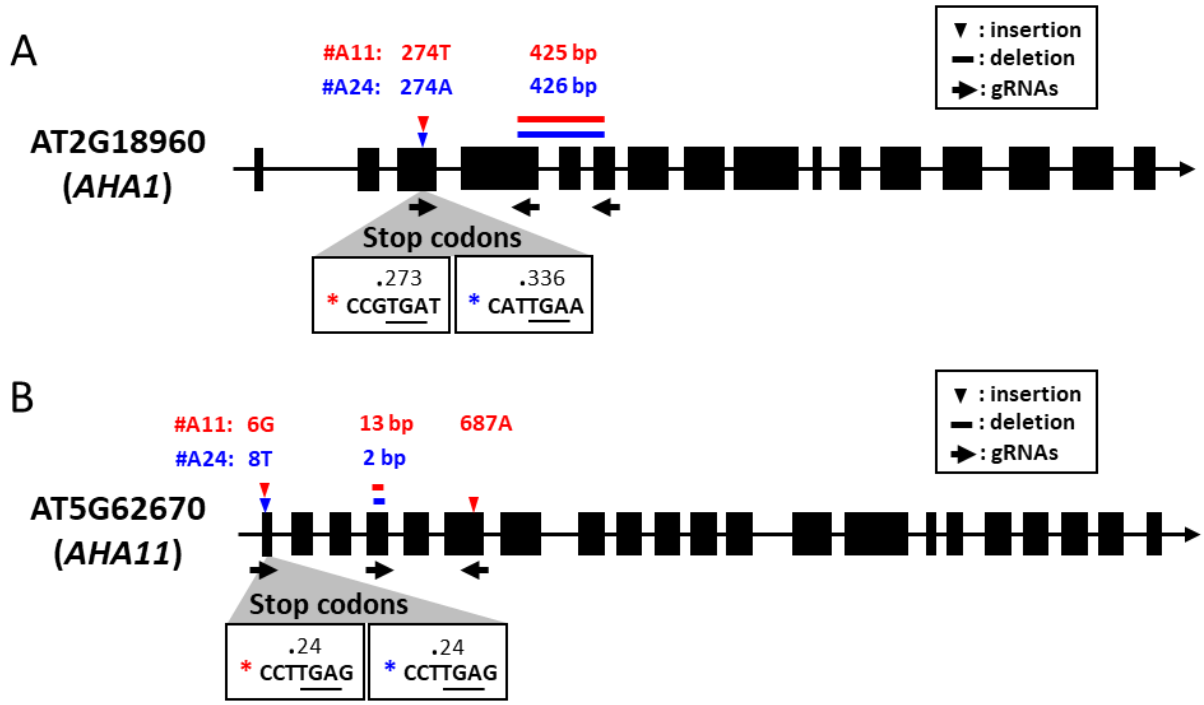

Figure 7.3 CRISPR-Cas9 *aha1 aha11* double mutants. Gene models for (A) *AHA1* and (B) *AHA11* indicating exons (black box) and guide RNAs target sites (black arrow). Two *aha1 aha11* double mutants (#A11 and #A24) were examined in detail. CRISPR-Cas9 mutations in #A11 (red) and #A24 (blue) lines are marked on the model. Base pair (bp) inserts are shown

with triangles and positions within coding sequence. The coloured lines and numbers indicate the length of deletions. The first stop codon found in #A11 and #A24 is highlighted in boxes with red or blue asterisks. The numbers in the boxes indicate positions within the coding sequence.

We also found mutations in *AHA3* and *AHA8* in the phloem group. It was quite surprising that several of the T1 individuals (No. 3, 5, 6, 11, 17, and 21) seemed to have *aha3* bi-allelic mutations (Figure 7.4A). This might be because CRISPR-Cas9 induced mutations directly in the embryo which could bypass the pollen development phenotype caused by *aha3* mutation (Robertson et al., 2004). So, with the CRISPR-Cas9 approach, we were able to examine phenotypes in bi-allelic *aha3* mutant backgrounds. However, and as expected, these bi-allelic *aha3* mutants were male sterile (Figure 7.4B). To examine bi-allelic *aha3* individuals, experiments should be conducted on the generation (T1) in which the Cas9 is working. This would be heavily dependent on the transformation efficiency. More efficient transformation would lead to more T1 individuals that could be tested. Furthermore, we found many of these T1 individuals also had *aha8* deletions, but none of these individuals showed a clear loss of PCR amplification products corresponding to the WT-like *AHA8* (Figure 7.4A). This suggested that the bi-allelic *aha8* mutation might be lethal. Therefore, none of the individuals obtain clear loss of the WT-sized PCR products.

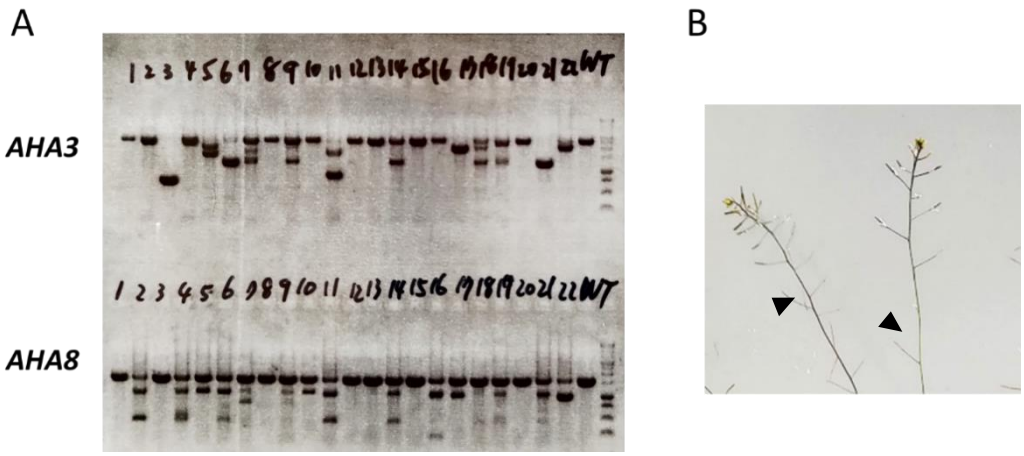

Figure 7.4 CRISPR-Cas9 *aha3* and *aha8* mutations in the T1 generation. (A) Genotyping PCR for *AHA3* and *AHA8*. (B) Male sterile phenotype in a bi-allelic *aha3* mutant.

This finding was supported by genotyping the clade II group (*AHA5, AHA6, AHA8, AHA9*) in the T2 generation (Figure 7.5). T2 lines were propagated from T1 individuals which showed mutations in *AHA6, AHA8,* and *AHA9*. The Cas9 and guide RNAs were removed in the T2 generation to eliminate additional CRISPR-Cas9 events. Three interesting features were found. Firstly, homozygous *aha6 aha9* double mutants were viable (No. 10 and 26 in Figure 7.5). Secondly, *aha6* and *aha9* single mutations did not occur with *aha8* mutations. Lastly, all the *aha8* mutants found were heterozygous. The *aha6 aha8 aha9* T-DNA mutants have fertility problems (Hoffmann et al., 2020). In that study, only 3-10 seeds were produced from each homozygous triple mutant plant. This supported our finding that the *aha6* and *aha9* mutations are incompatible with the *aha8* mutation (Figure 7.5). Thus, the CRISPR-Cas9 approach can generate *aha3* mutants and these experiments also revealed the potential lethality phenotype in *aha8* mutations for which no homozygous mutants were found. To reduce the complexity of our work, we then focused only on the phloem expressed group (AHA1, AHA3, AHA8, AHA11).

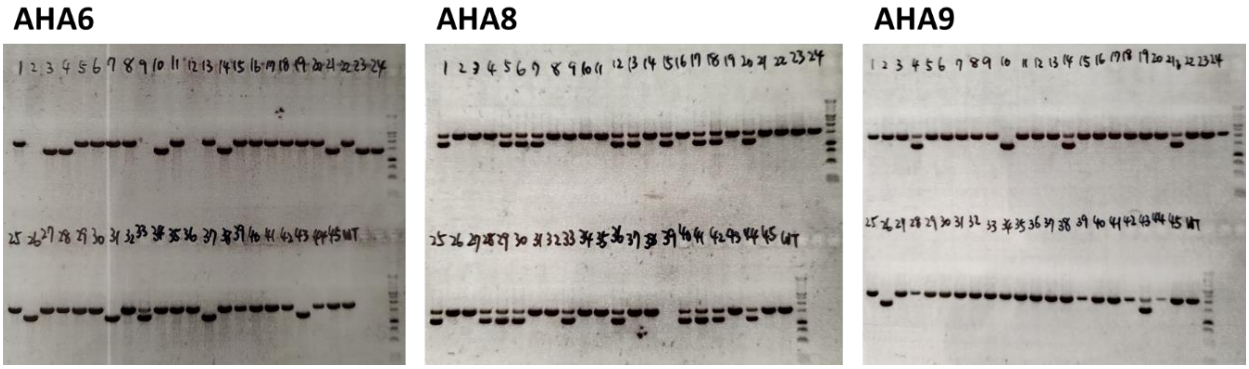

Figure 7.5 CRISPR-Cas9 *aha6*, *aha8*, *aha9* mutations segregating in the T2 generation. Genotyping PCR for *AHA6*, *AHA8*, and *AHA9*. Note the *aha6* and *aha9* mutations did not co-occur with heterozygous *aha8* mutation. No homozygous *aha8* mutant was found.

Mechanostimulated electrical signalling depends on phloem-expressed *AHA*s

Aurore Chételat genotyped many of the *aha* CRISPR-Cas9 mutants.

The mechanostimulation-induced electrical signal was associated with the vascular tissues, especially with the phloem (Chapter 4). *AHA1*, *AHA3*, *AHA8*, and *AHA11* were the highest expressed AHAs in the phloem (You et al., 2019). Two stable *aha1 aha11* double mutants (#A11 and #A24) were tested with bead mechanostimulations (Figure 7.6A). Very little difference in amplitude was found in line #A11 compared with WT (Figure 7.6B). Line #A24 didn't show any differences in both amplitudes and durations compared to the WT (Figure 7.6C). We assumed that this might be because of gene redundancy among the phloem-expressed AHAs.

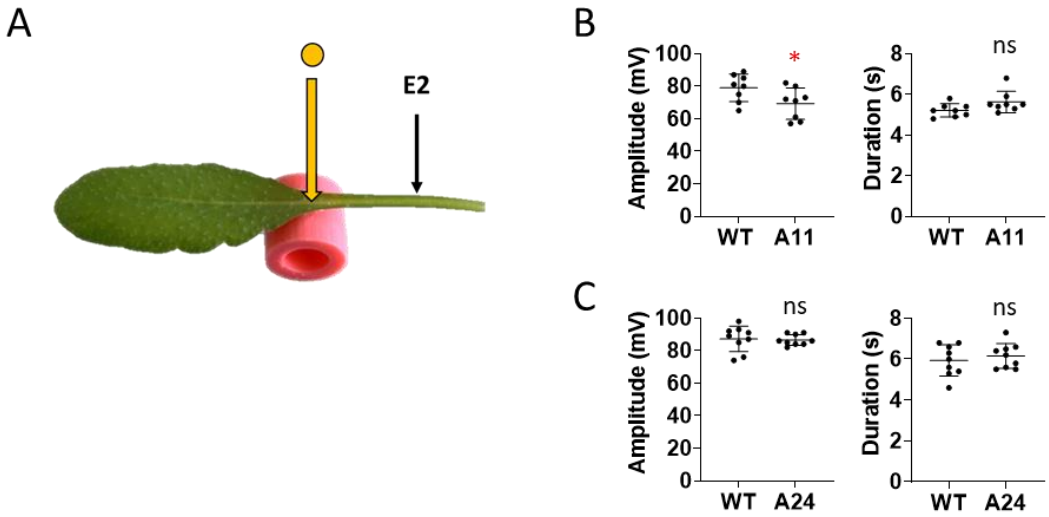

Figure 7.6 CRISPR-Cas9 *aha1 aha11* double mutants have little effect on mechanostimulation-induced electrical signals. (A) Mechanostimulation experimental design: 85 mg beads were dropped from an elevation of 2 cm onto the lamina/petiole junction. Estimated mechanostimulation force: 38 mN. ZT = 6-8. Amplitude and duration (B) #A11 (C) #A24. Bars are means ± SD. (n = 8-9). Student t-test: *P<0.05. ns = not significant.

As stated above, in the T1 generation, many plants in which we targeted *AHA3* seemed to have bi-allelic *aha3* mutations (two copies of *AHA3* were mutated), and all of these individuals had male-sterile phenotypes (Figure 7.4). We thus took advantage of this male-sterile phenotype. T1 individuals were backcrossed with WT. In the backcross generation, individuals should already have one copy of mutated *aha3*. Therefore, only one copy of *AHA3* would need to be mutated. This would increase the probability of producing bi-allelic *aha3* mutants. Using this approach, we found five bi-allelic *aha3* mutants among 12 individuals in the backcross generation (Figure 7.7A). These bi-allelic *aha3* mutants were confirmed to have male-sterile phenotypes (Figure 7.7B). This phenotype seemed not to be related to heterozygous *aha8* mutations. Plants No.15 and No.19 did not have clear deletions in *AHA8*, but both of them were male-sterile (Figure 7.7A and B). Mechanostimulation-induced electrical signals were

investigated in bi-allelic *aha3* mutants (Figure 7.7C). Interestingly, significant differences relative to the WT were found in signal amplitudes and durations (Figure 7.7D). But the effect was much weaker than the constitutively active mutant *ost2-2D* (Chapter 5).

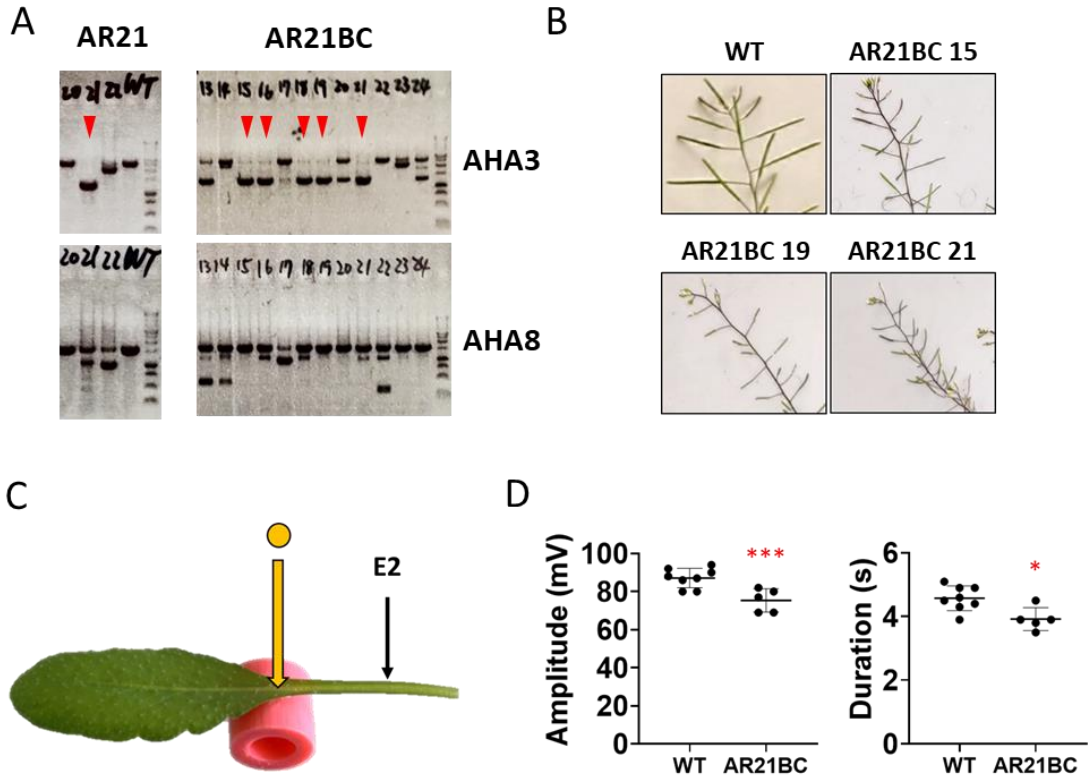

Figure 7.7 Bi-allelic *aha3* CRISPR-Cas9 mutations attenuated mechanostimulation-induced electrical signals. (A) Genotyping PCR for *AHA3* and *AHA8.* Red arrowheads indicated the bi-allelic *aha3* mutants in T1 (AR21) and in back crossed (AR21BC) generations. (B) Siliques of WT and male-sterile *aha3* mutants. (C) Mechanostimulation experimental design: Plant were stimulated with 85 mg beads dropped from elevation of 2 cm. Estimated mechanostimulation force: 38 mN. ZT = 6-8. (D) Amplitude and duration of mechanostimulation-induced electrical signals. Bars are means ± SD. (n = 5-8). Student *t*-test: *** P<0.001; * P<0.05.

The effect of heterozygous *aha8* mutation was investigated in the T3 population (Figure 7.8) propagated from the T2 individual (Figure 7.5) which showed clear deletions in *AHA8.* Because deletions in *AHA6* and *AHA9* did not occur with deletions in *AHA8* (Figure 7.5), these

T3 plants were highly likely to be *aha8* single mutants (Figure 7.8A and B). No difference in the amplitudes of mechanostimulation-induced electrical signals was found (Figure 7.8C and D). These findings suggested the phloem-expressed AHAs were important for mechanostimulation-induced electrical signal propagation.

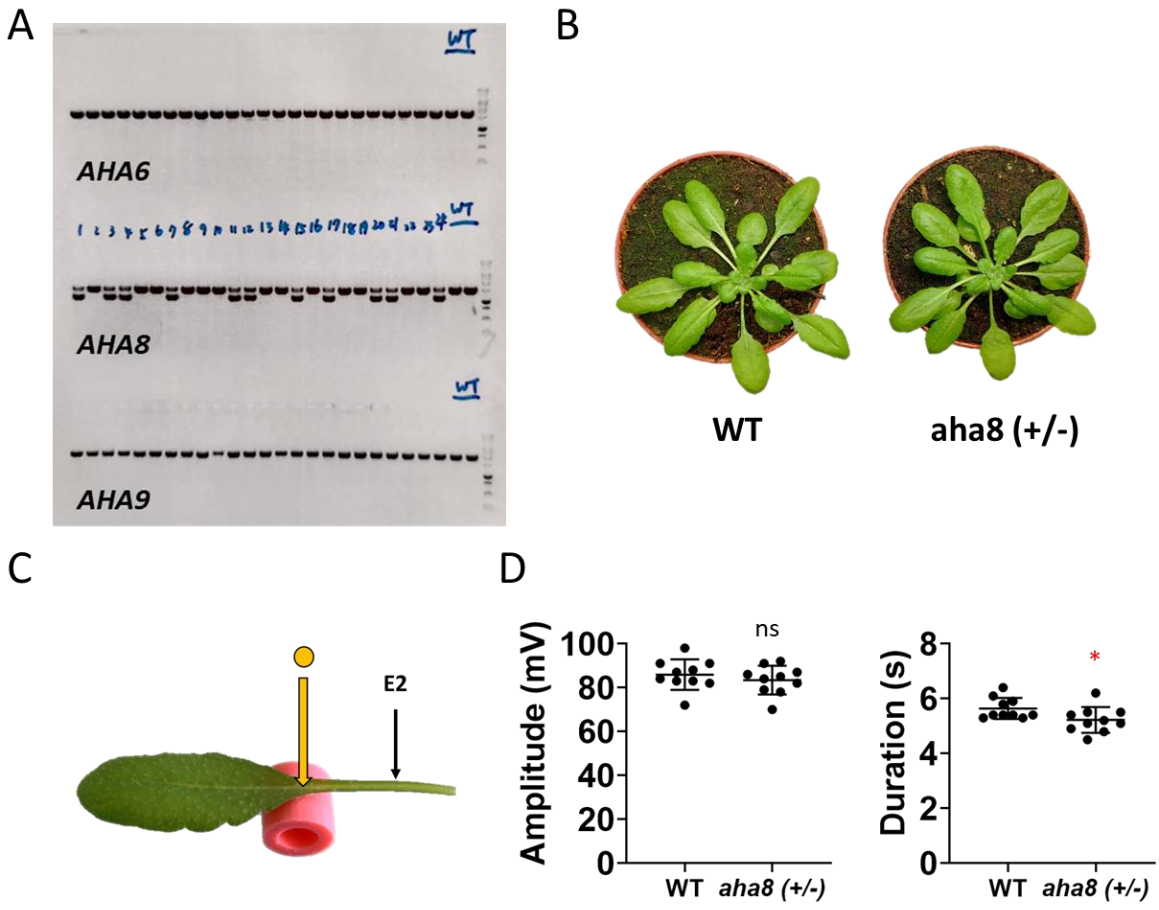

Figure 7.8 Heterozygous CRISPR-Cas9 *aha8* mutations have no effect on the amplitude of the mechanostimulation-induced electrical signal. T3 Plants propagated from the T2 individuals which show deletion in *AHA8* in Fig. 7.5. (A) Genotyping PCR for *AHA6*, *AHA8*, and *AHA9*. (B) Rosette phenotype of WT and heterozygous *AHA8/aha8* mutant. (C) Mechanostimulation experimental design: Plant were stimulated with 85 mg beads dropped from elevation of 2 cm. Estimated mechanostimulation force: 38 mN. ZT = 6-8. (D) Amplitudes and durations of mechanostimulation-induced electrical signals. Bars are means ± SD. n = 10. Student t-test: * $P<0.05$; ns = not significant.

To overcome the redundancy among phloem-expressed AHAs, a higher order mutant was required. Because of the male-sterile phenotype in bi-allelic *aha3* mutants, crossing *aha1 aha11* double mutants with *aha3 aha8* double mutants might not be an ideal strategy. We thus conducted a secondary CRISPR-Cas9 to target *AHA3* and *AHA8* in the #A11 (*aha1 aha11*) background (A11Re T1). If multiple *aha* mutations didn't kill the plant, triple or quadruple mutants should be found in the new T1 generation. Interestingly, we found five of A11Re T1 individuals have a slow-growth phenotype (Figure 7.9) although the majority of these T1 plants looked normal.

Figure 7.9 The rosette phenotype of 5-week-old A11Re T1 plants

Among the normal-sized T1 plants, only one (No.8) had obvious deletions in *AHA3* (Figure 7.10A). Because *UBQ10pro::Cas9* could create non-heritable mutations in somatic cells, the plant with somatic mutations would have more than two PCR products derived from different mutations in a gene. Multiple *AHA3* PCR products were found in plant No.8, suggesting somatic mutations in *AHA3*. T1 plants with clear CRISPR-Cas9 events in *AHA3* all showed a slow-growth phenotype (No. 15-19) (Figure 7.9 and Figure 7.10A, B). Notably, the slow-growth phenotype was more likely associated with the loss of *AHA3* function, because *aha8* mutations could not be homozygous, and the heterozygous *aha8* mutant did not have any

phenotype (Figure 7.8 and Figure 7.10A). Also, the No.15 individual had a slow-growth phenotype with only obvious bi-allelic *aha3* mutations and no obvious signs of *aha8* mutation (Figure 7.10A and B). The normal-growth T1 plants (No.1-14) were tested with mechanostimulations (Figure 7.10C). Strikingly, plant No.8 showed a significantly decrease in the amplitude of the mechanostimulation-induced electrical signal (Figure 7.10D). It was the only near normal-growth plant which has obvious *aha3* deletions (Figure 7.10A and B).

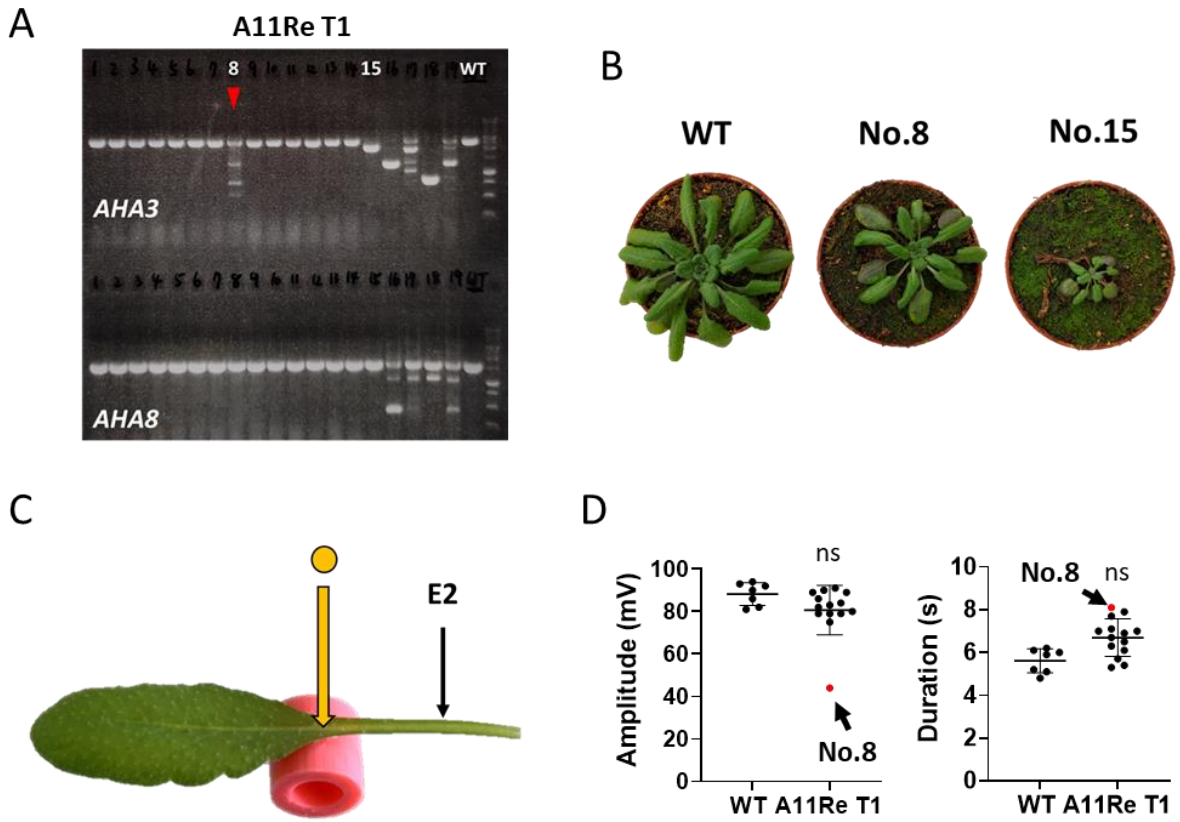

Figure 7.10 Effect of CRISPR-Cas9 mutations of *aha3* and *aha8* in the *aha1 aha11* background. T1 plants from this secondary CRISPR-Cas9 are referred to as A11Re T1. (A) Genotyping PCR for *AHA3* and *AHA8.* Red arrowhead indicates *aha3* mutation T1 No.8. (B) Rosette phenotype of WT, No.8 and No.15 of T1 plants. (C) Mechanostimulation experimental design: Plant were stimulated with 85 mg beads dropped from elevation of 2 cm. Estimated mechanostimulation force: 38 mN. ZT = 6-8. (D) Amplitude and duration of mechanostimulation-induced electrical

signals. Bars are means ± SD. WT (n = 8), T1 (n = 14). Amplitude and duration of No.8 plant shown as red dots. Student t-test: ns = not significant.

Bi-allelic *aha3* mutations lead to slow-growth in the *aha1 aha11* background (like No.15 and the No.16 plants in Figure 7.10B) and male-sterility phenotypes even in the WT (Figure 7.7B and Figure 7.11). The normal-growth No.8 plant seemed not to have bi-allelic *aha3* mutations (Figure 7.10B and Figure 7.11). Then, the reduction of the electrical signal in No.8 plant could be due to the heterozygous *aha3* mutation or somatic *aha3* mutations. In the case of somatic mutation, *aha3* was mutated in somatic cell populations that were necessary for mechanostimulation-induced electrical signals. This might cause a similar effect as bi-allelic *aha3* mutants. It was possible that plant No.8 have *aha3* mutations produced by *UBQ10pro::Cas9* specifically in the essential somatic cell populations. That is, in other words, knocking out *aha3* tissue specifically in plant No.8 was lucky.

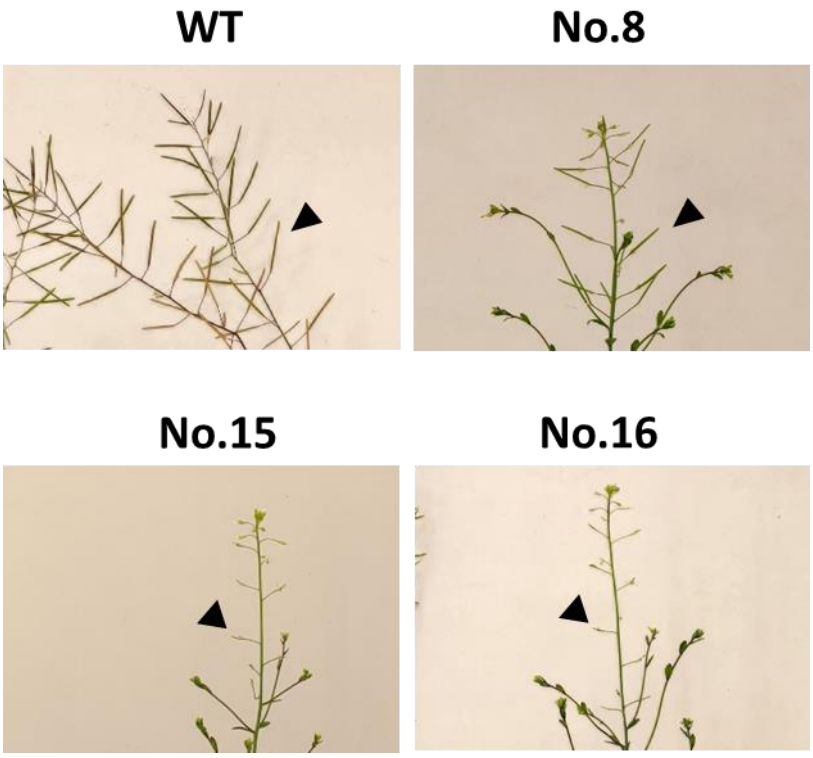

Figure 7.11 The siliques of WT and A11Re T1 plants.

To investigate the effect of heterozygous *aha3* mutations on mechanostimulation-induced electrical signals, plants No.15 and No.16 were backcrossed with line #A11. In the backcross generation, seeds without Cas9 were selected according to the absence of red fluorescence (Figure 7.2B). Stable deletions in *AHA3* would follow Mendelian inheritance. For example, 100 % of No.15 backcross offspring showed *aha3* deletions consistent with the T1 generation (Figure 7.12A). This indicated homozygous *aha3* deletions in T1 plant No.15. 50 % of No.16 backcross offspring showed consistent *aha3* deletions suggesting that the T1 No.16 individual had one copy of the *aha3* deletion and one copy of an *aha3* small mutation (Figure 7.11 and Figure 7.12A). The *aha3* small mutation allele was further mutated in somatic cells, thus producing a homozygous-like PCR result in T1 (Figure 7.10A). No obvious *aha8* deletions were found in backcross populations (Figure 7.12A).

Mechanostimulation-induced electrical signals were investigated in the plants with clear heterozygous *aha3* deletions (Figure 7.12B). None of the heterozygous mutants had severe growth phenotypes (Figure 7.12C). Interestingly, no differences were found in the amplitudes and durations of the mechanostimulation-induced electrical signals in those plants (Figure 7.12D). This finding suggested the reduction of the amplitude in No.8 T1 plant was not due to heterozygous *aha3* mutation. Therefore, a potential explanation for this observation was, that somatic mutations disrupted AHA3 functions in an essential cell population, producing a phenotype like homozygous *aha3* mutants in the mechanostimulation-induced electrical signal. However, the cell populations which were necessary for mechanostimulation-induced electrical signals were not yet identified. Therefore, we investigated the effect of bi-allelic *aha3* mutations in the *aha1 aha11* background (Figure 7.10 and Figure 7.11).

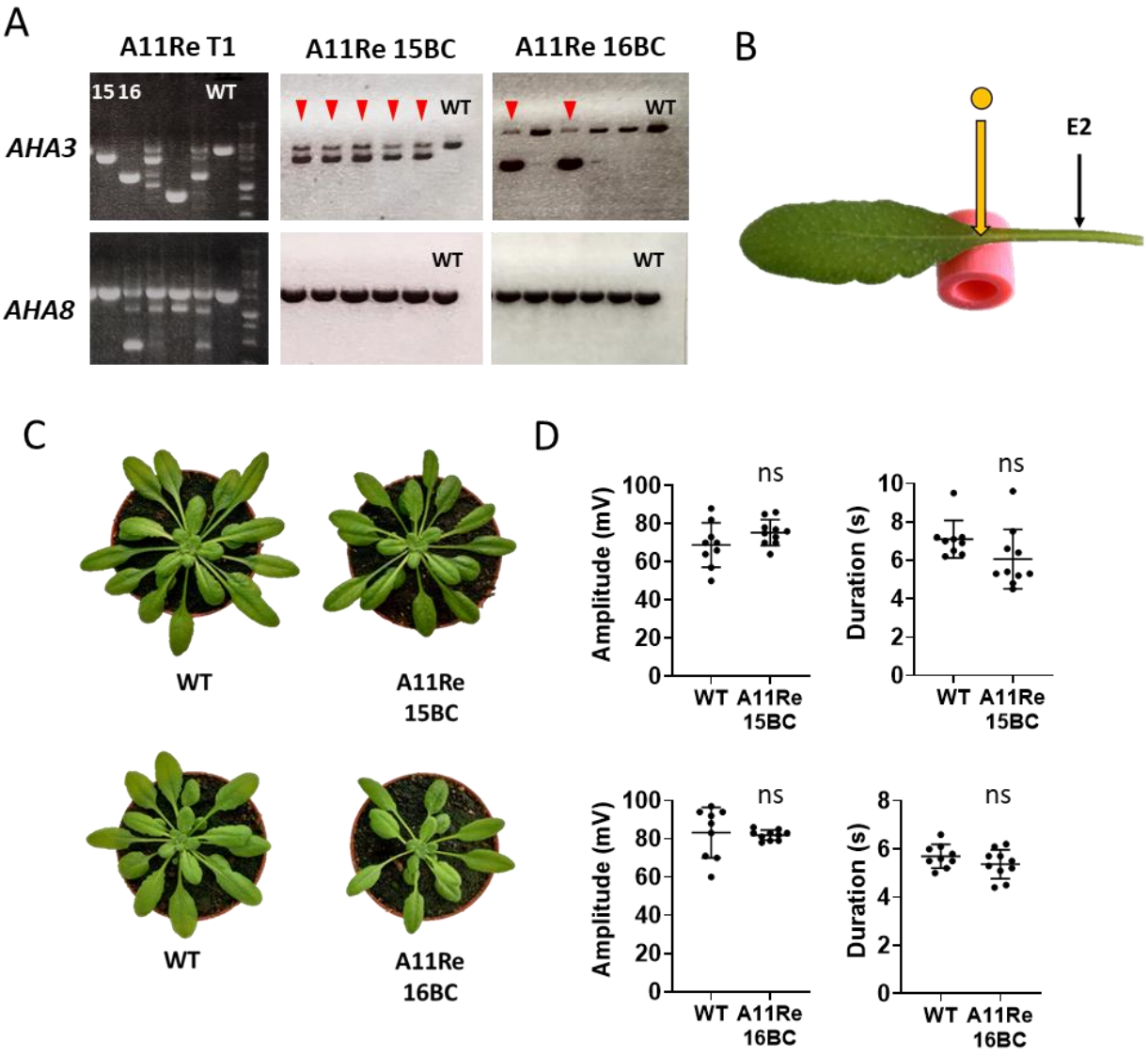

Figure 7.12 Effect of heterozygous *aha3* mutations in the *aha1 aha11* background. (A) Genotyping PCR for *AHA3* and *AHA8*. Red arrowheads indicate the individuals with *aha3* deletions in the backcrossed (A11Re15BC and A11Re16BC) generation. Note the presence of WT *AHA3* DNA in all plants tested. (B) Mechanostimulation experimental design: Plant were stimulated with 85 mg beads dropped from elevation of 2 cm. Estimated mechanostimulation force: 38 mN. ZT = 6-8. (C) Rosette phenotypes of WT, A11Re15BC and A11Re16BC plants. (D) Amplitude and duration of mechanostimulation-induced electrical signals. Bars are means ± SD. (n = 9-10). Student t-test: ns = not significant.

T2 seeds propagated from the No.8 T1 plant were selected using fluorescence markers (Figure 7.2B and Figure 7.11). The seeds without red fluorescence markers do not carry the Cas9 and guide RNAs construct and no further CRISPR-Cas9 events would happen in these seeds. The rosette phenotypes of the dark seeds was consistent with heterozygous *aha3* mutant lines (15BC and 16BC)(Figure 7.12C and Figure 7.13). With the activity of Cas9, the red fluorescent T2 seeds could undergo another round of CRISPR-Cas9 mutagenesis. Consistently, the potential bi-allelic *aha3* mutants in the T2 generation had similar slow-growth phenotypes (Figure 7.9. and Figure 7.13). The rosette phenotypes suggested new CRISPR-Cas9 events happening in the T2 generation.

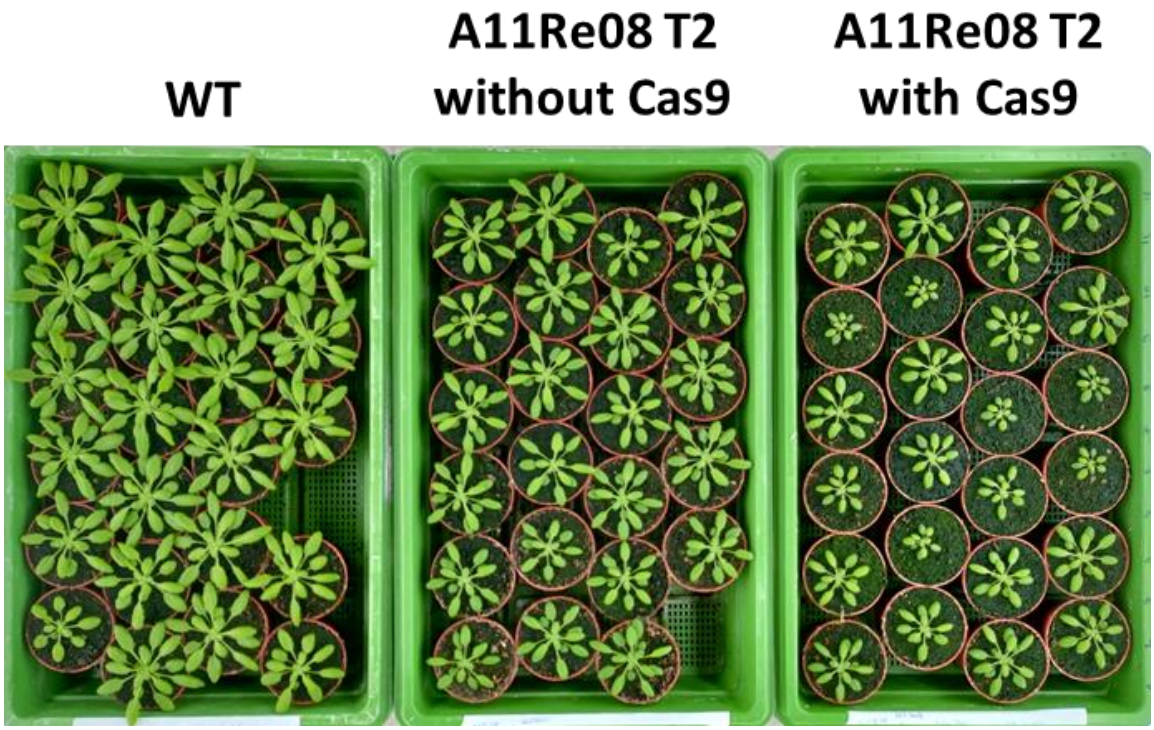

Figure 7.13 Rosette phenotype of WT and A11Re08 T2 plants. T2 plants propagated from A11Re No.8 T1 individual. Plants with and without Cas9 were selected according to the red fluorescence of T2 seeds.

The slow-growth A11Re08 T2 plants were genotyped for *AHA3* and *AHA8* (Figure 7.13 and Figure 7.14A). Some of the individuals showed novel large deletions in *AHA3*. Among all the individuals, no deletions were found in *AHA8*. However, due to the limitation of genotyping, small CRISPR-Cas9 events would not be visualized in the gels. Bi-allelic *aha3* mutations were confirmed by loss of fertility (Figure 7.14B). All the slow-growth T2 plants had male-sterile phenotypes, which was consistent with the T1 generation (Figure 7.9 and Figure 7.11). Therefore, the slow-growth T2 plants were highly likely to be homozygous *aha1 aha3 aha11* triple mutants. The 8-week-old slow-growth mutant had a similar rosette size to a 5-week-old WT (Figure 7.14C).

Mechanostimulation-induced electrical signals in T2 mutants and WT controls were investigated (Figure 7.14C and D). Strikingly, all of the slow-growth mutants showed similar reductions in signal amplitudes to No.8 T1 individual (Figure 7.10C and Figure 7.14E). The durations were not affected in T2 mutants (Figure 7.14F). Interestingly, 8-week-old WT plants showed reductions in amplitudes on average (Figure 7.14E). However, half of the 8-week-old WT plants displayed amplitudes similar to those of the 5-week-old WT. The signal durations were significantly increased in 8-week-old WT plants (Figure 7.14F). The *aha* mutations in T2 plants decreased the amplitudes to a T1-like level and had no effect in durations. Only the 8-week-old WT showed significant increases in durations. This evidence supported the conclusion that the slow-growth T2 mutants were likely to be the *aha1 aha3 aha11* triple mutants.

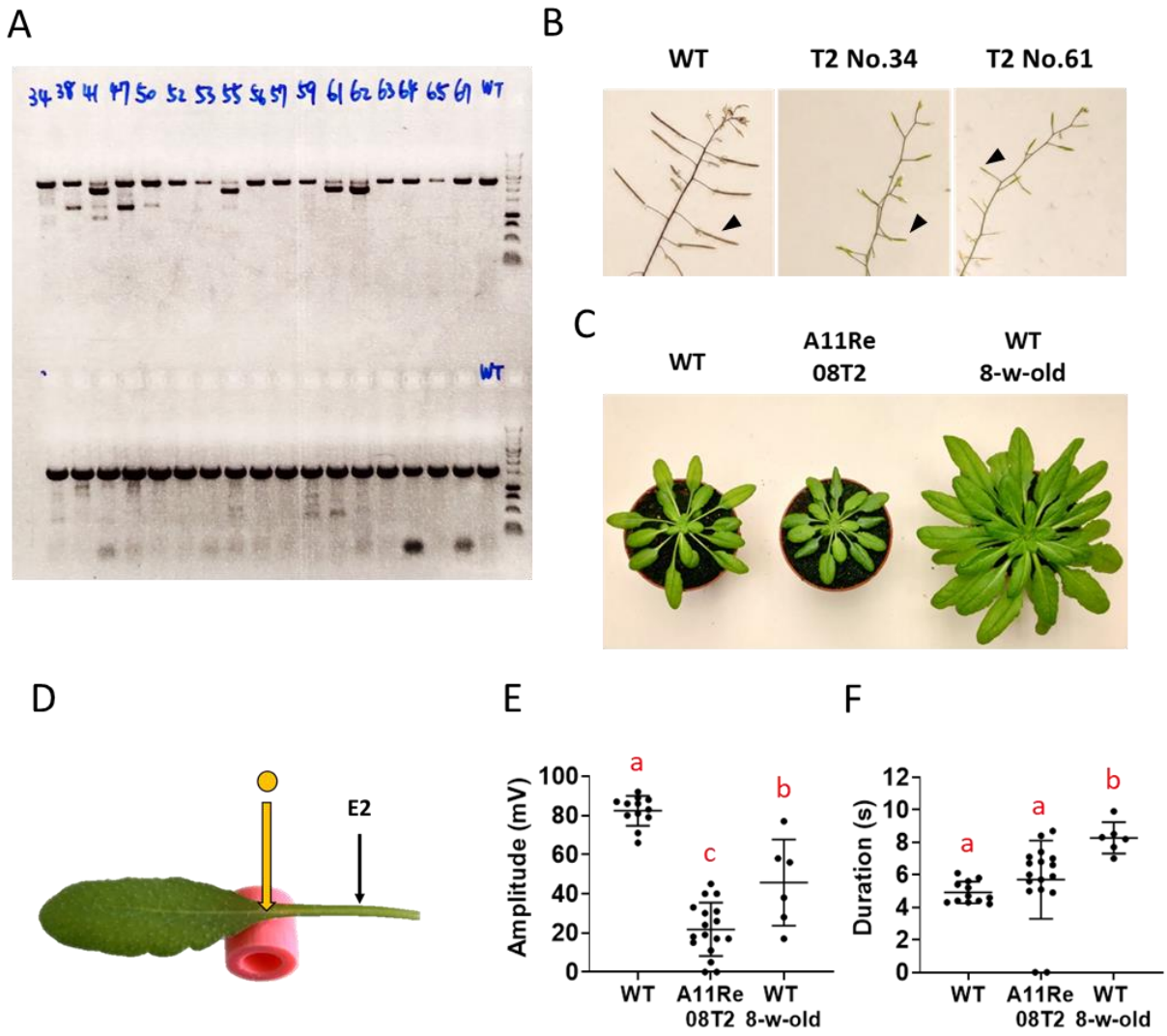

Figure 7.14 The slow-growing T2 plants had bi-allelic *aha3* mutant phenotypes. (A) Genotyping PCR for *AHA3* and *AHA8.* (B) Siliques of WT, No.34 and No.61 of T2 plants. (C) Rosette phenotype of 5-week-old WT, 8-week-old A11Re08 T2 plant and 8-week-old WT. (D) Mechanostimulation experimental design: Plant were stimulated with 85 mg beads dropped from elevation of 2 cm. Estimated mechanostimulation force: 38 mN. ZT = 6-8. (E) Amplitudes and (F) Durations of mechanostimulation-induced electrical signals. Bars are means ± SD. (n=6-14). Letters indicate significant differences, Tukey HSD test: $P<0.05$.

If the slow-growth mutants were *aha1 aha3 aha11* triple mutants, would the normal-growth plants in this T2 population have any phenotype? To address this question, we tested

the backcrossed line A11Re16BC. The backcrossed generation without the presence of Cas9 was used to examine the effect of heterozygous *aha3* mutations in the *aha1 aha11* background (Figure 7.12). In this experiment, red fluorescent seeds in the backcrossed generation were selected for the presence of Cas9 which should have produces new mutations in *AHA3* and *AHA8.* All the plants with the presence of Cas9 were grown until 8 weeks old. The normal-growth plants had similar rosette phenotypes to 8-week-old WT (Figure 7.14C and Figure 7.15A). No novel big deletions in *AHA3* or *AHA8* were detected, which suggested that any new CRISPR-Cas9 events produced small mutations or no mutations at all (Figure 7.15B). Consistently, both WT and the normal-growth mutants could produce seeds (Figure 7.15C). The slow-growth mutants were male-sterile which was similar to the result in A11Re08 T2 (Figure 7.14B and Figure 7.15C). A second independent line 16BC showed the slow-growth mutants were likely to be *aha1 aha3 aha11* triple mutants. We thus examined the mechanostimulation-induced electrical signals in this line (Figure 7.15D).

Strikingly, the electrophysiology data supported our hypothesis. The amplitudes in the 5-week-old WT were similar to the amplitudes in the 8-week-old normal-growth mutant (Figure 7.15E). The amplitudes in the potential *aha1 aha3 aha11* mutants were significantly decreased relative to the WT. Only the 8-week-old normal-growth mutants had significant increases in durations (Figure 7.15F). The increase in the duration was consistent with the mechanostimulation-induced electrical signals in 8-week-old WT (Figure 7.14F). In this experiment, we confirmed the normal-growth CRISPR-Cas9 mutants had no phenotypes that differed from the WT. Also, the second independent line of *aha1 aha3 aha11* mutant showed consistent results of the rosette growth phenotype, male-sterile phenotype, and reduction in the amplitudes of mechanostimulation-induced electrical signals.

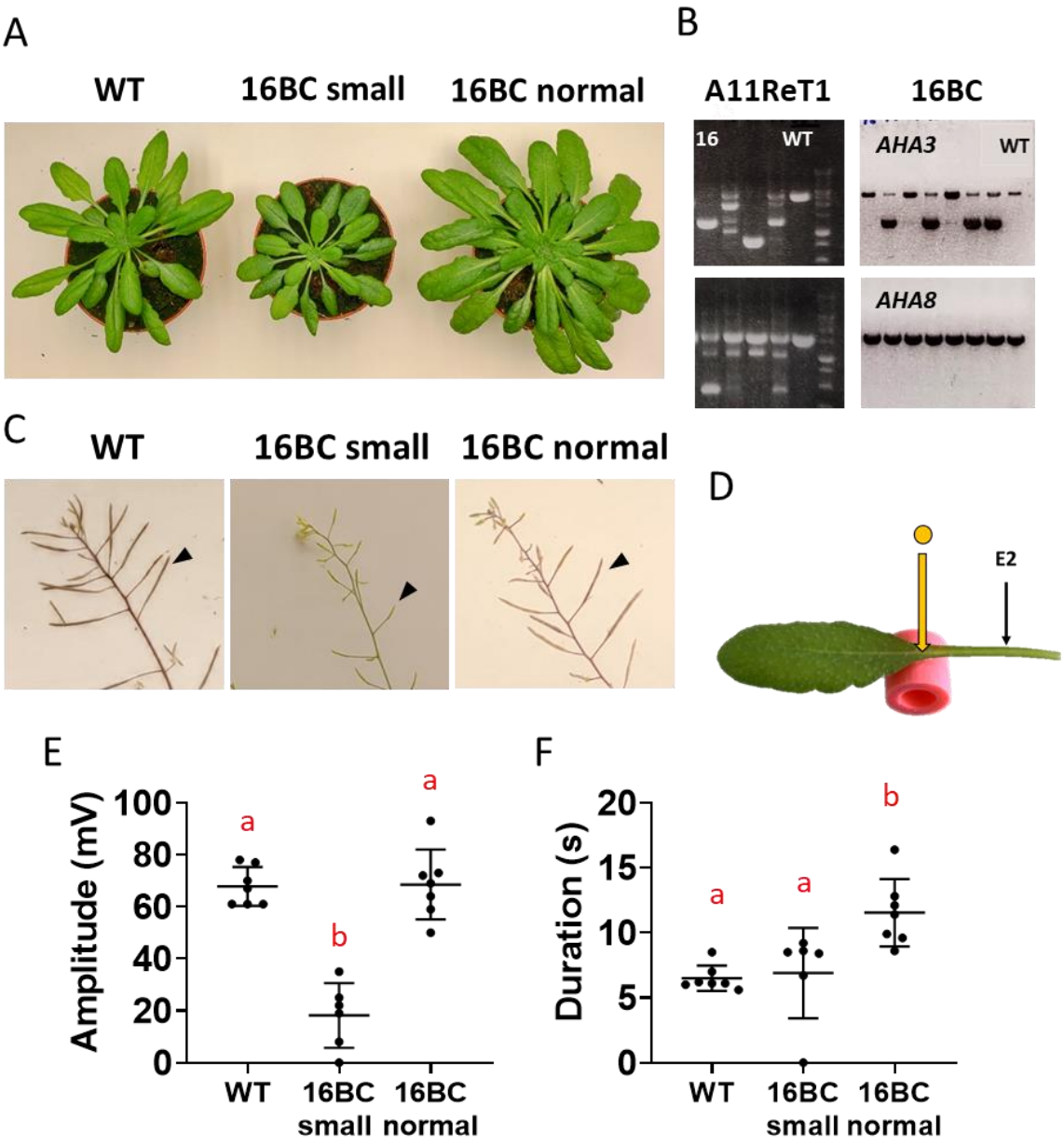

Figure 7.15 The normal-growth CRISPR-Cas9 A11ReBC16 mutants had WT-like phenotypes. (A) Rosette phenotypes of 5-week-old WT, 8-week-old 16BC slow-growth plant and 8-week-old 16BC normal-growth plant. (B) Genotyping PCR for *AHA3* and *AHA8*. (C) Siliques of WT, 16BC slow-growth plant and 16BC normal-growth plant. (D) Mechanostimulation experimental design: Plant were stimulated with 85 mg beads dropped from elevation of 2 cm. Estimated mechanostimulation force: 38 mN. ZT = 6-8. (E) Amplitudes and (F) Durations of mechano-stimulation-induced electrical signals. Bars are means ± SD. (n=6-7). Letters indicate significant differences, Tukey HSD test: $P<0.05$.

The potential *aha1 aha3 aha11* phenotypes were confirmed in a third independent line A11Re15BC. This backcrossed line was also used in the previous experiment testing the effect of heterozygous *aha3* mutations. The red fluorescent seeds were selected for the presence of Cas9 in this generation. The new CRISPR-Cas9 mutants with the slow-growth phenotype were chosen (Figure 7.16A). All the potential *aha1 aha3 aha11* mutants were shown to possibly be bi-allelic *aha3* deletions (Figure 7.16B). Some new deletions were found in *AHA8* but many of them might be somatic mutations (Figure 7.16B). Because more than two sizes of PCR products were found in *AHA8.* The potential *aha1 aha3 aha11* mutants were all male-sterile (Figure 7.16C). This was consistent with the results found in A11Re08T2 and A11Re16BC lines (Figure 7.14B and Figure 7.15C). Furthermore, the mechanostimulation-induced electrical signal was significantly reduced in signal amplitudes, and no difference in durations (Figure 7.16D, E, and F). The deletions found in *AHA8* did not affect the mechanostimulation-induced electrical signals. The electrophysiology results were consistent with previous experiments (Figure 7.14E, F, and Figure 7.15E, F).

To sum up, we identified a slow-growth phenotype which was likely due to bi-allelic *aha1 aha3 aha11* mutations (Figure 7.10A). Reproducible results were found in three independent CRISPR-Cas9 mutant lines. All the potential *aha1 aha3 aha11* individuals were male-sterile, which was similar to the bi-allelic *aha3* mutants (Figure 7.7B). The amplitudes of mechanostimulation-induced electrical signals were significantly reduced in *aha1 aha3 aha11* but the duration was not. However, the presence of heterozygous *aha8* mutations could not be excluded completely with this method. The guide RNAs targeted *AHA3* and *AHA8* were assembled in the same construct. In order to exclude the influence of heterozygous *aha8* mutations, further experiments were needed.

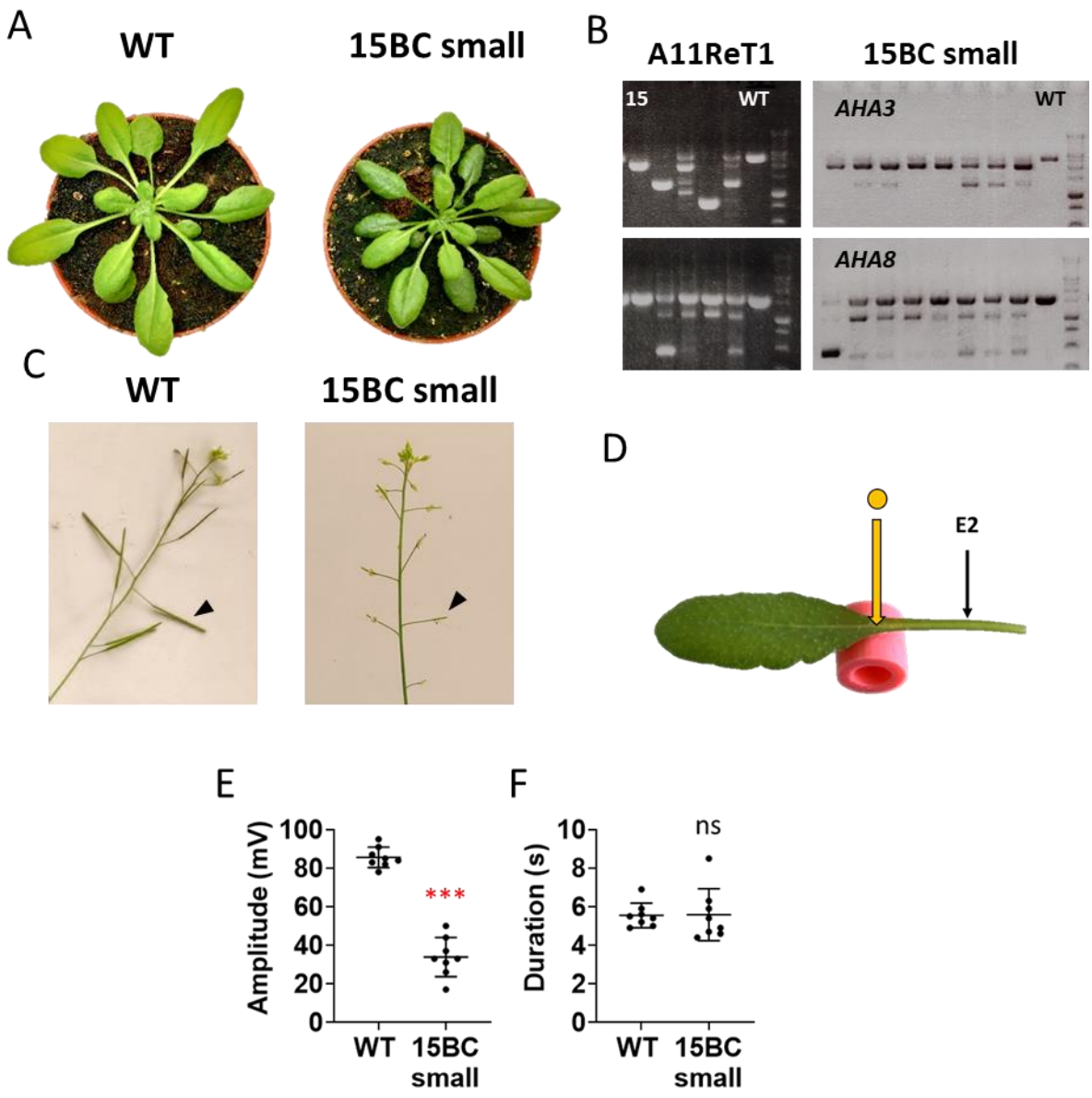

Figure 7.16 Consistent phenotype found in the third independent line (15BC) of CRISPR-Cas9 mutants. (A) Rosette phenotypes of 5-week-old WT and 15BC slow-growth mutant. (B) Genotyping PCR for *AHA3* and *AHA8*. (C) Siliques of WT and 15BC slow-growth mutant. (D) Mechanostimulation experimental design: Plant were stimulated with 85 mg beads dropped from elevation of 2 cm. Estimated mechanostimulation force: 38 mN. ZT = 6-8. (E) Amplitudes and (F) Durations of mechanostimulation-induced electrical signals. Bars are means ± SD. (n=8). Student t-test: *** $P<0.001$; ns = not significant.

Conclusion and Discussion:

Failing to find strong effects of a number of ion channel mutants on touch-responses electrical signalling. plasma membrane proton pumps (AHAs) were mutated with the CRISPR-Cas9 approach. Two independent homozygous *aha1 aha11* mutant lines showed minor effects on mechano-stimulation-induced electrical signals. Using CRISPR-Cas9, bi-allelic *aha3* mutations were identified. All the bi-allelic *aha3* mutations showed male-sterile phenotypes consistent with a previous study which found that T-DNA mutated *aha3* alleles cause male gametophyte lethality (Robertson et al., 2004). We found that CRISPR-Cas9-induced homozygous *aha8* mutations were not recoverable. This observation was consistent in two consecutive generations. Also, *aha6* and *aha9* mutations did not overlap with the heterozygous *aha8* mutation (Figure 7.5). This might be due to the severe retardation in pollen development and seed production in *aha6 aha8 aha9* (Hoffmann et al., 2020). However, in that study, the homozygous T-DNA *aha6 aha8 aha9* mutants have almost no detectable *AHA8* transcripts. This is different from our observation that homozygous *aha8* might be lethal. The T-DNA mutated genes might have minimum levels of *AHA8* expression remaining that kept the homozygous *aha8* T-DNA mutants alive (Hoffmann et al., 2020). These findings suggest that the CRISPR-Cas9 approach can provide new insights into the importance of plasma membrane proton pumps in *Arabidopsis*.

Potential bi-allelic loss-of-function *aha3* mutants are infertile (Figure 7.4). This was observed in the potential *aha1 aha3 aha11* mutant lines. The male-sterile phenotype in the potential *aha1 aha3 aha11* lines (A11Re08T2, A11Re15BC, and A11Re16BC) was coupled with a slow-growth phenotype. These mutants grew much slower than WT under short-day conditions. An 8-week-old slow-growth *aha1 aha3 aha11* had a similar rosette size to a 5-week-old WT. This slow-growth phenotype might be due to the decreased nutrient

transportation in these mutants. Plasma membrane proton pumps are important for nutrient transport in Arabidopsis (Palmgren, 2001). Moreover, many secondary transporters rely on electrochemical gradients built by plasma membrane proton pumps (Duby and Boutry, 2009). Reduced proton gradients in *aha1 aha3 aha11* would also inhibit the activity of secondary transporters. This would lead to growth rates much slower in the mutants than in the WT. On the other hand, the reduction of secondary transports might be able to serve as a support for the reduced proton gradient across the plasma membrane. The resting plasma membrane potential depends on the proton gradient buildup by plasma membrane proton pumps (Sze et al., 1999). Attenuated proton gradients on the plasma membrane not only inhibit secondary transporters but also reduce the strength of membrane depolarization. This is a likely reason why we found electrical signal amplitudes were largely attenuated in those *aha1 aha3 aha11* plants. The reduction of amplitudes was coupled with the slow-growth and male-sterile phenotypes. Neither 8-week-old WT plants nor 8-week-old normal-growth CRISPR-Cas9 mutants showed similar reductions in mechanostimulation-induced electrical signals. Additionally, the obvious *aha8* deletions in A11Re15BC did not enhance any of the phenotypes (electrical signal and growth) more than the lines (A11Re08T2 and A11Re16BC) without obvious *aha8* deletions. This might be because either heterozygous *aha8* mutations do not affect electrical signals or the other two lines (A11Re08T2 and A11Re16BC) have small *aha8* mutations that were not detected in PCR gels. To address these possibilities, we could redo transformation with constructs targeting *AHA3* only (without *AHA8*) into *aha1 aha11* background. If similar phenotypes (slow-growth, male-sterile, and reduced signal amplitudes) appeared, the effect of heterozygous *aha8* mutation could be ruled out.

Chapter 8: DISCUSSION AND PERSPECTIVES

Mechanostimulation activates jasmonate-dependent defense in *Arabidopsis* (Chehab et al., 2012). This thesis work identifies LOX2 and LOX6 as the most mechanostimulation-responsive jasmonate precursor-producing LOXs. This is consistent with their role in wound-induced jasmonate production (Figure 8.1). This might suggest that mechanostimulation-induced defenses share a similar level of importance to wound-induced defenses in plant biology. However, this would need to be tested. Plants grown in nature can receive multiple mechanostimulations on rainy or windy days. As shown in Chapter 6, the *Arabidopsis* grown in the field shows restricted rosette growth, similar to the observation of serial wounding-triggered growth inhibition (Yang et al., 2020). LOX3 and LOX4, essential for this growth inhibition are shown to be activated with repeated leaf bending in Chapter 6. Moreover, the refractory period of the touch-induced electrical signal characterized in Chapter 4 might be the key to controlling such growth regulation. We found that recovery periods between 30-90 minutes are required for triggering a second mechanostimulation-induced electrical signal. This observation coincidently matched with the time course of touch-induced *JAZ10* transcripts (Chapter 6). 90 minutes after mechanostimulation has the most pronounced induction. The refractory period controlling the responsiveness to the second mechanostimulation may have evolved to better regulate plant growth in nature since constant jasmonate production would be detrimental to the plant.

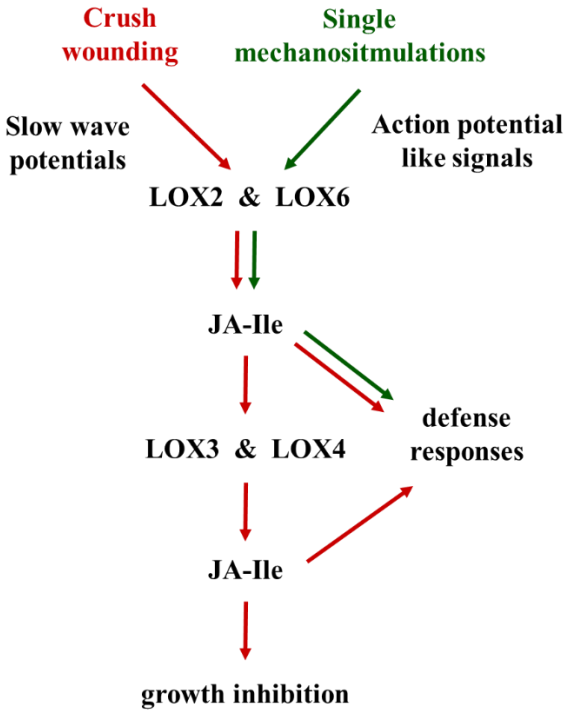

Figure 8.1 The interrelationship of responses to large wounds and to single gentle mechanostimulations. This figure integrates the two main aspect studied in the thesis.

Plants grown in nature are expected to receive numerous stimuli from the environment. A wild accession of *Arabidopsis* developed a smaller rosette when it grew on the University of Lausanne campus rather than in the laboratory as shown in Chapter 6. It was also shown that the constitutive active *ost2-2D* mutation attenuated both the wound (Kumari et al., 2019) and touch-response electrical signals (Chapter 5). Since the *ost2-2D* allele was identified from a forward genetic screen (Merlot et al., 2002), there is no transgenic T-DNA in the *ost2-2D* mutant plants. Therefore, it would be permitted to plant *ost2-2D* on the campus in Spring to observe its growth phenotype under the non-laboratory short-day conditions. We might thus be able to see if the *ost2-2D* mutation affects the environmental stimuli-triggered growth inhibition since both the wound and touch-response electrical signals were attenuated in *ost2-2D*. However, it would be also possible that the environmental stimuli activate downstream

responses that bypassed the effect of *ost2-2D*. It will require even further studies to address that. Exploring the growth of *ost2-2D* in nature would improve our knowledge of the relationship between electrical signals and growth regulation.

From a different point of view, mechanosensation might be positively associated with plant growth. It is known that the 24-hour rhythm is important for growth hormone regulation in humans. Sleep at night contributes more than 50 % of growth hormone production in a 24-hour cycle (Brandenberger and Weibel, 2004), and this is called the sleep-related growth hormone pulse. The night workers have reduced sleep-related growth hormone pulses but are compensated by the unpredictable pulses in the work period (Brandenberger and Weibel, 2004). In plants, it has been shown that the growth of hypocotyls peaked more than 6 hours post the zeitgeber time (Covington and Harmer, 2007). Exogenous auxin application causes maximum hypocotyl growth stimulation at night (Covington and Harmer, 2007). Interestingly, we found that the responsiveness of mechanostimulation-induced electrical signals depends on the time of day: 8 hours after the zeitgeber time plant have the most robust mechano-responsiveness (Chapter 4). This time-point also fits with the circadian leaf movement rhythm in the daytime (Dornbusch et al., 2014). The circadian mutant *elf3* mutant shows mechano-responsiveness throughout the day and early flower development as if it was grown under a continuous light condition (Chapter 5). The CRISPR-Cas9 *aha1 aha3 aha11* mutants show a reduction of mechanostimulation-induced electrical signals and also show slow-growth phenotypes compared with the WT (Chapter 7). Collectively, we find that mechanosensation depends on the time of day and the time-points coincidently associated with the circadian growth phenotypes reported in plants (Covington and Harmer, 2007; Dornbusch et al., 2014). Plants have altered mechanostimulation-induced electrical signalling and also show differences in the

growth phenotypes (Chapter 5 and Chapter 7). We suggest the possibility that mechano-responses positively contribute to plant growth regulation.

For the first time to our knowledge, we found the responsiveness of mechanostimulation-induced electrical signals depends on the time of day. The dysregulated circadian clock mutant *elf3* showed constant responsiveness to mechanostimulation throughout the day. We hypothesize that the responsiveness might be regulated by the phosphorylation status of plasma membrane proton pumps (AHAs) because the *elf3* mutation is known to cause an increased phosphorylation level of AHAs (Kinoshita et al., 2011). To explore this hypothesis further, we could in future examine mechano-responses in the phototropin mutant *phot1 phot2* which lost the ability to phosphorylate plasma membrane proton pumps in response to blue light stimulation (Ueno et al., 2005). In those plants, the phosphorylation status of AHAs might be similar throughout the day. Therefore, testing the mechano-responsiveness with the *phot1 phot2* would be an interesting perspective. Furthermore, the mechano-responsiveness in *Arabidopsis* was increased from 0 % at 11:00 to 100 % at 16:00. It would be very informative to test the time when the responsiveness starts to decrease after 16:00 and when the responsiveness is down to 0 %. With this information, we might be able to address if the phosphorylation status of the AHAs was regulated with time and possibly light conditions. However, a possible difficulty would be to operate experiments in a completely dark environment after 18:00. Moreover, Goodspeed et al. (2012) have shown that the day-night cycle of *Arabidopsis* plants and caterpillars affects the defense outcome. A synchronized day-night cycle results in a better-defended plant against caterpillar feeding. An *Allene oxide synthase* mutant and the *lux2* mutant both eliminate the day-night cycle-associated defense regulation (Goodspeed et al., 2012) suggesting that this effect depends on jasmonate and circadian rhythm. To investigate if this phenomenon is related to time-associated mechano-

responsiveness, we could repeat the clock-synchronization experiment with the *ost2-2D* mutant. Because the *ost2-2D* showed no influence on mechano-responsiveness and a reduction of the mechanostimulated electrical signals, it might reveal the effect of mechano-response without altering the circadian rhythm.

Similar time-dependent mechano-responsiveness was found in *Mimosa pudica* and *Arabidopsis thaliana*. Plasma membrane proton pumps are thought to underlie the high transmembrane potentials in *M. pudica* pulvinar motor cells (Fleurat-Lessard et al., 1997), which are important for leaf movement. We could thus transform the constitutive active *ost2-2D* cDNA into *Mimosa* to investigate the influence of plasma membrane proton pump activity in touch responses. A successful transgenic *Mimosa pudica* expressing the cytosolic calcium reporter GCaMP6f has been employed by Hagihara et al. (2022). With a similar approach, it would be possible to express the constitutively active plasma membrane H^+ATPase (*ost2-2D*) in the phloem, for example, with the *SUCROSE TRANSPORTER 2* (*SUC2*) promoter (Truernit and Sauer, 1995). Then we could see the effect of *ost2-2D* on the time-dependent mechano-responsiveness in the transgenic *Mimosa pudica.* It might improve our understanding of how does the constitutively active AHA1 attenuate the mechanostimulation-induced electrical signal in *Arabidopsis*.

The CRISPR-Cas9 approach allowed us to mutate multiple AHAs simultaneously. This, on the one hand, reduced the effect of gene redundancy. On the other hand, it would be difficult to tell which are the necessary mutations in multiple CRISPR-Cas9 mutants (eg. *aha1 aha3 aha8 aha11*). In Chapter 7, we found that *aha1 aha11* and *aha3 aha8* double mutants did not largely affect mechanostimulated electrical signals. It was exciting to find that the potential bi-allelic *aha1 aha3 aha11* mutants significantly reduced the signal amplitudes and the heterozygous *aha3* in the *aha1 aha11* background did not show any phenotype. However, we

could not identify if the other combinations of double mutants (eg. *aha3 aha11*) would have a similar effect on electrical signallings without making new mutants. Because of the male-sterile phenotypes in the bi-allelic *aha3* mutants, rescuing each *AHA* in the *aha1 aha3 aha11* mutant would not be suitable. To investigate this question, new CRISPR-Cas9 mutants (eg. re-mutate *aha3* in the *aha11* background) are inevitably needed.

There were contradictory findings in the loss-of-function and gain-of-function plasma membrane proton pump mutants in Chapter 5 and Chapter 7. We found the constitutively active *AHA1* mutants (*ost2-2D*) and the bi-allelic *aha1 aha3 aha11* mutants both show the reduction of the mechanostimulation-induced electrical signals. The *aha1 aha3 aha11* mutants might have a lower plasma membrane potential which leads to a smaller depolarization. However, if the *ost2-2D* mutant were constitutively active, would this generate a higher plasma membrane potential? How would a higher plasma membrane potential result in a smaller amplitude and a shorter duration? In this scenario, the reduced electrical signals in the *ost2-2D* mutant did not make much sense. A possible explanation would be that transient inhibition of proton pumps was required for the initial phase of membrane depolarization (Julien and Frachisse, 1992; Stahlberg and Cosgrove, 1996), but it is not clear how a constitutively active proton pump influences the electrical signals by affecting the transient inhibition event. Furthermore, it would be also possible that the constitutively active proton pumps were too efficient. The charges traveling across the plasma membrane in the depolarization phase were immediately complemented by the activity of the proton pumps. This would explain the fact that the signal durations were both decreased in the *ost2-2D* mutant and with fusicoccin treatment as well. Measuring the absolute membrane potential (Lazzari-Dean et al., 2021) in the phloem of the CRISPR-Cas9 mutants as well as the *ost2-2D* mutant would provide additional useful

information. Also, additional experiments are required to examine how a more active plasma membrane proton pump (*ost2-2D*) reduces the mechanostimulation-induced electrical signals.

V-type proton pumps (V-ATPase or VHA) are mostly localized in the subcellular compartments (Frogac M., 2007; Lupanga et al., 2020) and P-type proton pumps (P-ATPase or AHA) are mostly localized on the plasma membrane (Rodrigues et al., 2014; Hoffmann et al., 2019; Hoffmann et al., 2020). The VHAs would pump protons from the compartments to the cytosol differing from the AHAs which pump protons from the cytosol to the apoplast. Mutating the VHAs would theoretically decrease the proton gradient in the cytosol, and this effect might be similar to the constitutive active AHA1 mutation (*ost2-2D*). However, the results of *vha* T-DNA mutants showed increases in signal amplitudes which was contrary to the *ost2-2D* (Chapter 7). Our data suggest that VHAs and AHAs might influence the electrical signals in a different way, but investigating how the proton gradients change without directly monitoring the pH is difficult. Hence, monitoring the subcellular proton gradient changes with pH reporters would be a possible future perspective. Once a reliable pH reporter can be visualized in leaf veins, we could monitor the subcellular pH changes during the depolarization and repolarization phases of electrical signals. Thus we might be able to answer the question that how do VHAs and AHAs contribute to the proton gradient changes in mechanostimulation.

Mechanical force sensing mechanisms appear to be necessary for plant survival in nature. For instance, plant roots need to penetrate the ground to develop the underground root system. These mechanosensation mechanisms remain largely unknown in plants. Mechanosensation in animals depends in part on the well-known PIEZO channels (Coste et al., 2010; Kefauver et al., 2020). In *Arabidopsis,* PIEZO1 is localized on the tonoplast and facilitates mechanical force transduction in the roots and in pollen tubes (Mousavi et al., 2021; Radin et al., 2021). However, *Arabidopsis pzo1* mutants have normal (ie. WT-like) touch-

triggered growth reduction in the shoots (Darwish et al., 2022) and also display WT-like electrical signalling (Table 7.2). This suggests that mechanical force sensation in shoots relies on different mechanisms.

We identified the activities of plasma membrane proton pumps (AHAs) controlling mechanostimulation-induced electrical signalling in the leaf vasculature in Chapter 5. Genetically and pharmaceutically activating AHAs attenuated mechanostimulated electrical signals significantly. This proton pump machinery was further investigated in detail with the CRISPR-Cas9 approach in Chapter 7. Using CRISPR-Cas9 to mutate phloem-expressed *AHA*s specifically (*AHA1*, *AHA3*, and *AHA11*) reduced the signal amplitudes from 80 mV to 20 mV on average. The loss of these AHAs may result in lower membrane potentials in resting plasma membranes. A lower resting membrane potential would be responsible for a reduced depolarization, thus reducing the signal amplitudes. In this view, mechanostimulated surface potentials would be attenuated significantly if the plasma membrane potential was reduced in the phloem (eg. in *aha1 aha3 aha11*). This evidence would further support the findings in Chapter 4 which indicate that phloem may be the vascular tissue most responsive to mechanostimulation. Bead mechanostimulations triggered surface potentials and sieve element electrical signals in *Arabidopsis*. In both cases, vascular tissues appear to be very important in sensing and/or responding to mechanical stimulation. The time duration of the mechanostimulation-induced sieve element signal was much shorter than the surface potentials. Considering the surface potentials might be a summation of electrical potential changes on the measuring position, additional cell types within the vasculature would be responding to bead mechanostimulation as well. However, to date, we do not have methods that can probe electrical signals specifically in cell types other than the sieve element.

To explore the cell type-specific mechano-responses further, we may be able to use the cytosolic calcium sensors (eg. a GCaMP). It had shown that the wound-responses GCaMP3 signals appeared together with the electrical signals (Nguyen et al., 2018). Both of these two wound-induced signals depended on the vasculature for propagation. We have also shown that mechanostimulation with borosilicate bead dropping and repeated leaf bending both induced cytosolic calcium signals (monitored with GCaMP3) in cells surrounding the trichomes and in the veins. These results suggested that the cytosolic calcium signal would possibly serve as a complementary measurement to the electrical signal in response to touch. Furthermore, using the *SUC2* promoter (Truernit and Sauer, 1995) and the *LOX6* promoter (Chauvin et al., 2013) we could express the reporters (eg. GCaMP6) in the phloem and in xylem contact cells, respectively. If a genetically encoded voltage sensor (Matzke and Matzke, 2015) can be visualized in leaf veins this would also provide much useful information. We may thus investigate the mechano-responses in the specific cell types within the bundle sheath. The aim would be to identify which of the vascular cell types are the most mechanosensitive in *Arabidopsis*. Moreover, caterpillar walking triggers mechano-responses on the leaf surface but not in the veins as shown in Chapter 4. We might be able to further address our hypothesis that this is due to a different mechanosensitivity between each tissue with the use of tissue-specific reporters. The tools we have developed will be useful to explore more of the biology of touch responses in plants.

References:

- Acosta IF, Farmer EE. Jasmonates. Arabidopsis Book. 2010.
- Alabadí D, Oyama T, Yanovsky MJ, Harmon FG, Más P, Kay SA. Reciprocal regulation between TOC1 and LHY/CCA1 within the Arabidopsis circadian clock. Science. 2001, 293, 880-883.
- Alfonso E, Stahl E, Glauser G, Bellani E, Raaymakers TM, Van den Ackerveken G, Zeier J, Reymond P. Insect eggs trigger systemic acquired resistance against a fungal and an oomycete pathogen. New Phytol. 2021, 232, 2491-2505.
- Bear M, Connors B, Paradiso MA. Neuroscience: Exploring the Brain. Jones & Bartlett Learning, LLC. 2015.
- Barbier-Brygoo H, De Angeli A, Filleur S, Frachisse JM, Gambale F, Thomine S, Wege S. Anion channels/transporters in plants: from molecular bases to regulatory networks. Annu Rev Plant Biol. 2011, 62, 25-51.
- Beyhl D, Hörtensteiner S, Martinoia E, Farmer EE, Fromm J, Marten I, Hedrich R. The fou2 mutation in the major vacuolar cation channel TPC1 confers tolerance to inhibitory luminal calcium. Plant J. 2009, 58, 715-723.
- Boari F, Malone M. Wound-induced hydraulic signals: survey of occurrence in a range of species. Journal of Experimental Botany 1993, 44, 741-746.
- Bonaventure G, Gfeller A, Proebsting WM, Hörtensteiner S, Chételat A, Martinoia E, Farmer EE. A gain-of-function allele of TPC1 activates oxylipin biogenesis after leaf wounding in Arabidopsis. Plant J. 2007, 49, 889-898.
- Bose JC, Nervous Mechanism of Plants (Longmans, Green and Co., London, 1926).
- Bose JC, Plant Autographs and Their Revelations (Longmans, Green and Co., London, 1927).
- Brandenberger G, Weibel L. The 24-h growth hormone rhythm in men: sleep and circadian influences questioned. J Sleep Res. 2004, 13, 251-255.
- Burri JT, Saikia E, Läubli NF, Vogler H, Wittel FK, Rüggeberg M, Herrmann HJ, Burgert I, Nelson BJ, Grossniklaus U. A single touch can provide sufficient mechanical stimulation to trigger Venus flytrap closure. PLoS Biol. 2020, 18:e3000740.
- Caldelari D, Wang G, Farmer EE, Dong X. Arabidopsis lox3 lox4 double mutants are male sterile and defective in global proliferative arrest. Plant Mol Biol. 2011, 75, 25-33.

- Chauvin A, Caldelari D, Wolfender JL, Farmer EE. Four 13-lipoxygenases contribute to rapid jasmonate synthesis in wounded Arabidopsis thaliana leaves: a role for lipoxygenase 6 in responses to long-distance wound signals. New Phytol. 2013, 197, 566-575.
- Chauvin A, Lenglet A, Wolfender JL, Farmer EE. Paired Hierarchical Organization of 13-Lipoxygenases in Arabidopsis. Plants (Basel). 2016, 24:16.
- Chehab EW, Yao C, Henderson Z, Kim S, Braam J. Arabidopsis touch-induced morphogenesis is jasmonate mediated and protects against pests. Curr Biol. 2012, 22, 701-706.
- Chini A, Fonseca S, Fernández G, Adie B, Chico JM, Lorenzo O, García-Casado G, López-Vidriero I, Lozano FM, Ponce MR, Micol JL, Solano R. The JAZ family of repressors is the missing link in jasmonate signalling. Nature. 2007, 448, 666-671.
- Choi HW, Klessig DF. DAMPs, MAMPs, and NAMPs in plant innate immunity. BMC Plant Biol. 2016, 16: 232.
- Chung HS, Howe GA. A critical role for the TIFY motif in repression of jasmonate signaling by a stabilized splice variant of the JASMONATE ZIM-domain protein JAZ10 in Arabidopsis. Plant Cell. 2009, 21, 131-145.
- Coste B, Mathur J, Schmidt M, Earley TJ, Ranade S, Petrus MJ, Dubin AE, Patapoutian A. Piezo1 and Piezo2 are essential components of distinct mechanically activated cation channels. Science. 2010, 330, 55-60.
- Coste B, Xiao B, Santos JS, Syeda R, Grandl J, Spencer KS, Kim SE, Schmidt M, Mathur J, Dubin AE, Montal M, Patapoutian A. Piezo proteins are pore-forming subunits of mechanically activated channels. Nature. 2012, 483, 176-181.
- Coutand C, Dupraz C, Jaouen G, Ploquin S, Adam B. Mechanical stimuli regulate the allocation of biomass in trees: demonstration with young Prunus avium trees. Ann Bot. 2008, 101, 1421-1432.
- Creelman RA, Mullet JE. BIOSYNTHESIS AND ACTION OF JASMONATES IN PLANTS. Annu Rev Plant Physiol Plant Mol Biol. 1997, 48, 355-381.
- Darwish E, Ghosh R, Ontiveros-Cisneros A, Tran HC, Petersson M, De Milde L, Broda M, Goossens A, Van Moerkercke A, Khan K, Van Aken O. Touch signaling and thigmomorphogenesis are regulated by complementary CAMTA3- and JA-dependent pathways. Sci Adv. 2022, 8:eabm2091.

- Davies, E, Stankovic, B. Electrical signals, the cytoskeleton, and gene expression: a hypothesis on the coherence of the cellular responses to environmental insult. Communication in Plants. 2006, 21, 309-320, Springer Berlin Heidelberg.
- Degli Agosti RD. Touch-induced action potentials in Arabidopsis thaliana. Archives des Sciences 2014, 67, 125-138.
- DeWitt ND, Sussman MR. Immunocytological localization of an epitope-tagged plasma membrane proton pump (H(+)-ATPase) in phloem companion cells. Plant Cell. 1995, 7, 2053-2067.
- Dodd AN, Jakobsen MK, Baker AJ, Telzerow A, Hou SW, Laplaze L, Barrot L, Poethig RS, Haseloff J, Webb AA. Time of day modulates low-temperature Ca signals in Arabidopsis. Plant J. 2006, 48, 962-973.
- Dornbusch T, Michaud O, Xenarios I, Fankhauser C. Differentially phased leaf growth and movements in Arabidopsis depend on coordinated circadian and light regulation. Plant Cell. 2014, 26, 3911-3921.
- Evans MJ, Morris RJ. Chemical agents transported by xylem mass flow propagate variation potentials. Plant J. 2017, 91, 1029-1037.
- Farmer EE, Gao YQ, Lenzoni G, Wolfender JL, Wu Q. Wound- and mechanostimulated electrical signals control hormone responses. New Phytol. 2020, 227, 1037-1050.
- Farmer EE, Ryan CA. Interplant communication: airborne methyl jasmonate induces synthesis of proteinase inhibitors in plant leaves. Proc Natl Acad Sci U S A. 1990, 87, 7713-7716.
- Farmer EE, Ryan CA. Octadecanoid Precursors of Jasmonic Acid Activate the Synthesis of Wound-Inducible Proteinase Inhibitors. Plant Cell. 1992, 4, 129-134.
- Ferrari S, Savatin DV, Sicilia F, Gramegna G, Cervone F, Lorenzo GD. Oligogalacturonides: plant damage-associated molecular patterns and regulators of growth and development. Front Plant Sci. 2013, 4, 49.
- Fleurat-Lessard P, Bouche-Pillon S, Leloup C, Bonnemain JL. Distribution and Activity of the Plasma Membrane H+-ATPase in Mimosa pudica L. in Relation to Ionic Fluxes and Leaf Movements. Plant Physiol. 1997, 113, 747-754.
- Forgac M. Vacuolar ATPases: rotary proton pumps in physiology and pathophysiology. Nat Rev Mol Cell Biol. 2007, 8, 917-929.

- Forterre Y, Skotheim JM, Dumais J, Mahadevan L. How the Venus flytrap snaps. Nature. 2005, 433, 421-425.
- Fromm J. Control of phloem unloading by action potentials in Mimosa. Physiologia Plantarum 1991, 83, 529-533.
- Fromm J, Lautner S. Electrical signals and their physiological significance in plants. Plant Cell Environ. 2007, 30, 249-257.
- Gasperini D, Chauvin A, Acosta IF, Kurenda A, Stolz S, Chételat A, Wolfender JL, Farmer EE. Axial and Radial Oxylipin Transport. Plant Physiol. 2015, 169, 2244-2254.
- Glauser G, Dubugnon L, Mousavi SA, Rudaz S, Wolfender JL, Farmer EE. Velocity estimates for signal propagation leading to systemic jasmonic acid accumulation in wounded Arabidopsis. J Biol Chem. 2009, 284, 34506-34513.
- Green TR, Ryan CA. Wound-Induced Proteinase Inhibitor in Plant Leaves: A Possible Defense Mechanism against Insects. Science. 1972, 175, 776-777.
- Gottwald JR, Krysan PJ, Young JC, Evert RF, Sussman MR. Genetic evidence for the in planta role of phloem-specific plasma membrane sucrose transporters. Proc Natl Acad Sci U S A. 2000, 97, 13979-13984.
- Gouhier-Darimont C, Schmiesing A, Bonnet C, Lassueur S, Reymond P. Signalling of Arabidopsis thaliana response to Pieris brassicae eggs shares similarities with PAMP-triggered immunity. J Exp Bot. 2013, 64, 665-674.
- Guan L, Denkert N, Eisa A, Lehmann M, Sjuts I, Weiberg A, Soll J, Meinecke M, Schwenkert S. JASSY, a chloroplast outer membrane protein required for jasmonate biosynthesis. Proc Natl Acad Sci U S A. 2019, 116,10568-10575.
- Guo J, Zeng W, Jiang Y. Tuning the ion selectivity of two-pore channels. Proc Natl Acad Sci U S A. 2017, 114, 1009-1014.
- Hagihara T, Mano H, Miura T, Hasebe M, Toyota M. Calcium-mediated rapid movements defend against herbivorous insects in Mimosa pudica. Nat Commun. 2022 13, 6412.
- Han D, Antunes F, Canali R, Rettori D, Cadenas E. Voltage-dependent anion channels control the release of the superoxide anion from mitochondria to cytosol. J Biol Chem. 2003, 278, 5557-5563.

- Haruta M, Burch HL, Nelson RB, Barrett-Wilt G, Kline KG, Mohsin SB, Young JC, Otegui MS, Sussman MR. Molecular characterization of mutant Arabidopsis plants with reduced plasma membrane proton pump activity. J Biol Chem. 2010, 285, 17918-17929.
- Haruta M, Gray WM, Sussman MR. Regulation of the plasma membrane proton pump (H(+)-ATPase) by phosphorylation. Curr Opin Plant Biol. 2015, 28, 68-75.
- Hedrich R, Neher E. Venus Flytrap: How an Excitable, Carnivorous Plant Works. Trends Plant Sci. 2018, 23, 220-234.
- Heil M, Ibarra-Laclette E, Adame-Álvarez RM, Martínez O, Ramirez-Chávez E, Molina-Torres J, Herrera-Estrella L. How plants sense wounds: damaged-self recognition is based on plant-derived elicitors and induces octadecanoid signaling. PLoS One. 2012, 7, e30537.
- Hicks KA, Millar AJ, Carré IA, Somers DE, Straume M, Meeks-Wagner DR, Kay SA. Conditional circadian dysfunction of the Arabidopsis early-flowering 3 mutant. Science. 1996, 274, 790-792.
- HODGKIN AL, HUXLEY AF. A quantitative description of membrane current and its application to conduction and excitation in nerve. J Physiol. 1952 Aug;117(4):500-44.
- Hodick D, Sievers A. The action potential of Dionaea muscipula Ellis. Planta. 1988, 174, 8-18.
- Hoffmann RD, Portes MT, Olsen LI, Damineli DSC, Hayashi M, Nunes CO, Pedersen JT, Lima PT, Campos C, Feijó JA, Palmgren M. Plasma membrane H+-ATPases sustain pollen tube growth and fertilization. Nat Commun. 2020, 11, 2395.
- Homblé F, Krammer EM, Prévost M. Plant VDAC: facts and speculations. Biochim Biophys Acta. 2012, 1818,1486-1501.
- Howe GA, Major IT, Koo AJ. Modularity in Jasmonate Signaling for Multistress Resilience. Annu Rev Plant Biol. 2018, 69, 387-415.
- Huber AE, Bauerle TL. Long-distance plant signaling pathways in response to multiple stressors: the gap in knowledge. J Exp Bot. 2016, 67, 2063-2079.
- Jentsch TJ. CLC chloride channels and transporters: from genes to protein structure, pathology and physiology. Crit Rev Biochem Mol Biol. 2008, 43, 3-36.
- Katsir L, Schilmiller AL, Staswick PE, He SY, Howe GA. COI1 is a critical component of a receptor for jasmonate and the bacterial virulence factor coronatine. Proc Natl Acad Sci U S A. 2008, 105, 7100-7105.

- Kefauver JM, Ward AB, Patapoutian A. Discoveries in structure and physiology of mechanically activated ion channels. Nature. 2020, 587, 567-576.
- Kim S, Mochizuki N, Deguchi A, Nagano AJ, Suzuki T, Nagatani A. Auxin Contributes to the Intraorgan Regulation of Gene Expression in Response to Shade. Plant Physiol. 2018, 177, 847-862.
- Kinoshita T, Doi M, Suetsugu N, Kagawa T, Wada M, Shimazaki K. Phot1 and phot2 mediate blue light regulation of stomatal opening. Nature. 2001, 414, 656-660.
- Kinoshita T, Ono N, Hayashi Y, Morimoto S, Nakamura S, Soda M, Kato Y, Ohnishi M, Nakano T, Inoue S, Shimazaki K. FLOWERING LOCUS T regulates stomatal opening. Curr Biol. 2011, 21, 1232-1238.
- Kinoshita T, Shimazaki Ki. Blue light activates the plasma membrane H(+)-ATPase by phosphorylation of the C-terminus in stomatal guard cells. EMBO J. 1999, 18, 5548-5558.
- Kisnieriene V, Lapeikaite I, Pupkis V. Electrical signalling in Nitellopsis obtusa: potential biomarkers of biologically active compounds. Funct Plant Biol. 2018, 45,132-142.
- Krysan PJ, Young JC, Tax F, Sussman MR. Identification of transferred DNA insertions within Arabidopsis genes involved in signal transduction and ion transport. Proc Natl Acad Sci U S A. 1996, 93, 8145-8150.
- Kumari A, Chételat A, Nguyen CT, Farmer EE. Arabidopsis H+-ATPase AHA1 controls slow wave potential duration and wound-response jasmonate pathway activation. Proc Natl Acad Sci U S A. 2019, 116, 20226-20231.
- Kurenda A, Nguyen CT, Chételat A, Stolz S, Farmer EE. Insect-damaged Arabidopsis moves like wounded Mimosa pudica. Proc Natl Acad Sci U S A. 2019, 116, 26066-26071.
- Koo AJ, Howe GA. The wound hormone jasmonate. Phytochemistry. 2009, 70, 1571-80.
- Lee D, Polisensky DH, Braam J. Genome-wide identification of touch- and darkness-regulated Arabidopsis genes: a focus on calmodulin-like and XTH genes. New Phytol. 2005, 165, 429-444.
- Lazzari-Dean JR, Gest AMM, Miller EW. Measuring Absolute Membrane Potential Across Space and Time. Annu Rev Biophys. 2021, 50, 447-468.

- Lee Y, Satter RL. H Uptake and Release during Circadian Rhythmic Movements of Excised Samanea Motor Organs : Effects of Mannitol, Sorbitol, and External pH. Plant Physiol. 1987, 83, 856-862.
- Lehmann J, Jørgensen ME, Fratz S, Müller HM, Kusch J, Scherzer S, Navarro-Retamal C, Mayer D, Böhm J, Konrad KR, Terpitz U, Dreyer I, Mueller TD, Sauer M, Hedrich R, Geiger D, Maierhofer T. Acidosis-induced activation of anion channel SLAH3 in the flooding-related stress response of Arabidopsis. Curr Biol. 2021, 31, 3575-3585.
- Lenglet A, Jaślan D, Toyota M, Mueller M, Müller T, Schönknecht G, Marten I, Gilroy S, Hedrich R, Farmer EE. Control of basal jasmonate signalling and defence through modulation of intracellular cation flux capacity. New Phytol. 2017, 216, 1161-1169.
- Lupanga U, Röhrich R, Askani J, Hilmer S, Kiefer C, Krebs M, Kanazawa T, Ueda T, Schumacher K. The Arabidopsis V-ATPase is localized to the TGN/EE via a seed plant-specific motif. Elife. 2020, 9, e60568.
- Malone, M, Alarcon, JJ. Palumbo, L. An hydraulic interpretation of rapid, long-distance wound signalling in the tomato. Planta 1994, 193, 181-185.
- Marhavý P, Kurenda A, Siddique S, Dénervaud Tendon V, Zhou F, Holbein J, Hasan MS, Grundler FM, Farmer EE, Geldner N. Single-cell damage elicits regional, nematode-restricting ethylene responses in roots. EMBO J. 2019, 38, e100972.
- Martí Ruiz MC, Jung HJ, Webb AAR. Circadian gating of dark-induced increases in chloroplast- and cytosolic-free calcium in Arabidopsis. New Phytol. 2020, 225, 1993-2005.
- Matsumura M, Nomoto M, Itaya T, Aratani Y, Iwamoto M, Matsuura T, Hayashi Y, Mori T, Skelly MJ, Yamamoto YY, Kinoshita T, Mori IC, Suzuki T, Betsuyaku S, Spoel SH, Toyota M, Tada Y. Mechanosensory trichome cells evoke a mechanical stimuli-induced immune response in Arabidopsis thaliana. Nat Commun. 2022, 13, 1216.
- Matzke AJ, Matzke M. Expression and testing in plants of ArcLight, a genetically-encoded voltage indicator used in neuroscience research. BMC Plant Biol. 2015, 15, 245.
- McWatters HG, Bastow RM, Hall A, Millar AJ. The ELF3 zeitnehmer regulates light signalling to the circadian clock. Nature. 2000, 408, 716-720.
- Merlot S, Leonhardt N, Fenzi F, Valon C, Costa M, Piette L, Vavasseur A, Genty B, Boivin K, Müller A, Giraudat J, Leung J. Constitutive activation of a plasma membrane

H(+)-ATPase prevents abscisic acid-mediated stomatal closure. EMBO J. 2007, 26, 3216-3226.

- Merlot S, Mustilli AC, Genty B, North H, Lefebvre V, Sotta B, Vavasseur A, Giraudat J. Use of infrared thermal imaging to isolate Arabidopsis mutants defective in stomatal regulation. Plant J. 2002, 30, 601-609.
- Mielke S, Gasperini D. Interplay between Plant Cell Walls and Jasmonate Production. Plant Cell Physiol. 2019, 60, 2629-2637.
- Mielke S, Zimmer M, Meena MK, Dreos R, Stellmach H, Hause B, Voiniciuc C, Gasperini D. Jasmonate biosynthesis arising from altered cell walls is prompted by turgor-driven mechanical compression. Sci Adv. 2021, 7, eabf0356.
- Miller G, Schlauch K, Tam R, Cortes D, Torres MA, Shulaev V, Dangl JL, Mittler R. The plant NADPH oxidase RBOHD mediates rapid systemic signaling in response to diverse stimuli. Sci Signal. 2009, 2, ra45.
- Moe-Lange J, Gappel NM, Machado M, Wudick MM, Sies CSA, Schott-Verdugo SN, Bonus M, Mishra S, Hartwig T, Bezrutczyk M, Basu D, Farmer EE, Gohlke H, Malkovskiy A, Haswell ES, Lercher MJ, Ehrhardt DW, Frommer WB, Kleist TJ. Interdependence of a mechanosensitive anion channel and glutamate receptors in distal wound signaling. Sci Adv. 2021, 7, eabg4298.
- Mousavi SA, Chauvin A, Pascaud F, Kellenberger S, Farmer EE. GLUTAMATE RECEPTOR-LIKE genes mediate leaf-to-leaf wound signalling. Nature. 2013, 500, 422-426.
- Mousavi SAR, Dubin AE, Zeng WZ, Coombs AM, Do K, Ghadiri DA, Keenan WT, Ge C, Zhao Y, Patapoutian A. PIEZO ion channel is required for root mechanotransduction in Arabidopsis thaliana. Proc Natl Acad Sci U S A. 2021, 118, e2102188118.
- Nguyen CT, Kurenda A, Stolz S, Chételat A, Farmer EE. Identification of cell populations necessary for leaf-to-leaf electrical signaling in a wounded plant. Proc Natl Acad Sci U S A. 2018, 115, 10178-10183.
- Nohales MA, Kay SA. Molecular mechanisms at the core of the plant circadian oscillator. Nat Struct Mol Biol. 2016, 23, 1061-1069.

- Oppenheimer DG, Herman PL, Sivakumaran S, Esch J, Marks MD. A myb gene required for leaf trichome differentiation in Arabidopsis is expressed in stipules. Cell. 1991, 67, 483-493.
- Ozalvo R, Cabrera J, Escobar C, Christensen SA, Borrego EJ, Kolomiets MV, Castresana C, Iberkleid I, Brown Horowitz S. Two closely related members of Arabidopsis 13-lipoxygenases (13-LOXs), LOX3 and LOX4, reveal distinct functions in response to plant-parasitic nematode infection. Mol Plant Pathol. 2014, 15, 319-332.
- Park JH, Halitschke R, Kim HB, Baldwin IT, Feldmann KA, Feyereisen R. A knock-out mutation in allene oxide synthase results in male sterility and defective wound signal transduction in Arabidopsis due to a block in jasmonic acid biosynthesis. Plant J. 2002, 31, 1-12.
- Radin I, Richardson RA, Coomey JH, Weiner ER, Bascom CS, Li T, Bezanilla M, Haswell ES. Plant PIEZO homologs modulate vacuole morphology during tip growth. Science. 2021, 373, 586-590.
- Ramesh SA, Tyerman SD, Xu B, Bose J, Kaur S, Conn V, Domingos P, Ullah S, Wege S, Shabala S, Feijó JA, Ryan PR, Gilliham M. GABA signalling modulates plant growth by directly regulating the activity of plant-specific anion transporters. Nat Commun. 2015, 6, 7879.
- Reymond P, Bodenhausen N, Van Poecke RM, Krishnamurthy V, Dicke M, Farmer EE. A conserved transcript pattern in response to a specialist and a generalist herbivore. Plant Cell. 2004, 16, 3132-3147.
- Ribot C, Zimmerli C, Farmer EE, Reymond P, Poirier Y. Induction of the Arabidopsis PHO1;H10 gene by 12-oxo-phytodienoic acid but not jasmonic acid via a CORONATINE INSENSITIVE1-dependent pathway. Plant Physiol. 2008, 147, 696-706.
- Ricca U. Transmission of stimuli in plants. Nature 1926, 117, 654-655.
- Robertson WR, Clark K, Young JC, Sussman MR. An Arabidopsis thaliana plasma membrane proton pump is essential for pollen development. Genetics. 2004, 168, 1677-1687.
- Salvador-Recatalà V, Tjallingii WF, Farmer EE. Real-time, in vivo intracellular recordings of caterpillar-induced depolarization waves in sieve elements using aphid electrodes. New Phytol. 2014, 203, 674-684.

- Sasaki T, Tsuchiya Y, Ariyoshi M, Ryan PR, Furuichi T, Yamamoto Y. A domain-based approach for analyzing the function of aluminum-activated malate transporters from wheat (Triticum aestivum) and Arabidopsis thaliana in Xenopus oocytes. Plant Cell Physiol. 2014, 55, 2126-2138.
- Schaller A, Stintzi A. Enzymes in jasmonate biosynthesis - structure, function, regulation. Phytochemistry. 2009, 70, 1532-1538.
- Sehr EM, Agusti J, Lehner R, Farmer EE, Schwarz M, Greb T. Analysis of secondary growth in the Arabidopsis shoot reveals a positive role of jasmonate signalling in cambium formation. Plant J. 2010, 63, 811-822.
- Sharma T, Dreyer I, Kochian L, Piñeros MA. The ALMT Family of Organic Acid Transporters in Plants and Their Involvement in Detoxification and Nutrient Security. Front Plant Sci. 2016, 7, 1488.
- Shimada TL, Shimada T, Hara-Nishimura I. A rapid and non-destructive screenable marker, FAST, for identifying transformed seeds of Arabidopsis thaliana. Plant J. 2010, 61, 519-28.
- Shimmen T. Involvement of receptor potentials and action potentials in mechano-perception in plants. Aust. J. Plant Physiol. 2001, 28, 567-576.
- Sibaoka T. Action potentials in plant organs. Symp Soc Exp Biol. 1966, 20, 49-73.
- Simons PJ. The role of electricity in plant movements. New Phytologist 1981, 87, 11-37.
- Spartz AK, Ren H, Park MY, Grandt KN, Lee SH, Murphy AS, Sussman MR, Overvoorde PJ, Gray WM. SAUR Inhibition of PP2C-D Phosphatases Activates Plasma Membrane H+-ATPases to Promote Cell Expansion in Arabidopsis. Plant Cell. 2014, 26, 2129-2142.
- Stahlberg R, Cosgrove DJ. Induction and ionic basis of slow wave potentials in seedlings of Pisum sativum L. Planta. 1996, 200, 416-425.
- Stahlberg R, Cosgrove DJ. Mannitol inhibits growth of intact cucumber but not pea seedlings by mechanically collapsing the root pressure. Plant Cell Environ. 1997, 20, 1135-1144.
- Staswick PE, Serban B, Rowe M, Tiryaki I, Maldonado MT, Maldonado MC, Suza W. Characterization of an Arabidopsis enzyme family that conjugates amino acids to indole-3-acetic acid. Plant Cell. 2005, 17, 616-627.

- Staswick PE, Tiryaki I, Rowe ML. Jasmonate response locus JAR1 and several related Arabidopsis genes encode enzymes of the firefly luciferase superfamily that show activity on jasmonic, salicylic, and indole-3-acetic acids in an assay for adenylation. Plant Cell. 2002, 14, 1405-1415.
- Steinhorst L, Kudla J. Calcium and reactive oxygen species rule the waves of signaling. Plant Physiol. 2013, 163, 471-485.
- STUHLMAN O Jr, DARDEN EB. The action potentials obtained from venus's-flytrap. Science. 1950, 111, 491-492.
- Sze H, Li X, Palmgren MG. Energization of plant cell membranes by H+-pumping ATPases. Regulation and biosynthesis. Plant Cell. 1999, 11, 677-690.
- Szechyńska-Hebda M, Lewandowska M, Witoń D, Fichman Y, Mittler R, Karpiński SM. Aboveground plant-to-plant electrical signaling mediates network acquired acclimation. Plant Cell. 2022, 34, 3047-3065.
- Tazawa M, Shimmen T, Mimura T. Membrane control in the characeae. Ann. Rev. Plant physiol. 1987, 38, 95-117.
- Thines B, Katsir L, Melotto M, Niu Y, Mandaokar A, Liu G, Nomura K, He SY, Howe GA, Browse J. JAZ repressor proteins are targets of the SCF(COI1) complex during jasmonate signalling. Nature. 2007, 448, 661-665.
- Tjallingii, W.F. ELECTRONIC RECORDING OF PENETRATION BEHAVIOUR BY APHIDS. Entomologia Experimentalis et Applicata, 1978, 24, 721-730.
- Tjallingii, WF. Continuous Recording of Stylet Penetration Activities by Aphids. In: Campbell, R.K. and Eikenbary, R.D., Eds., Aphid-Plant Genotype Interactions, Elsevier, Amsterdam, 1990, 89-99.
- Toyota M, Spencer D, Sawai-Toyota S, Jiaqi W, Zhang T, Koo AJ, Howe GA, Gilroy S. Glutamate triggers long-distance, calcium-based plant defense signaling. Science. 2018, 361, 1112-1115.
- Tran D, Girault T, Guichard M, Thomine S, Leblanc-Fournier N, Moulia B, de Langre E, Allain JM, Frachisse JM. Cellular transduction of mechanical oscillations in plants by the plasma-membrane mechanosensitive channel MSL10. Proc Natl Acad Sci U S A. 2021, 118, e1919402118.

- Truernit E, Sauer N. The promoter of the Arabidopsis thaliana SUC2 sucrose-H+ symporter gene directs expression of beta-glucuronidase to the phloem: evidence for phloem loading and unloading by SUC2. Planta. 1995, 196, 564-570.
- Ueda M, Nakamura Y. Chemical basis of plant leaf movement. Plant Cell Physiol. 2007, 48, 900-907.
- Ueno K, Kinoshita T, Inoue S, Emi T, Shimazaki K. Biochemical characterization of plasma membrane H+-ATPase activation in guard cell protoplasts of Arabidopsis thaliana in response to blue light. Plant Cell Physiol. 2005, 46, 955-963.
- Ursache R, De Jesus Vieira Teixeira C, Dénervaud Tendon V, Gully K, De Bellis D, Schmid-Siegert E, Grube Andersen T, Shekhar V, Calderon S, Pradervand S, Nawrath C, Geldner N, Vermeer JEM. GDSL-domain proteins have key roles in suberin polymerization and degradation. Nat Plants. 2021, 7, 353-364.
- Ursache R, Fujita S, Dénervaud Tendon V, Geldner N. Combined fluorescent seed selection and multiplex CRISPR/Cas9 assembly for fast generation of multiple Arabidopsis mutants. Plant Methods. 2021, 17, 111.
- van Bel AJ, Furch AC, Will T, Buxa SV, Musetti R, Hafke JB. Spread the news: systemic dissemination and local impact of Ca^{2+} signals along the phloem pathway. J Exp Bot. 2014, 65, 1761-1787.
- Vodeneev V, Orlova A, Morozova E, Orlova L, Akinchits E, Orlova O, Sukhov V. The mechanism of propagation of variation potentials in wheat leaves. J Plant Physiol. 2012, 169, 949-954.
- Wasternack C, Hause B. Jasmonates: biosynthesis, perception, signal transduction and action in plant stress response, growth and development. An update to the 2007 review in Annals of Botany. Ann Bot. 2013, 111, 1021-1058.
- Würtele M, Jelich-Ottmann C, Wittinghofer A, Oecking C. Structural view of a fungal toxin acting on a 14-3-3 regulatory complex. EMBO J. 2003, 22, 987-994.
- Xia Y, Yu K, Navarre D, Seebold K, Kachroo A, Kachroo P. The glabra1 mutation affects cuticle formation and plant responses to microbes. Plant Physiol. 2010, 154, 833-846.
- Yan Y, Stolz S, Chételat A, Reymond P, Pagni M, Dubugnon L, Farmer EE. A downstream mediator in the growth repression limb of the jasmonate pathway. Plant Cell. 2007, 19, 2470-2483.

- Yang TH, Lenglet-Hilfiker A, Stolz S, Glauser G, Farmer EE. Jasmonate Precursor Biosynthetic Enzymes LOX3 and LOX4 Control Wound-Response Growth Restriction. Plant Physiol. 2020, 184, 1172-1180.
- You Y, Sawikowska A, Lee JE, Benstein RM, Neumann M, Krajewski P, Schmid M. Phloem Companion Cell-Specific Transcriptomic and Epigenomic Analyses Identify MRF1, a Regulator of Flowering. Plant Cell. 2019, 31, 325-345.
- Zagotta MT, Hicks KA, Jacobs CI, Young JC, Hangarter RP, Meeks-Wagner DR. The Arabidopsis ELF3 gene regulates vegetative photomorphogenesis and the photoperiodic induction of flowering. Plant J. 1996, 10, 691-702.
- Zhou LH, Liu SB, Wang PF, Lu TJ, Xu F, Genin GM, Pickard BG. The Arabidopsis trichome is an active mechanosensory switch. Plant Cell Environ. 2017, 40, 611-621.
- Zhu Z, Quint M, Anwer MU. Arabidopsis EARLY FLOWERING 3 controls temperature responsiveness of the circadian clock independently of the evening complex. J Exp Bot. 2022, 73, 1049-1061.
- Zimmermann MR, Felle HH. Dissection of heat-induced systemic signals: superiority of ion fluxes to voltage changes in substomatal cavities. Planta. 2009, 229, 539-547.